**THESIS**

# AN OBSERVATIONAL ANALYSIS OF TWO GULF SURGE EVENTS DURING THE 2004 NORTH AMERICAN MONSOON EXPERIMENT

Submitted by

Peter James Rogers

Department of Atmospheric Science

In partial fulfillment of the requirements

For the Degree of Master of Science

Colorado State University

Fort Collins, Colorado

Fall 2005

COLORADO STATE UNIVERSITY

3 November 2005

WE HEREBY RECOMMEND THAT THE THESIS PREPARED UNDER OUR SUPERVISON BY PETER JAMES ROGERS ENTITLED AN OBSERVATIONAL ANALYSIS OF TWO GULF SURGE EVENTS DURING THE 2004 NORTH AMERICAN MONSOON EXPERIMENT BE ACCEPTED AS FULFILLING IN PART REQUIREMENTS FOR THE DEGREE OF MASTER OF SCIENCE.

Committee on Graduate Work

_____

_____

_____

Advisor

_____

Department Head

## ABSTRACT OF THESIS

## AN OBSERVATIONAL ANALYSIS OF TWO GULF SURGE EVENTS DURING THE 2004 NORTH AMERICAN MONSOON EXPERIMENT

Gulf surges are northward propagating disturbances along the Gulf of California (GOC) that are responsible for advecting large quantities of cool, moisture-laden air from the GOC or eastern tropical Pacific Ocean into the low deserts of the southwest United States and northwest Mexico during the North American Monsoon. Although numerous observational and modeling studies have examined the gross synoptic patterns, initiation mechanisms, general structure, and precipitation tendencies associated with gulf surges, little attention has been given to the dynamical mechanism(s) by which these disturbances propagate northward along the GOC. In this study, high temporal and spatial observational measurements collected during the 2004 North American Monsoon Experiment (NAME) field campaign (1 July – 15 August) are used to describe the detailed vertical/ horizontal structure and probable dynamical mechanism(s) of two gulf surge events on a case-by-case basis. Of greatest interest was the deployment of three National Center for Atmospheric Research Integrated Sounding Systems (ISS) along the east coast of the GOC, in addition to a relatively dense network of rawinsonde sites across the North American Monsoon geographical domain.

The observations show that gulf surges occur amid extremely complex synoptic, mesoscale, and convective environments. Preceded by anomalous warming, gulf surge passage occurs in the early morning hours and is accompanied by increased south-southeasterly flow that appears to deepen and strengthen with time. Considerable low-level anomalous cooling and moistening primarily confined below 800 hPa also occurs. At the northern ISS sites, gulf surge onset appears to significantly increase the depth of the well-mixed boundary layer. Anomalous surface pressure increases associated with this deepening can be tracked from site to site, resulting in gulf surge propagation speeds of approximately 20 m $s^{-1}$. Overall, these patterns are best observed at sites along the northern GOC and become increasingly difficult to discern farther south.

A conceptual model is proposed in which substantial convective evaporational cooling over the central or southern GOC, its coastal plain, and Sierra Madre Occidental (SMO) foothills induces a northward propagating linear Kelvin wave-like disturbance along the north-south barrier of the SMO, thus initiating the gulf surge. As the surge propagates north, it encounters an environment favorable for the development of nonlinearities along its leading edge. These nonlinearities are exhibited as atmospheric bore or solitary wave-like characteristics at the surface and within the boundary layer. The observed rapid propagation and surface pressure rises are consistent with this interpretation.

Peter James Rogers
Department of Atmospheric Science
Colorado State University
Fort Collins, Colorado 80523-1372
Fall 2005

## ACKNOWLEDGEMENTS

This research was supported by National Science Foundation (NSF)/North American Monsoon Experiment (NAME) grant ATM-0340602 and by a one-year American Meteorological Society Graduate Fellowship.

I want to thank Dr. Steven Rutledge from the Department of Atmospheric Science and Dr. Holger Kley from the Department of Mathematics for their willingness to serve as members of my graduate thesis committee, and after having reviewed this manuscript, provided valuable comments and suggestions as a means to improve its content. I would also like to thank my academic advisor, Dr. Richard Johnson, for his guidance, support, and encouragement in all aspects of this project – from presenting me with the opportunity to participate in the 2004 NAME field campaign to the countless hours he dedicated to one-on-one meetings with me. It was these important times where he helped me analyze data, better understand relevant concepts, and edit this manuscript. His valuable insight and direction were also much appreciated.

Special thanks are also in order to several members of the Johnson Mesoscale Meteorology Research Group. To Paul Ciesielski for his time and effort in data acquisition, quality control, and generating the gridded datasets; to Rick Taft, Brian

McNoldy, and Russ Schumacher for their patience in helping me with computer related issues, including coding; to Daniel Lindsey for providing the satellite data;
and to Paul Quelet and Gail Cordova for their continuous words of encouragement and support.

Finally, I want to thank my parents, Kevin and Kristi, and my sister, Sarah, for their love, prayers, and support during my endeavors while at Colorado State University. Most important, I thank my wife, Elizabeth, for her unconditional love, devotion, and personal sacrifice in order to make this work a reality.

## CONTENTS

## FIGURES

## TABLES

# CHAPTER 1

# INTRODUCTION AND MOTIVATION

The North American Monsoon (NAM hereafter) is an atmospheric circulation phenomenon most often characterized by a marked increase in convective activity and precipitation, beginning in early July and continuing through mid-September across much of northwest Mexico and the southwest United States (Bryson and Lowry 1955, Douglas et al. 1993, Adams and Comrie 1997, Stensrud et al. 1997). Given similar thermal, pressure, and circulation patterns to its Asian counterpart over the Tibetan Plateau (Tang and Reiter 1984), the NAM can be considered a "true" monsoon (Adams and Comrie 1997), or seasonal wind (Glickman et al. 2000), since it is accompanied by a low-level wind reversal over the Gulf of California (GOC hereafter) from northwesterly during the winter months to southerly or southeasterly during the summer (Badan-Dangon et al. 1991, Bordoni et al. 2004). A mid- to upper-tropospheric wind shift also occurs during this time from westerly to easterly or southeasterly (Jurwitz 1953, Bryson and Lowry 1955, Reitan 1957, Sellers and Hill 1974, Douglas et al. 1993).

Early NAM literature focused almost exclusively on Arizona and the southwest United States (Jurwitz 1953, Bryson and Lowry 1955, Reitan 1957, Sellers and Hill 1974). However, a prominent feature of the NAM is its region of maximum precipitation that parallels the western slopes of the Sierra Madre Occidental (SMO hereafter) in

northwest Mexico (Douglas et al. 1993, Gochis et al. 2004). Increased precipitation over the southwest United States is only the northernmost extent of this pattern. The NAM geographical domain, therefore, encompasses an area stretching from the Pacific Ocean east to the Gulf of Mexico and Great Plains, and from the Great Basin, Colorado Plateau, and Rocky Mountains south to the Mexican Plateau. This region of interest includes the Peninsular Range of Baja California, GOC, SMO, Sonoran Desert, and Colorado River Basin (Fig. 1).

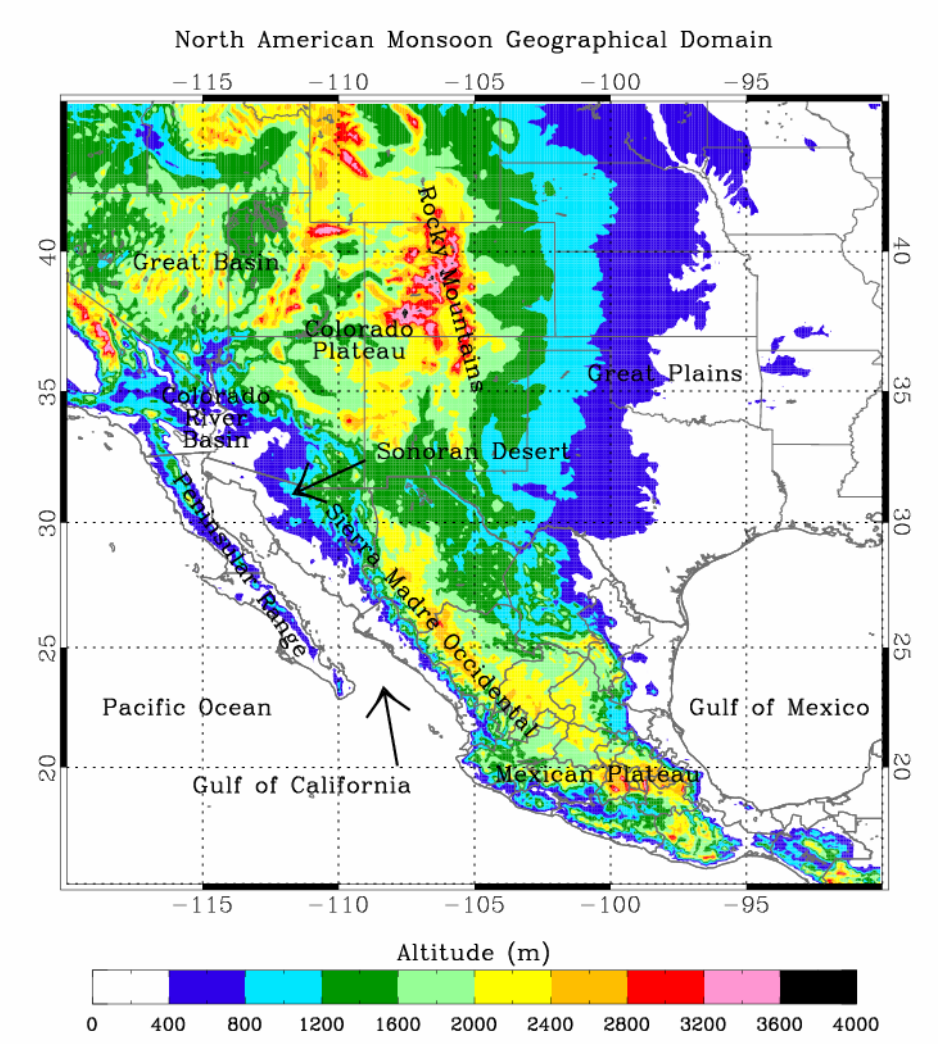


Figure 1: North American Monsoon geographical domain. Colored contours represent altitude above sea level (m).

Numerous reasons exist to continue NAM research and better understand its various circulation features, including gulf surges (defined below). The NAM is responsible for approximately 40% to 60% of Arizona's (Jurwitz 1953) and 60% to 80% of northwest Mexico's (Douglas et al. 1993) annual precipitation. In addition, Arizona's total population increased nearly 40% from 1990 to 2000 (U.S. Census Bureau 2005). These statistics emphasize the increasing challenges for water management in the southwest United States. Dramatically rising populations also increase the risk for property damage and personal injury and/or death resulting from NAM heavy rains, flash floods, and strong winds (McCollum et al. 1995, Stensrud et al. 1995). In addition, Eta (recently renamed to NAM or North American Mesoscale) and NGM (Nested Grid Model) forecast models perform poorly when simulating low-level moisture, subsequent convection, and precipitation over Arizona (Dunn and Horel 1994a,b), and coarsely gridded National Centers for Environmental Prediction (NCEP hereafter) reanalyses products fail to capture the basic low-level wind reversal during the NAM over the GOC (Bordoni et al. 2004).

The progression from extremely dry to moist conditions over the NAM domain, or monsoon onset, was originally attributed to the westward extension of the southeast United States subtropical high (Jurwitz 1953, Bryson and Lowry 1955, Reitan 1957, Sellers and Hill 1974), resulting in a mid-tropospheric wind shift from dry westerlies with Pacific Ocean origins to moist southeasterlies with Gulf of Mexico origins. Reitan (1957), however, discovered that 50% of the total precipitable water over Phoenix was below 800 hPa (~ 2 km above sea level) when examining sounding data. Hence,

questions arose as to how water vapor from the Gulf of Mexico could traverse up and over the SMO into Arizona given the large extent of this mountain range above this level (Fig. 1). In addition, Rasmusson (1967) showed that there is a strong northward water vapor flux from the GOC into the southwest United States that is detached from an even stronger Gulf of Mexico water vapor flux into the central United States east of the Continental Divide.

Given these findings, Hales (1972) and Brenner (1974) were among the earliest studies to introduce the GOC moisture "gulf" surge (hereafter gulf surge) as a mechanism for advecting low-level moisture-laden air from the eastern tropical Pacific and GOC into the deserts of the southwest United States and northwest Mexico during the NAM. Several other studies have since provided further evidence in support for the eastern tropical Pacific and GOC as the dominant low-level monsoon moisture source for northwest Mexico and western Arizona (Carleton 1986, Douglas et al. 1993, Douglas 1995, Stensrud et al. 1995, Stensrud et al. 1997). However, many studies still agree that the Gulf of Mexico moisture source cannot be ignored, especially east of central Arizona, and is most important in the mid- to upper-troposphere (Hales 1974, Carleton 1986, Stensrud et al. 1995, Schmitz and Mullen 1996, Higgins et al. 1997).

Following the studies of Hales (1972) and Brenner (1974), gulf surge research received little attention until the Southwest Area Monsoon Project (SWAMP) (Stensrud et al. 1997) in 1990 (Douglas 1995) and 1993 (Douglas and Li 1996). Both field campaigns placed emphasis on severe thunderstorm development over Arizona and the

surrounding areas, corresponding synoptic flow patterns, and circulation features over the GOC and low deserts. An unprecedented abundance of rawinsonde, pilot balloon, and aircraft observations served as the basis for several studies (Douglas 1995, McCollum et al. 1995, Stensrud et al. 1995, Douglas and Li 1996, Douglas et al. 1998) that sparked a renewed interest in gulf surges (Stensrud et al.1997, Anderson et al. 2000b, Fuller and Stensrud 2000, Douglas and Leal 2003, Higgins et al. 2004). Further interest in gulf surges has been generated by the planning and execution of the 2004 North American Monsoon Experiment (NAME hereafter) (Higgins et al. 2006).

Although past observational and modeling studies have provided tremendous insight towards a better understanding of gulf surges, there are still a number of aspects of this phenomenon that remain a mystery. Most importantly, the dynamical mechanism(s) by which gulf surges propagate northward along the GOC is still a matter of debate (Zehnder 2004). It is not known whether gulf surges are best described as coastally trapped gravity currents, atmospheric bores, Rossby waves, Kelvin waves, or a combination of these mechanisms. Observational measurements collected during the NAME allow for detailed studies of the structure and dynamical mechanism(s) of gulf surges given the data's unprecedented high temporal and spatial resolution. Of particular importance is the deployment of three National Center for Atmospheric Research (NCAR hereafter) Integrated Sounding Systems (ISS hereafter) along the east coast of the GOC to sample the lower troposphere throughout the 46-day extent of the NAME field campaign (1 July – 15 August 2004) (see Section 3.3 for further explanation). The ISS data, along with

other instrumentation platforms, will be an integral part of this study of the vertical/ horizontal structure and dynamical mechanism(s) of gulf surges.

The remainder of this paper is outlined as follows. Chapter 2 will discuss the breadth of literature aimed at better understanding NAM circulation and thermodynamic patterns, and more specifically the details surrounding gulf surges. Chapter 3 will describe the NAME field campaign, its observational network, and the data used for this study. Data analyses methods will also be discussed in this chapter. Chapter 4 will detail the synoptic and convective environments that accompanied the two gulf surge events observed. Chapter 5 will examine the gulf surge vertical and horizontal structures. Chapter 6 will describe the propagation characteristics of both gulf surge events, as well as suggest a probable dynamical mechanism for propagation. Finally, Chapter 7 will provide a brief summary and conclusions.

# CHAPTER 2

# BACKGROUND AND LITERATRUE REVIEW

## 2.1 Mean Tropospheric Upper Air Analyses over the NAM Geographical Domain

The troposphere over the NAM geographical domain can be divided into two primary layers due to the complex topography of the region (Fig. 1). The mid- to upper-troposphere, or free atmosphere, is the layer in which atmospheric flow is predominately unaffected by the surrounding terrain and includes pressures less than or equal to 700 hPa (~ 3 km above sea level). Conversely, the lower troposphere is the layer in which atmospheric flow is significantly altered by the surrounding terrain and includes pressures greater than 700 hPa. Since much of the terrain surrounding the GOC rises 1-2 km above sea level, lower tropospheric flow over the NAM geographical domain is most important over the GOC, surrounding coasts, SMO and Peninsular Range foothills, and the low deserts of northwest Mexico and southwest United States.

Using rawinsonde data from the United States, Mexico, and countries south of Mexico, Douglas et al. (1993) computed the mean July mid-tropospheric dewpoints and atmospheric flow for an 11-year period (1979-1989) (Fig. 2). Atmospheric flow at 500 hPa (Fig. 2a) is dominated by the westward extension of the southeast United States subtropical high centered over eastern New Mexico and north central Texas. This pattern

results in broad easterlies across much of eastern and central Mexico, and south-southeasterlies over northwest Mexico and Arizona. The southeast United States subtropical high still dominates atmospheric flow at 700 hPa (Fig. 2b), though the pattern is shifted farther east. This eastward displacement results in broad southeasterly flow across all of Mexico, except for northwest regions where the flow is southerly. It is interesting to note that at both levels, drier air is advected westward from the Gulf of Mexico and regions of maximum dewpoints are primarily west of the Continental Divide. From this, Douglas et al. (1993) suggest that mid-tropospheric moisture west of the SMO may be due to vertical transport from low-levels by convection and/or afternoon upslope mountain circulations – a theory also suggested by Stensrud et al. (1995).

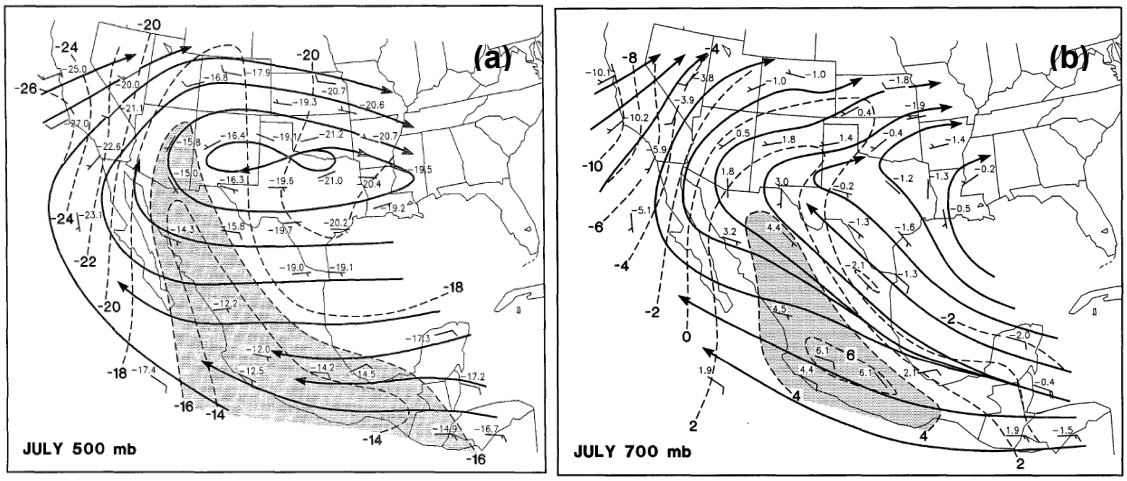


Figure 2: Mean winds, streamlines, and dewpoint (°C) analysis at (a) 500 hPa and (b) 700 hPa for July. Means are for 1200 UTC data for the 11-year interval 1979-1989. Areas with dewpoints greater than (a) -16°C and (b) 4°C are shaded. From Douglas et al. (1993) Fig. 8c and Fig. 10.

Following the SWAMP 1990 field campaign (10 July – 15 August), Douglas (1995) analyzed the lower tropospheric flow over northwest Mexico and southwest United States

using data from nine pilot balloon sites in Mexico and one in Yuma, AZ (Fig. 3). Mean lower tropospheric flow surrounding the northern and central GOC at 1200 UTC (0600 LST) was dominated by south-southeasterly flow that paralleled the coasts and SMO axis with a wind speed maximum centered over the northern half of the gulf (Fig. 3a). This low-level jet (LLJ hereafter) was present approximately 75% of the mornings at Yuma during SWAMP 1990 with the strongest winds located between 300-600 m and maximum speeds reaching 20 m $s^{-1}$. Further analysis by Douglas et al. (1998) using data collected during a short field campaign in 1995 suggests that the LLJ is strongest at 0100 LST along the eastern shores of the northern gulf. At 0000 UTC (1800 LST), mean south-southeasterly flow still dominated areas immediately over the northern and central GOC (Fig. 3b), but due to daytime heating, strong local sea breezes and upslope flow along the coasts and foothills replaced the weak downslope flow during the morning hours. In utilizing a PSU (Pennsylvania State University)-NCAR mesoscale model, Stensrud et al. (1995) was able to reproduce many of these low-level circulation patterns.

While it is likely that mean south-southeasterly flow over the northern gulf at both 0000 and 1200 UTC is largely a result of topographic channeling, albeit much stronger in the morning (Badan-Dangon et al. 1991, Douglas et al. 1993, Douglas 1995, Stensrud et al. 1995, Anderson et al. 2000a), circulation patterns over the southern gulf seem to be affected to a greater extent by the turning of the wind around the southern tip of Baja California – from northwest flow over the Pacific Ocean to south-southeast flow over the central and northern GOC. This flow feature is shown in greater detail at the surface with QuikSCAT wind data over the oceans from Bordoni et al. (2004).

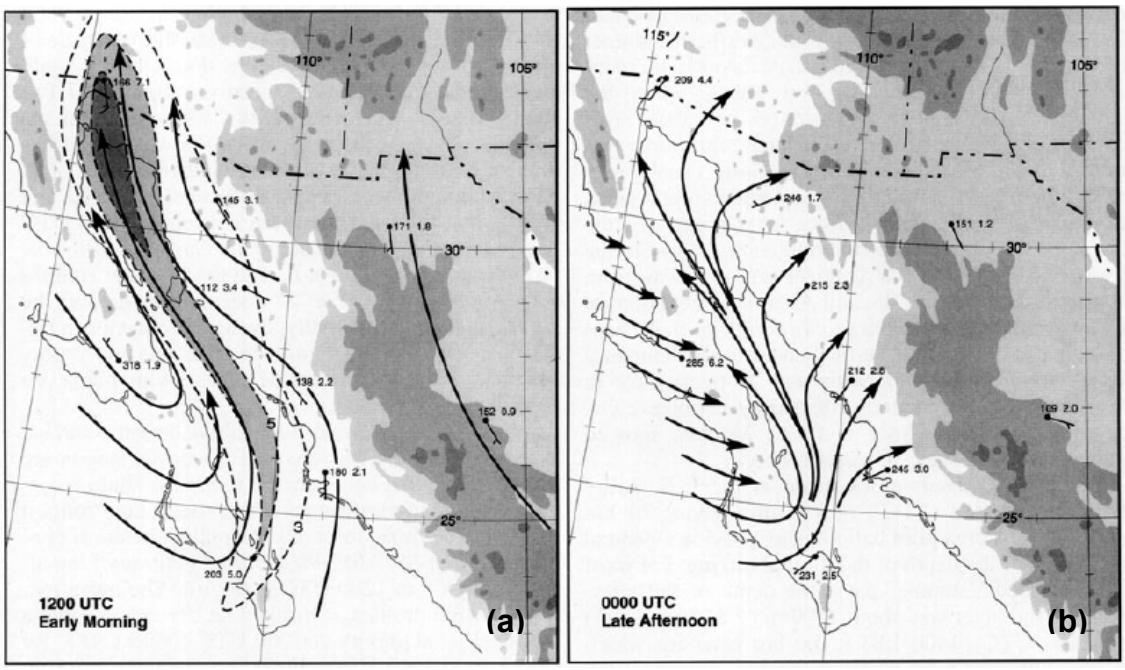


Figure 3: Mean pilot balloon winds and streamline analyses at 450 m AGL at 1200 (a) and 0000 (b) UTC. Isotachs with contours at 3, 5, and 7 m $s^{-1}$ are also shown at 1200 UTC. Jet core is also shaded. Wind direction and speed is plotted next to each station in the form: *ddd f.f* where *ddd* is the direction in degrees and *f.f* is the speed in meters per second; *xx* denotes missing data. Shading of topography (light, intermediate, and darkest) indicates elevations above 915 m, 1830 m, and 2745 m, respectively. From Douglas (1995) Fig. 4.

Although focused on the low deserts of Arizona and northwest Mexico and not the GOC, Douglas and Li (1996) computed the mean surface flow using surface observations collected during the SWAMP 1993 field campaign (27 July – 14 August) (Fig. 4). Not surprisingly, the basic diurnal mountain circulations discussed by Douglas (1995) along the GOC were also observed over Arizona with downslope conditions at 1200 UTC (Fig. 4a) and upslope conditions at 0000 UTC (Fig. 4b). These patterns generate confluence and convergence in the morning and generate diffluence and weak divergence in the evening over the Colorado River Basin and low deserts. The authors suggest that this diurnal cycle may help explain the trend for nighttime thunderstorms over the Arizona

low deserts. At both times, there is significant cyclonic curvature centered near the California/Arizona border. This feature is associated with the well-documented southwest United States thermal heat low, which is due to extreme daytime desert temperatures. Also observable at 925 or 850 hPa from Douglas and Li (1996) (not shown), the heat low does not expand above 700 hPa (Rowson and Colucci 1992).

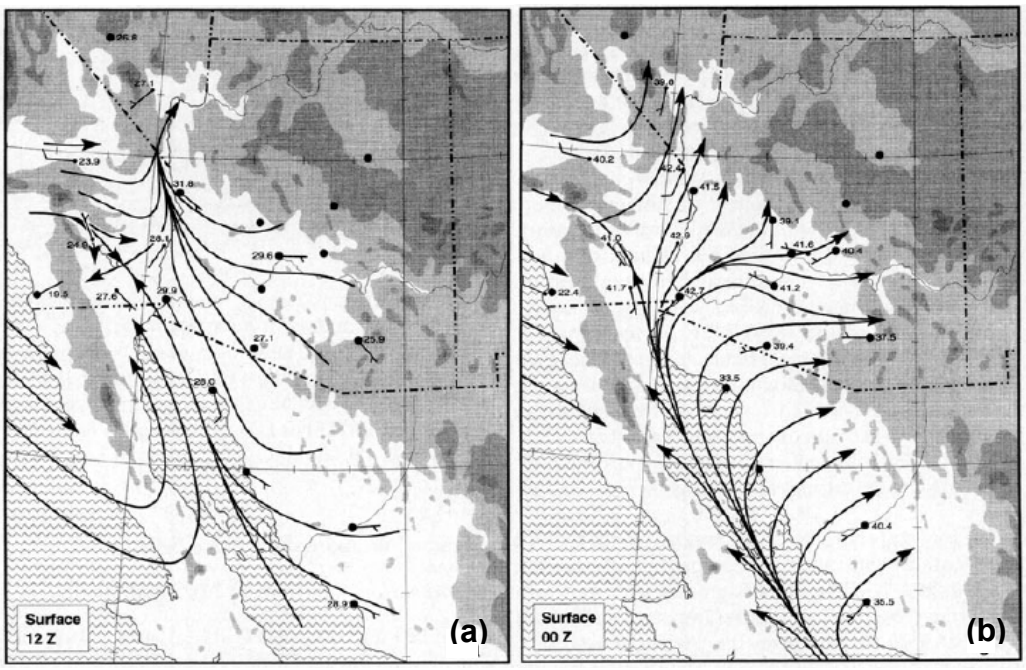


Figure 4: Mean streamlines and isotherms (°C) for the period 28 July – 14 August 1993, based on selected low-altitude surface observations. Full barb is 5 m $s^{-1}$ and half barb is 2.5 m $s^{-1}$. Temperatures (°C) are plotted: (a) 1200 UTC streamlines and (b) 0000 UTC streamlines. From Douglas and Li (1996) Figs. 2a and 2c.

Considering thermal patterns over the NAM geographical domain, Douglas (1995) found that within the mean flow surrounding the GOC during SWAMP 1990, there is increasing anticyclonic vorticity with height over northern regions and increasing cyclonic vorticity with height over southern regions (not shown). Thus, from the quasi-geostrophic vorticity equation (Holton 1992), there exists a strong thermal gradient along

the GOC with relatively warm air to the north and relatively cool air to the south. In addition, Douglas (1995) showed that based on 11 years (1979-1989) of rawinsonde observations from Tucson and Mazatlan, Sinaloa, the thermal gradient (Tucson minus Mazatlan mean July temperature) is greatest at the surface and decreases to near zero by 500 hPa, agreeing with the modeling results of Stensrud et al. (1995). It is the intensification or disturbance of this thermal and hence pressure gradient that was first used to argue the triggering mechanism for gulf surges (Hales 1972, Brenner 1974).

### 2.2 Brief Gulf Surge Overview

Four independent case studies presented by Hales (1972) using surface, rawinsonde, and satellite data provided an in-depth observational first-look at what are now readily referred to as gulf surges. In noting the terrain features surrounding the GOC (Peninsular Range to the west and SMO to the east), Hales (1972) suggested that a natural channel (~200 miles in width) existed in which moisture-laden air from the tropical Pacific Ocean could propagate northward into the low deserts of the southwest United States and northwest Mexico during the NAM. Due to decreased frictional effects over water, gulf surges are strongest over the GOC and follow the path of least resistance, thus continuing most forcefully up the Colorado River Basin upon reaching the northernmost extent of the GOC (Hales 1972, Brenner 1974). Observationally, gulf surges have been found to traverse the entire length of the gulf in 17 hours or at a speed of approximately 30 kts (~15.4 m $s^{-1}$) (Hales 1972). However, gulf surges appear to quicken when passing through the northern gulf, and fan out in an arc-like fashion and slow over the deserts

upon exiting the channel provided by the terrain surrounding the GOC (Brenner 1974) (Fig. 5). Further modeling studies by Stensrud et al. (1997) simulate gulf surge propagation speeds of 10-23 m $s^{-1}$, typically slowing during the afternoon hours when diurnal heating is greatest.

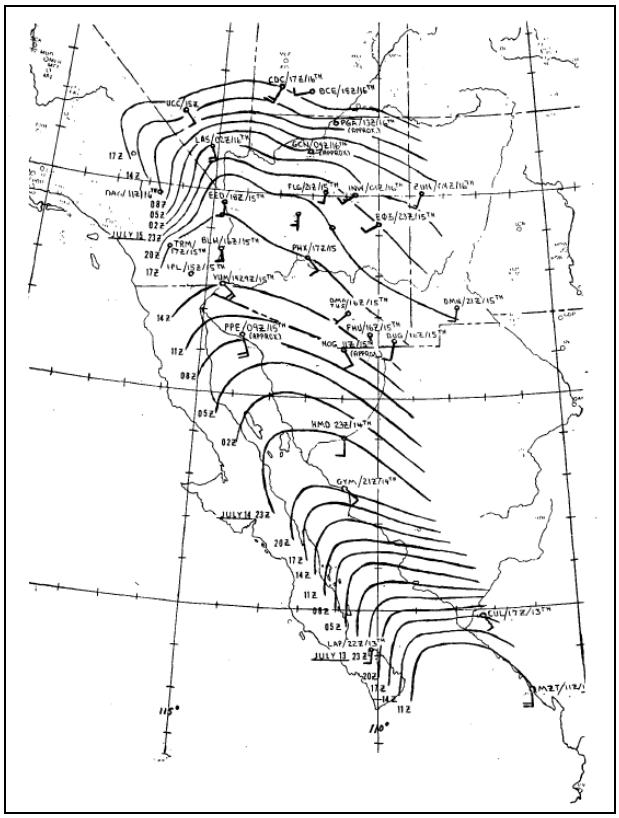

Figure 5: Isochrones (3 h intervals) of passage of leading edge of the moisture surge (13 July – 16 July 1972). From Brenner (1974) Fig. 19.

Despite little high resolution upper air observations in time and space, Hales (1972) and Brenner (1974) noted several common characteristics associated with gulf surges:

- Gulf surge onset is accompanied by a significant decrease in surface temperature, an increase in sea-level pressure, an increase in surface dewpoint temperature

(relative humidity) relative to the changing air masses, a surface wind shift with an increased southerly component, and an increased low-level cloudiness.

- Atmospheric modifications associated with gulf surges (cooling and moistening) are greatest just above the surface and decrease in intensity with height.
- Gulf surges are strongest at their onset, but steadily decrease in intensity once having fanned out over the low-deserts of Arizona.
- Deep gulf surges result in increased convective activity across much of Arizona.

Many of these characteristics provided the basis for surge identification criterion in other studies (Stensrud et al. 1997, Anderson et al. 2000b, Fuller and Stensrud 2000, Douglas and Leal 2003, Higgins et al. 2004). Stensrud et al. (1997), Fuller and Stensrud (2000), and to a certain extent Higgins et al. (2004) identified surges by noting increases in hourly surface dewpoint temperature that persisted for several days above a certain threshold at Yuma and/or Tucson, as well as requiring southerly surface flow with speeds above a certain threshold at surge onset. Anderson et al. (2000b) identified surges by noting modeled southerly or southeasterly winds over Empalme, Sonora for periods longer than 24 hours followed by a large 24-hour increase in meridional velocity over Puerto Peñasco, Sonora. However, in using rawinsonde observations from Empalme over a nine-year period (1980-1988), Douglas and Leal (2003) developed the most complex identification scheme that required an increase in integrated surface-to-850 hPa moisture transport greater than 50 kg $m^{-1}$ $s^{-1}$, a decrease in temperature at 925 hPa greater than 3°C, and an increase in the surface pressure of more than 3 hPa.

## 2.3 Initiation Mechanisms and Associated Synoptic Circulations

In studying satellite photographs, Hales (1972) discovered a relationship between large cloud masses over the central and/or southern GOC and subsequent surges of moisture, implying a disturbance in the low-level thermal-dynamic (pressure) balance along the GOC. Strengthening domes of higher pressure over the central and southern gulf related to convective activity, evaporational cooling from precipitation, and/or differential heating in and outside the cloud were suggested as mechanisms for such a disturbance. Intensification of the southwest United States thermal heat low can also work in combination with this process to disrupt the normal thermal gradient along the GOC. The amplification of the along-gulf pressure gradient thus provides the impetus necessary to advect moisture northward, analogous to a very strong sea breeze (Hales 1972, Brenner 1974). The question naturally arises, however, as to what causes the cloud masses to develop – an issue that has received much attention.

Hales (1972) proposed two gulf surge types. The first navigates the entire length of the gulf, is relatively deep (8,000-12,000 ft), and is triggered by a thick cloud canopy near the mouth of the gulf. This cloud canopy can be associated with a tropical disturbance (i.e. easterly wave, tropical storm, or hurricane) that generally propagates from west-central Mexico or the eastern Pacific Ocean west to the south of Baja California. The second is confined to the northern GOC, is relatively shallow (3,000-5,000 ft), and is triggered by a cloud mass over the central or southern GOC. This cloud mass can be associated with a mesoscale convective system (Adams and Comrie 1997)

that propagates from the SMO west to the central gulf. Since this taxonomy, other studies have primarily focused on gulf surges and their relationship to tropical disturbances, although it should be noted that not all easterly waves, tropical storms, or hurricanes affecting the NAM geographical domain are followed by a gulf surge (Stensrud et al. 1997, Fuller and Stensrud 2000).

Stensrud et al. (1997), utilizing 32 successive 24-hour simulations (11 July – 11 August 1990) generated by the PSU-NCAR mesoscale model, produced 800 hPa time-longitude Hovmöller diagrams of v-component winds south of 30°N to investigate the relationship between gulf surges and easterly waves. The authors found the existence of simulated westerly propagating tropical disturbances passing over Mexico approximately every six days at 8 m $s^{-1}$ with wavelengths from 2700-4100 km. These waves were most prominent at latitudes below 20°N and maintained a horizontal southwest to northeast orientation. When focused on 19°N, there was a strong relationship between easterly wave passages at 110°W and observed increases in southerly wind at Yuma approximately one day later. However, this apparent relationship did not explain gulf surge strength.

To investigate circulation features that may be related to gulf surge strength, Stensrud et al. (1997) also generated a 300 hPa time-longitude Hovmöller diagram of v-component winds at 40°N. From this, the authors concluded that strong simulated gulf surges only occurred when a midlatitude trough traversed the western United States a day or two before the passage of a tropical disturbance over the same longitudes. Weak gulf surges

were not accompanied by such a pattern. Hence Stensrud et al. (1997) proposed a conceptual synoptic model necessary for the occurrence of strong gulf surges. A midlatitude trough propagates across the western United States resulting in increased subsidence and a strong low-level stable layer over the GOC. Soon after, an easterly wave propagates over west-central Mexico resulting in increased convective activity due to associated convergence and vertical motion. Finally, low-level convective outflows or easterly wave convergence initiates the gulf surge, resulting in a northward propagation that decreases in intensity and speed upon entering the low deserts of Arizona.

In an attempt to validate the modeling results of Stensud et al. (1997), Fuller and Stensrud (2000) examined hourly surface data at Yuma and European Centre for Medium-Range Weather Forecasts (ECMWF hereafter) 850 hPa meridional wind reanalysis data during July and August of 1979-1993, excluding the year 1992 (14 years). During this period, 85 gulf surges were identified at Yuma. Also during this 14-yr period, 850 hPa time-longitude Hovmöller diagrams were constructed from 10°N-22.5°N and 65°W-130°W using the ECMWF data. From these diagrams, 85 westward propagating easterly waves were identified, which typically propagated at 6-8 m $s^{-1}$ and had wavelengths of 2500-3800 km, in relative agreement with Stensrud et al. (1997). When comparing these phenomena, it was found that out of the 85 gulf surge events at Yuma, 63 (~74%) were preceded by the passage of an easterly wave at 110°W within three days, thus signifying an important relationship. However, when identifying midlatitude troughs over the western United States using a 200 hPa time-longitude Hovmöller diagram at 40°N, it was found that only 15 (~18%) of the 85 gulf surge events

at Yuma were preceded by a midlatitude trough within three days of an easterly wave passage. Eleven of these events were associated with strong surges and the other four associated with weak surges. Although there seemed to be a relationship between midlatitude trough passage and gulf surge strength, the occurrence of such a phase relationship occurred infrequently.

Analysis by Douglas and Leal (2003) using rawinsonde observations over the southwest United States and Mexico over a nine-year period (1980-1988) lent itself to a further understanding of the basic synoptic patterns associated with gulf surges, including easterly waves. Mean anomaly (from July-August climatological profiles) streamline composites based on 38 identified strong gulf surges were generated at 925 hPa (Fig. 6) and 600 hPa (Fig. 7) from two days before to two days after gulf surge passage at Empalme. At 925 hPa (Fig. 6), the most important changes as noted by the authors include a marked wind shift from northwesterly to southeasterly over the GOC and replacement of a cyclonic anomaly south of the gulf with an anticyclonic anomaly after surge onset. Consistent southeasterly flow over the GOC after gulf surge onset is argued by Anderson et al. (2000b), using a nested regional modeling system, to be the result of low-level geostrophic flow around the cyclonic anomaly to the south and west of Baja California. In addition from Fig. 6, there are generally positive temperature and negative specific humidity anomalies north of Empalme prior to surge onset, and negative temperature and positive specific humidity anomalies after surge onset.

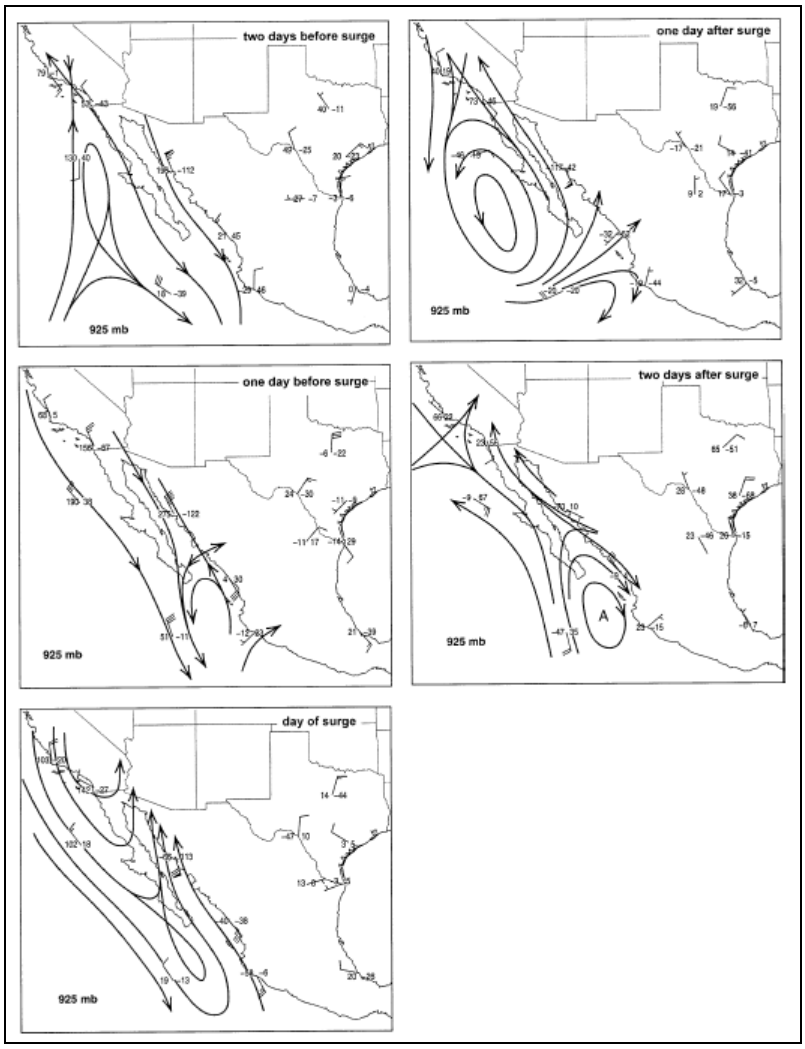


Figure 6: Anomaly streamline analyses at 925 hPa based on radiosonde data composited with respect to the surge data at Empalme. The plotting convention is one full shaft is 0.5 m $s^{-1}$ and one flag is 2.5 m $s^{-1}$. Numbers to the left of station are temperature anomalies (from long-term mean) in hundredths of a degree Celsius; numbers to right are specific humidity anomalies (from long-term mean) in hundredths of a gram per kilogram. Only winds (streamlines) are analyzed. From Douglas and Leal (2003) Fig. 11.

At 600 hPa (Fig. 7), the most important changes include the progression of an anticyclonic anomaly from northwest Mexico to Arizona, the westward movement of a cyclonic anomaly over Mexico to the tropical Pacific Ocean south of Baja California, and the development and eventual stationary presence of a cyclonic curvature anomaly oriented southwest to northeast over north-central Mexico and west Texas. The

westward progression of a cyclonic anomaly from Mexico to the oceans is analogous to the tropical disturbance/easterly wave phenomenon discussed by Stensrud et al. (1997) and Fuller and Stensrud (2000). Interestingly, Douglas and Leal (2003) discovered 16 of the 38 identified gulf surges during the study period were related to tropical storms or hurricanes. Temperature and specific humidity anomalies at 600 hPa are much weaker than at 925 hPa, in basic agreement with Douglas (1995).

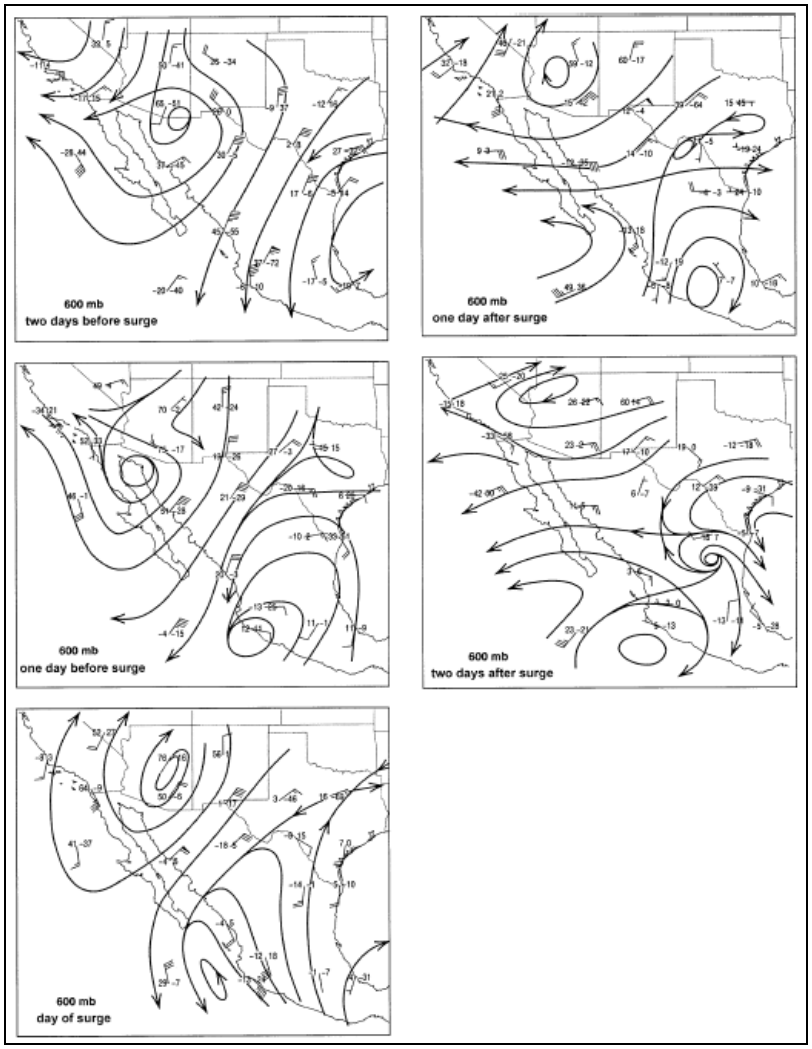


Figure 7: Same as in Fig. 6 but at 600 hPa. From Douglas and Leal (2003) Fig. 12.

Douglas and Leal (2003) also generated a mean anomaly streamline composite at 200 hPa for only the day of surge passage at Empalme (not shown). At this level, the authors note the most important feature consists of a southwest to northeast tilted trough, whose axis stretches from southern Baja California to west Texas. This results in increased easterlies (westerlies) across the southern United States (northern and central Mexico). Interestingly, though, there has been relatively little attention given to anomalous upper-tropospheric synoptic patterns in the literature as they relate to the NAM and gulf surges. However, upper-tropospheric phenomena during the NAME were noted through the issuance of daily forecasts and discussions for the NAM region by the NAME Forecast Operations Center (FOC hereafter) located in Tucson (Joint Office for Science Support 2005) (see Section 3.2 for further discussion). Among other features discussed in these reports, special attention was given to the location and propagation of inverted troughs, or tropical upper-tropospheric trough (TUTT hereafter) lows.

As a means to better understand TUTT lows over the western north Pacific Ocean, Kelley and Mock (1982) generated a composite based on 117 identified lows over four summers (1967, 1969-1971) using rawinsonde data from four island stations. Examining north-south and east-west cross sections through the composite low's center, the authors found that the feature tilts to the north and east with height and is primarily constrained between 700 and 100 hPa, with maximum relative vorticity values at 200 hPa. Maximum anomalous cooling occurs to the north of the low center at 300 hPa and extends weakly to the surface, whereas maximum anomalous warming occurs in line with the low center at 125 hPa. Confined primarily between 900 and 100 hPa, vertical motion is at its

maximum at 300 hPa. However, relative to the composite low's 200 hPa center, sinking motion and relatively little cloud cover accompany quadrants to the north and west, while rising motion and substantial cloud cover accompany quadrants to the south and east.

Several years later, Whitfield and Lyons (1992) conducted a case study of a quasi-stationary TUTT low over Texas during the summer of 1988. Interestingly, the authors found nearly identical TUTT low characteristics to those presented by Kelley and Mock (1982) using National Meteorological Center global gridded analyses from NCAR, daily rainfall data from 660 rain gauges, and satellite imagery provided by the National Oceanic and Atmospheric Administration (NOAA hereafter). In addition, Whitfield and Lyons (1992) found that the Texas TUTT low moistened the troposphere as it strengthened and was responsible for significant rainfall over much of the state. Of greater interest, though, the authors attributed the feature's initial vorticity source to the conservation of absolute vorticity, vorticity convergence along the TUTT low's axis, and positive vorticity advection from midlatitudes.

Preliminary examination of eleven TUTT cold lows over the NAM geographical domain during the 2004 NAME by Pytlak et al. (2005), however, suggested that such systems do not necessarily follow the synoptically driven vertical motion profiles proposed by Kelley and Mock (1982) and Whitefield and Lyons (1992). As TUTT lows interact with the NAM flow regime, Pytlak et al. (2005) proposed that in addition to the southeast quadrant, areas to the west of the low may play an important role in convective initiation and development. This is argued to be the case due to significant upper-level

divergence, and thus rising motion throughout the column, that can occur as TUTT lows interact with the southwest quadrant of the subtropical ridge to the north (not shown). In addition, the authors note that many of the TUTT lows affecting the NAM domain originate from the Gulf of Mexico. However, others originate in the midlatitude westerlies as short-wave troughs that propagate around the southeast United States subtropical high and become embedded within the tropical easterlies.

Complementing these results in a seemingly unrelated study, Thorncroft et al. (1993) used a baroclinic spectral model to describe in great detail two midlatitude baroclinic-wave life cycles, the first of which offers support for TUTT low initiation. Specifically, the authors found that southwest to northeast tilted eastward propagating midlatitude baroclinic systems that develop on the anticyclonic side of the jet stream tend to thin as they extend equatorward with time. In the decaying stage of these baroclinic waves, the thinning troughs can be cut-off across the southern United States as a closed cyclonic vorticity maximum south of the main baroclinic system, which can then serve as the initial starting point for a TUTT low.

### 2.4 Mean Gulf Surge Vertical Structure

Although case studies presented by Hales (1972) and Brenner (1974), along with the observational data collected during the SWAMP 1990 and 1993 field campaigns provided valuable insight into the structure of gulf surges, no mean vertical structure was proposed until the examination of rawinsonde data at Empalme by Douglas and Leal

(2003). Averaging the 0000 and 1200 UTC composites based on 38 strong gulf surges from 1980-1988, Douglas and Leal (2003) investigated the temperature, specific humidity, wind, and horizontal moisture flux profiles from two days prior to two days after surge onset at Empalme up to 500 hPa (Fig. 8).

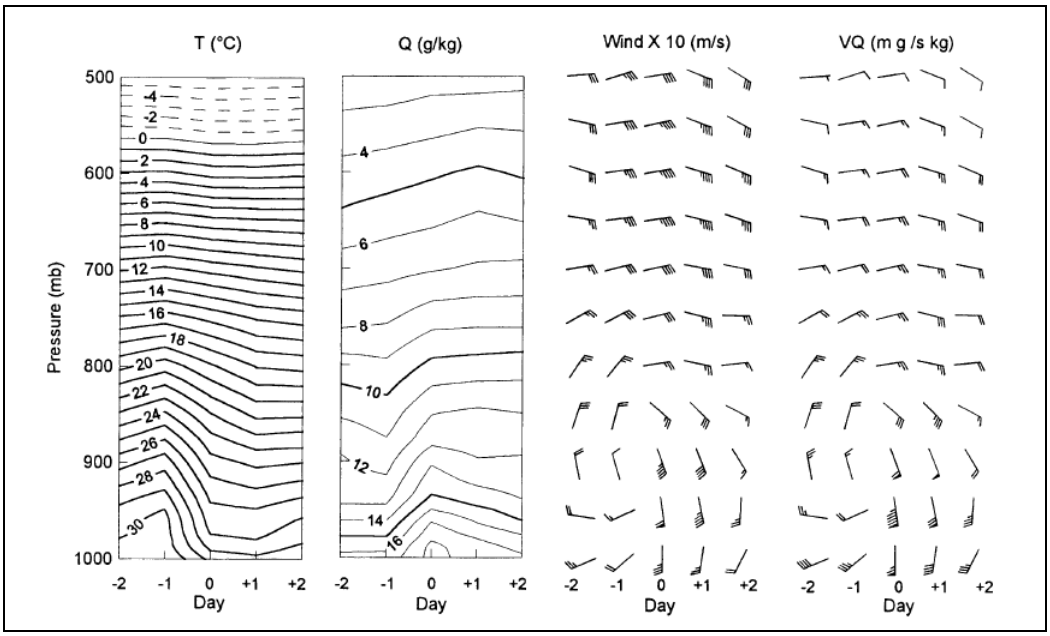


Figure 8: Time-pressure sections of the (a) temperature, (b) specific humidity, (c) wind, and (d) moisture flux at Empalme during the composite surge passage [(a)-(d) correspond to the panels from left to right]. Winds are plotted to enhance the signal; full barb is 1 m $s^{-1}$, half barb is 0.5 m $s^{-1}$. Contour interval for temperature is 1°C; for specific humidity it is 1 g $kg^{-1}$; for moisture flux one barb equals 10 m g $s^{-1}$ $kg^{-1}$; a flag is 50 m g $s^{-1}$ $kg^{-1}$. From Douglas and Leal (2003) Fig. 5.

From the time-pressure profiles in Fig. 8, the most distinct changes associated with gulf surge passage occur below 800 hPa, in agreement with Douglas (1995) and Stensrud et al. (1997). One day prior to surge onset, significant warming occurs in this layer (Fig. 8a) concurrent with slight decreases in specific humidity (Fig. 8b). Conversely, on the day of surge onset, significant cooling occurs in this layer concurrent with dramatic

increases in specific humidity. Whereas near surface wind speeds change little during the times examined most likely due to frictional effects, there is a strong wind shift from northerly to southerly at 900 hPa (Fig. 8c). Horizontal moisture flux patterns are similar to those of the wind field (Fig. 8d), but more intense at day zero and 950 hPa due to the multiplicative effects of increased specific humidity and southerly wind component.

The warming/cooling, drying/moistening, and wind shift tendencies associated with gulf surge passages, however, are better viewed through time-pressure anomaly (from July-August climatological values) profiles (Fig. 9). The pre-surge warming is stronger and deeper than the post-surge cooling, although the cooling effects seem to slope upward with time (Fig. 9a). Conversely, the post-surge low-level moistening is stronger than the pre-surge drying, but also slopes upward with time (Fig. 9b). This sloping feature is also evident in time-pressure potential temperature and static stability anomaly plots (not shown), implying a post-surge dome of cool air capped by a stable layer as noted by the authors. The wind (Fig. 9c) and horizontal moisture flux (Fig. 9d) anomaly patterns are qualitatively similar to those in Fig. 8. However, the gulf surge associated wind shift (north to south) patterns occur to some extent from the surface up to 800 hPa rather than at just one level. It is important to note that Douglas and Leal (2003) reiterate that these results are based on composites and therefore individual gulf surge events may deviate significantly from the patterns discussed here.

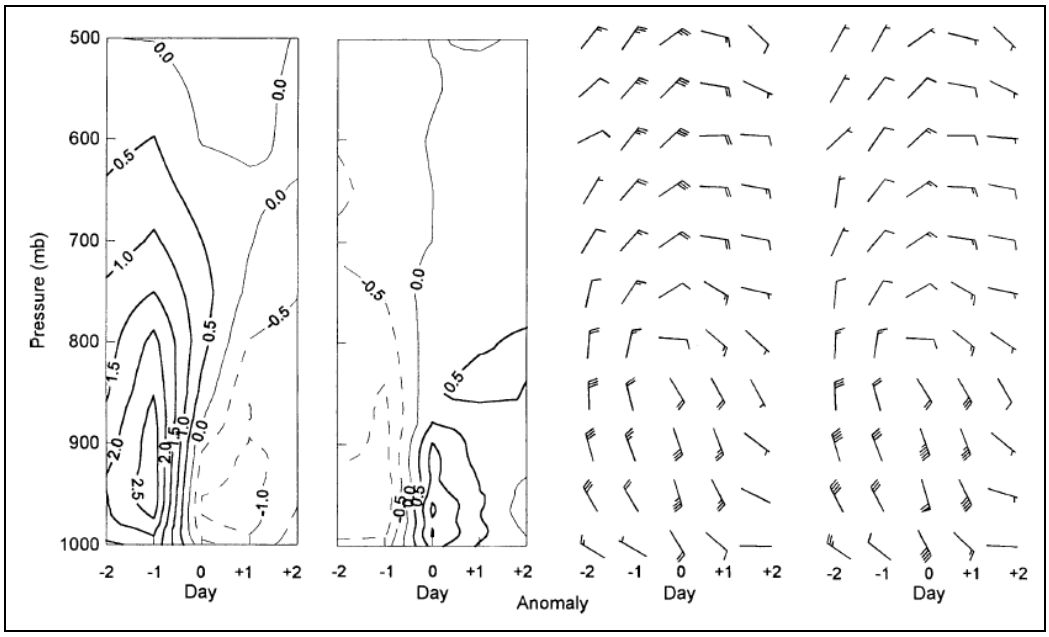


Figure 9: Same as in Fig. 8 except all figures are anomalies from the Jul-Aug climatological profiles, and contour intervals are 0.5°C for temperature and 0.5 g $kg^{-1}$ for specific humidity. Positive contours are solid; negative contours are dashed. From Douglas and Leal (2003) Fig. 6.

## 2.5 Precipitation Tendencies

Early gulf surge studies (Hales 1972, Brenner 1974) suggested that convective activity, and thus precipitation, increased upon passage of a gulf surge. This theory seems qualitatively acceptable since the importance of moisture in thunderstorm development is well-documented during the NAM (McCollum et al. 1995). However, Douglas and Leal (2003) provided one of the first quantitative examinations of this proposed relationship. Using rainfall data from the Mexican climatological network, Douglas and Leal (2003) calculated the daily mean rainfall keyed to surge onset at Empalme for the states of Sonora and Sinaloa, given approximately 60 stations per state. The authors found that mean rainfall amounts increased 1-2 days before surge onset in

Sinaloa, but coincided with surge onset in Sonora. However, rainfall increased only 15-30% after gulf surge onset at Empalme when compared to periods long before and after the event. A more robust finding was that relatively dry conditions before surge passage were followed by nearly a doubling of precipitation values after onset. Hence, these quantitative results seem to validate the conceptual relationship argued by Hales (1972) and Brenner (1974) between gulf surge onset and precipitation along the eastern shores of the GOC.

Complementing the results of Doulgas and Leal (2003), Gochis et al. 2004 used precipitation data from the NAME 2003 Event Rain Gauge Network (NERN) to investigate gulf surge-related precipitation patterns from July-September. Having recognized nine gulf surge passages at Guaymas, Sonora during this period using subjective identification criterion proposed by forecasters with the National Weather Service (NWS hereafter), the authors showed evidence of a northward propagating region of precipitation (fraction of wet days) along the east coast of the GOC in association with gulf surges. Interestingly, however, this precipitation pattern seemed to be confined to lower elevations well below the high terrain of the SMO.

Examination of the relationship between gulf surges and precipitation by Higgins et al. (2004) challenged the basic premise that all gulf surges are related to enhanced precipitation. Using hourly surface observations from Yuma and Tucson along with precipitation data from the Climate Prediction Center's Unified Raingauge Database and additional observations from the Mexican Weather Service, the authors identified four

different types of gulf surges – strong, weak, wet, and dry. The strength of the surge depended on 25-hour running mean dewpoint temperatures increasing (strong) or decreasing (weak) during a three-day period after onset, whereas the wetness of the surge depended on positive (wet) or negative (dry) precipitation anomalies during a five-day period after onset over an area covering much of eastern Arizona and western New Mexico (32°-36°N, 112.5°-107.5°W). From these definitions, 57% (43%) of all identified surges were strong (weak) and 54% (46%) were wet (dry) at Yuma, and 59% (41%) of all identified surges were strong (weak) and 63% (37%) were wet (dry) at Tucson during July-August 1977-2001. Obviously, not all gulf surges were accompanied by enhanced rainfall.

Geographic composite maps were generated showing the progression of precipitation anomalies across the United States and Mexico before and after all, strong, weak (Fig. 10), wet, and dry gulf surge onsets at Yuma. When considering all gulf surges (Fig. 10a), there is a distinct southeast to northwest progression of positive precipitation anomalies along the east coast of the GOC and into the southwest United States. Prior to surge onset at Yuma, northern Mexico is dominated by negative precipitation anomalies, while southern Mexico is dominated by positive precipitation anomalies. By surge onset, the positive precipitation anomalies over southern Mexico progress northwestward to northwest Mexico and continue into Arizona two to four days later. The authors also note that this overall pattern is enhanced for strong surges (Fig. 10b) and suppressed for weak surges (Fig. 10c). Composites for wet surges (not shown) closely resemble those for strong surges, except that positive precipitation anomalies are stronger and more

extensive, whereas composites for dry surges (not shown) are overwhelmed by negative precipitation anomalies across much of the NAM geographical domain.

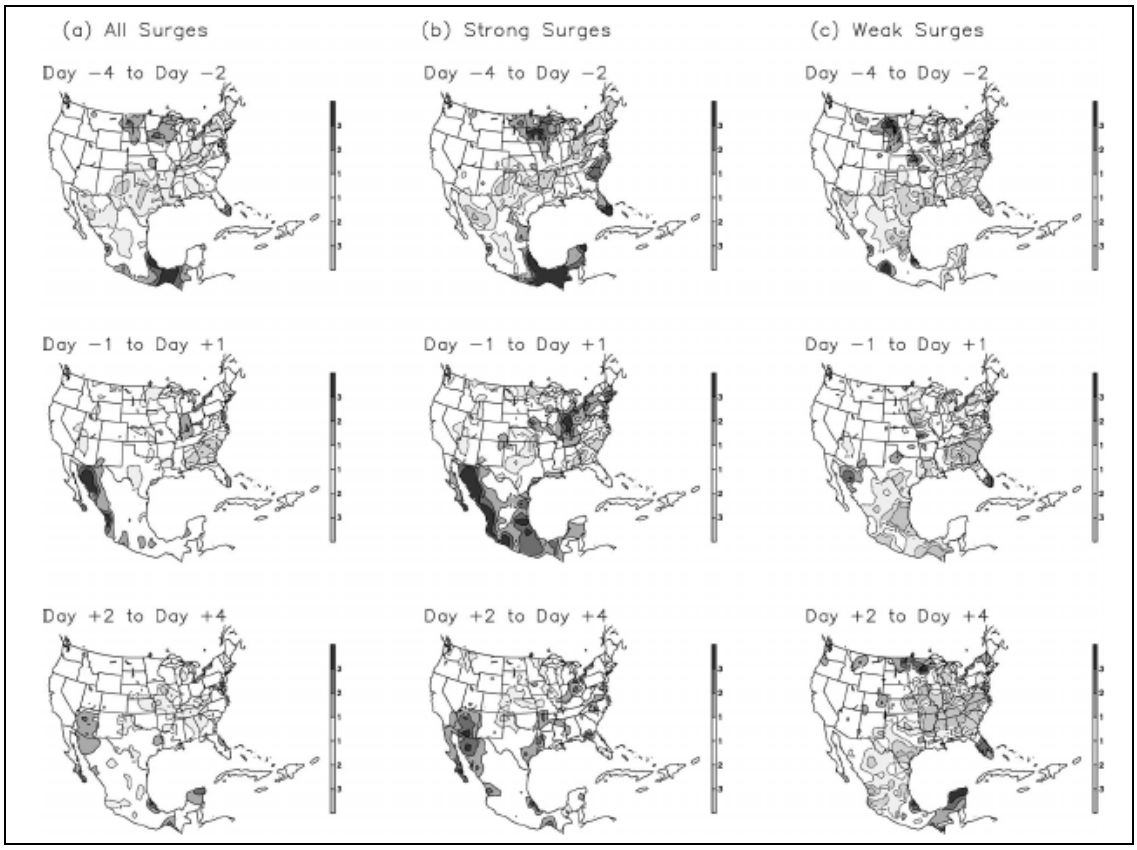


Figure 10: Composite evolution of precipitation anomalies (mm) for (a) all, (b) strong, and (c) weak surges keyed to Yuma. Day 0 is the onset date of the surges at Yuma. The average period relative to onset is indicated on each panel. The contour interval is 1 mm day$^{-1}$, the zero contour is omitted for clarity, and values greater than 1 mm day$^{-1}$ (less than -1 mm day$^{-1}$) are shaded dark (light). From Higgins et al. (2004) Fig. 6.

Since gulf surge-related precipitation is not strictly dependent upon surge strength, Higgins et al. (2004) examined NCEP-NCAR reanalysis winds to determine if large-scale circulation features explained differences between wet and dry surge precipitation patterns. Having generated a composite streamline and vector wind anomaly plot at 700 hPa across the NAM geographical domain (not shown), the authors proposed a

conceptual model at this level to help explain these differences (Fig. 11). Both wet and dry surges are accompanied by a low pressure system centered to the south and/or west of Baja California as a result of westward propagating tropical disturbances (i.e. easterly waves) across Mexico. Geostrophic flow around the cyclonic circulation center transports moist southerly flow across much of the GOC and western Mexico. Thus, it is primarily the midlatitude high pressure system's location that defines whether a surge is wet or dry. For wet surges, the anticyclonic axis is aligned to the east of Arizona/New Mexico over the Upper Midwest. Hence, southerly geostrophic flow around the west side of this high enhances the flow over the GOC associated with the easterly wave, allowing deep plumes of moisture to penetrate well into the low desert regions resulting in increased convective activity. For dry surges, the anticyclonic axis is aligned to the west of Arizona/New Mexico over the Pacific Northwest. Hence, northerly geostrophic flow around the east side of this high suppresses the southerly flow over the GOC associated with the easterly wave and caps the atmosphere from any convective development despite abundant low-level moisture.

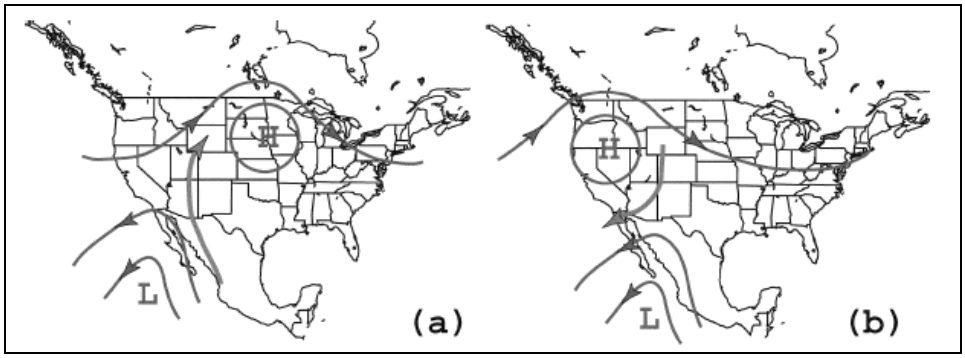


Figure 11: Schematic mapping of the typical 700-hPa circulation features (heights and winds) that accompany (a) wet and (b) dry surges keyed to Yuma. From Higgins et al. (2004) Fig. 13.

## 2.6 Gulf Surge Dynamical Mechanisms

The dynamical mechanism(s) for which gulf surges propagate northward along the GOC has received little attention in the literature, especially from an observational standpoint. This is most likely due to the fact that reliable high resolution data has been unavailable across the NAM geographical domain except for brief periods during the SWAMP 1990 and 1993 field campaigns. Although gulf surges were noted by Fuller and Stensrud (2000) as coastally trapped disturbances, gulf surge dynamical mechanisms are not currently well-understood. However, Zehnder (2004) systematically examined the validity of four possible linear gulf surge dynamical mechanisms through a series of dynamical arguments and modeling experiments. The author proposed four mechanisms including gravity currents, ageostrophic isallobaric flow, Rossby edge waves, and barrier Kelvin waves.

Gravity currents associated with cool convective downdrafts or outflow boundaries can propagate away from thunderstorms assuming a significant density contrast across the leading edge. Hence, Zehnder (2004) showed that a 4 hPa pressure difference along the initial front would result in a gravity current propagation speed of 20 m $s^{-1}$. Although this value seems to qualitatively agree with gulf surge propagation speeds, the author notes that gravity currents are subject to Coriolis deflections if the current's traveled distance is greater than the Rossby radius of deformation. Hence, assuming a Rossby radius of deformation of 320 km, this mechanism may explain gulf surges that initiate

along the northern GOC due to mesoscale convective system outflows, but does not help to explain gulf surges that initiate near the mouth of the GOC.

Ageostrophic isallobaric flow is possible when the geostrophic balance along the GOC is disrupted by the passing of an easterly wave across Mexico. Using the horizontal momentum equations on an *f*-plane and making multiple simplifying assumptions, Zehnder (2004) conducted a scale analysis of the ageostrophic wind component to discover an isallobaric wind slightly less than 2 m $s^{-1}$, or significantly slower than observed gulf surge propagation speeds. Thus, it is very unlikely that this dynamical mechanism can be used to explain northward propagating gulf surges.

In order to investigate the proposed edge trapped gulf surge mechanisms, Zehnder (2004) notes that Rossby edge waves propagate within potential vorticity gradients generated by the terrain surrounding the GOC whereas barrier Kelvin waves must be blocked by the topography. This contrast may be examined by noting the orientation of isentropic (potential temperature) surfaces relative to the SMO and Peninsular Range. For Rossby edge waves, isentropes follow the curvature of the surface and are tightly packed near the summits, and for barrier Kelvin waves, isentropes intersect the surface.

With this is mind, Zehnder (2004) conducted modeling studies using a shallow water model to discuss Rossby edge waves and a two-layer channel model to discuss barrier Kelvin waves. Both models included idealized topography profiles of the SMO and Peninsular Range. From these simulations, the author found that the terrain-induced

potential vorticity gradients along the SMO provided the conditions necessary to support Rossby edge waves that resembled gulf surges. The potential vorticity gradient along the Peninsular Range tends to slow the waves, but northward propagation still results as a vortex near the mouth of the GOC moves to the left of the primary potential vorticity gradient. When considering barrier Kelvin waves, the simulated vortex located against the SMO mountain barrier seemed to support self-induced propagation, but the inertial stability of the original flow hindered cross-isobaric motion, characteristic of such a phenomenon. In addition, flow patterns characteristic of gulf surges were located along the mountain barrier and not over or nearby the GOC. From these results, barrier Kelvin waves appear to be an unrealistic mechanism for gulf surges to propagate northward whereas Rossby edge waves seem probable.

Other nonlinear dynamical mechanisms or a combination of those discussed here may also be linked to gulf surge propagation. A time-height profile of virtual potential temperature of a coastally trapped disturbance along the California coast from Ralph et al. (1998) shows an initial front-like structure, similar to that of gulf surges as discussed by Brenner (1974). Using a 3D hydrostatic model, Skamarock et al. (1999) showed that these same phenomena initiate with impinging flow along the coast, thus deepening the marine layer. This layer progresses northward as a Kelvin wave, which may later transition into an atmospheric bore or gravity current. Further observational studies conducted by Ralph et al. (2000) have likened coastally trapped disturbances along California to a mixed Kelvin wave-bore. Despite various gulf surge modeling (Stensrud et al. 1997, Anderson et al. 2000b) and observational compositing (Douglas and Leal

2003, Higgins et al. 2004) studies, it is not until high resolution observational data or mesoscale model output over the NAM geographical domain is examined on a case-by-case basis that the dynamical mechanism(s) of the gulf surge will be better understood (Zehnder 2004).

Therefore, the primary objective of this study is to use the high temporal and spatial observational data collected during the 2004 NAME field campaign to attempt to describe in unprecedented detail the vertical/horizontal structure and dynamical mechanism(s) of gulf surges. Among many different analyses, case studies of two gulf surge events will be presented and discussed.

# CHAPTER 3

# THE NORTH AMERICAN MONSOON EXPERIMENT, DATA, AND ANALYSIS METHODS

## 3.1 NAME Primary Objectives and Structure

The primary objective of the NAME is to determine the "sources and limits of predictability of warm season precipitation over North America, with emphasis on time scales ranging from seasonal-to-interannual" (NAME Science Working Group 2005). As an internationally coordinated CLIVAR-GEWEX (Climate Variability and Predictability World Climate Research Program-Global Energy and Water Cycle Experiment) project, a multi-scaled (tiered) structure was developed for the 2004 NAME field campaign to address several different scientific issues concerning the NAM.

Tier 1 (20°-35°N, 105°-115°W) encompasses the core NAM region. The primary objective within Tier 1 is to resolve with high temporal and spatial resolution the wind, temperature, and moisture fields surrounding the GOC. In addition, a better understanding of the synoptic and mesoscale circulation patterns associated with gulf surge events are of keen interest. Tier 2 (10°-40°N, 90°-120°W) encompasses a region including much of southwest North America and the eastern subtropical Pacific Ocean. The primary objective within Tier 2 is to explain and better understand phenomena that

are associated with intra-seasonal variability of the NAM. Finally, Tier 3 (5°-50°N, 75°-125°W) encompasses a region stretching from the United States-Canada border south to the northernmost reaches of South America, and includes vast extents of the Caribbean Sea and eastern tropical Pacific Ocean. The primary objective within Tier 3 is to explain and better understand continental-scale NAM variability by examining relations between warm season precipitation, associated circulation patterns, and dominant boundary forcing. The analyses and results of this study are almost exclusively focused within the Tier 1 domain and are aimed to better answer those questions associated with the core NAM region.

The primary extended observing period (EOP hereafter) associated with the NAME field campaign was conducted from 1 June – 30 September 2004, although many instrumentation platforms (i.e. ISS sites) were only in operation from 1 July – 15 August. In addition, some of these platforms were not fully operational until 7 July due to difficulties associated with transporting equipment and personnel across the United States-Mexico border. During 1 July –15 August, 20 intensive observing period (IOP hereafter) days were allocated over eight different time frames (IOP #1-8), each of which was intended to investigate different aspects of the NAM (Table 1). Observationally, IOPs were accompanied by an increased frequency of rawinsonde launches at numerous sites (Fig. 12) and NOAA P-3 aircraft flights in the vicinity of the GOC. A ninth IOP was conducted from 0600 UTC 17 September – 0000 UTC 20 September to investigate Hurricane Javier and a gulf surge, but was only accompanied by increased rawinsonde launches at a few sites.

Table 1: 2004 NAME field campaign IOP number, duration, and investigated phenomena.

| IOP # | DURATION | INVESTIGATED PHENOMENA |
|---|---|---|
| 1 | 1200 UTC 7 July - 0600 UTC 10 July | Monsoon onset |
| 2 | 0000 UTC 12 July - 0000 UTC 15 July | Tropical cyclone and gulf surge |
| 3 | 0000 UTC 20 July - 0000 UTC 23 July | Normal monsoon conditions |
| 4 | 0000 UTC 28 July - 0000 UTC 30 July | Suppressed monsoon conditions |
| 5 | 0000 UTC 1 August - 0000 UTC 2 August | Moisture flux, tropical jet, and MCS |
| 6 | 0000 UTC 3 August - 0000 UTC 4 August | Tropical wave and MCS |
| 7 | 1200 UTC 5 August - 1200 UTC 8 August | Inverted trough, MCS, and gulf surge |
| 8 | 1800 UTC 9 August - 0000 UTC 14 August | Tropical wave and backdoor cold front |

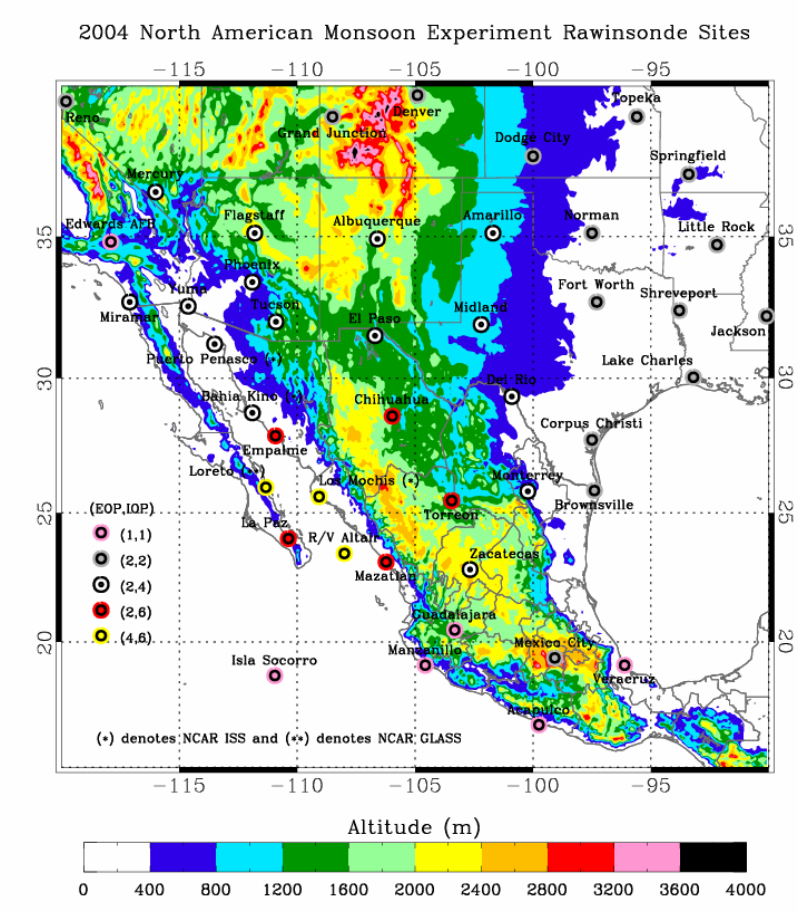


Figure 12: 2004 NAME EOP rawinsonde sites. Site color code refers to number of rawinsonde launches per day during the EOP and eight IOPs. Colored contours represent altitude above sea level (m).

### 3.2 Gulf Surge Identification

Although prior studies have used numerous methods to identify gulf surge onsets at various sites, one distinct advantage during the 2004 NAME EOP was the issuance of daily discussions and forecasts for the NAM region by the FOC, as briefly introduced in Section 2.3. Hence, FOC forecasters noted gulf surge events in the Day Zero Discussions using all available data, including those collected near real-time in the field at the ISS sites. While gulf surge identification techniques will not be investigated or validated with this study, special observational focus will be given to a subset of those gulf surge periods identified by the FOC.

Two gulf surge events will be analyzed in this study, both of which were captured by IOPs. Initial onset of the first gulf surge (GS #1 hereafter) occurred on 13 July (IOP #2), whereas initial onset of the second (GS #2 hereafter) occurred on 21 July (IOP #3). It is important to note that GS #2 was followed by a stronger surge on 22 July, but is not analyzed in as great of detail within this report for reasons of brevity, and the author's desire to identify possible dynamical mechanisms. This task was made easier if the gulf surge was not closely preceded by other significant atmospheric phenomena, as was the 22 July surge by GS #2. In order to properly diagnose pre- and post- surge atmospheric conditions, analyses presented in this study will focus on periods ranging from three days prior to three days after the day of surge onset at Puerto Peñasco based on the times identified by the FOC. Thus, the period of interest for GS #1 was 0000 UTC 10 July – 0000 UTC 17 July and 0000 UTC 18 July – 0000 UTC 25 July for GS #2.

## 3.3 NCAR ISS and GLASS Rawinsonde Sites

Maintained by NCAR, three ISSs (Puerto Peñasco, Sonora, Bahia Kino, Sonora, and Los Mochis, Sinaloa) and one Global Positioning System (GPS hereafter) Loran Atmospheric Sounding System (GLASS hereafter) (Loreto, Baja California Sur) were deployed during the NAME EOP from 1 July – 15 August (Fig. 12). The ISS consisted of a GPS balloon-borne atmospheric rawinsonde system, a 915 MHz Doppler clear-air wind profiling radar, a Radio Acoustic Sounding System (RASS), and an enhanced surface observing station. The GLASS sounding system only consisted of the GPS rawinsonde system. All collected data were initially processed in an onsite trailer. Subsets of the full dataset were then relayed near real-time via satellite to a data server at NCAR's Atmospheric Technology Division (ATD hereafter) and to the Global Telecommunications System (GTS) in an effort to quickly disseminate data and enhance operational forecasting decisions by the FOC.

### *3.3.1 GPS Atmospheric Rawinsonde System*

Vaisala RS-80 rawinsondes (Fig. 13a) tethered to helium-filled rubber balloons (Fig. 13b) were used to measure at one-second resolution upper-air pressure, temperature, relative humidity, and wind speed and direction, which were calculated from the instrument/balloon position. After termination of the launch or a popped balloon, the raw sounding data were run through the NCAR-developed Atmospheric Sounding Processing Environment (ASPEN) quality control program which smoothed the profiles and

removed suspicious data points. Further quality control performed by NCAR ATD included visual checks, generating scatter plots to check ranges of pressure, temperature, and relative humidity, and profile comparisons to check for major discrepancies (W. Brown 2004, personal communication).

Additional detailed quality control checks were conducted by the Colorado State University (CSU hereafter) Mesoscale Dynamics Group (P. E. Ciesielski 2005, personal communication). This procedure for each site included the following steps:

- Linearly interpolate one-second data to uniform 5 hPa intervals.
- Compute statistical temporal means and standard deviations at each 5 hPa level.
- Using these statistics as a method to check gross limits, objectively flag data as questionable or bad based on the number of standard deviations from the mean.
- Using good data, linearly interpolate in *log(p)* over missing data gaps if gap is less than 200 hPa.
- Visually inspect each sounding manually and flag any remaining suspicious data.
- Examine vertical profiles of temporal means and standard deviations, time series, and diagnostic fields to check for any inconsistencies.

It is important to note that this quality control procedure was performed on sounding data from all sites (Fig. 12) during the EOP and not just for the ISS and GLASS systems. High resolution data (i.e. one second) were used when possible for both thermodynamic parameters and wind information. Otherwise lower-resolution GTS data (i.e. mandatory

and significant levels) were employed. This was the case for the NWS rawinsonde wind data, as unrealistic high-frequency noise accompanied the high resolution dataset in over 50% of the launches (P. E. Ciesielski 2005, personal communication).

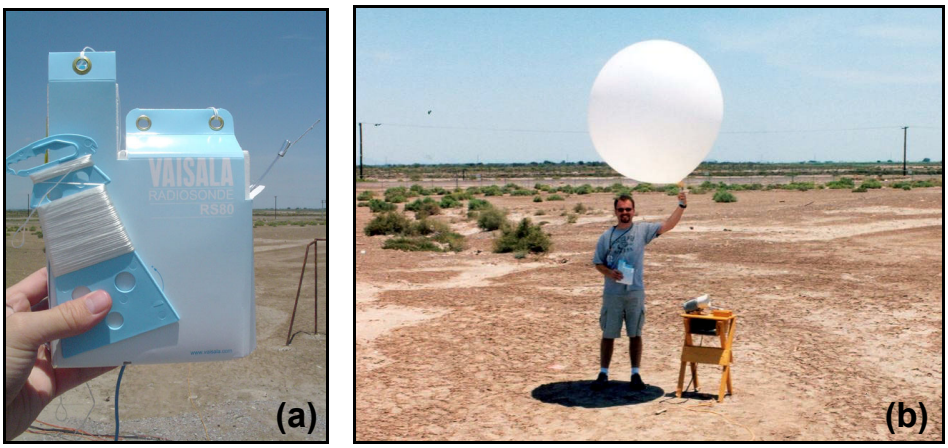


Figure 13: Vaisala RS-80 rawinsonde (a) and rawinsonde tethered to helium-filled rubber balloon (b) at ISS 4 Los Mochis.

As a means to determine the vertical structure and atmospheric modification characteristics (i.e. moistening and cooling) of the two gulf surge events noted above, quality controlled rawinsonde data from the three ISS sites along with data from Yuma, Empalme, and Mazatlan were linearly interpolated in time to uniform half-hour intervals. Additional interpolation was conducted over data points flagged as bad or questionable from the quality control procedure and a 1-2-1 filter was applied in the vertical to smooth high frequency noise. Numerous time-pressure plots were generated at these sites for different atmospheric parameters and their anomalies from 5 July-August 16 means. In addition to the interpolated plots, individual soundings were also carefully examined to describe the structure and evolution of the boundary layer for both pre- and post- gulf surge onset periods.

*3.3.2 915 MHz Doppler Clear-Air Wind Profiling Radar*

The 915 MHz Doppler clear-air wind profiling radar (Fig. 14) (profiler hereafter) at each of the three ISS sites measured wind speed and direction up to several kilometers above ground level by tracking changes within the air's index of refraction due to evolving turbulent eddies (Earth Observing Laboratory 2005). Operated by NOAA's Environmental Technology Laboratory (ETL hereafter), there was a similar profiler unit onboard the Mexican Navy Vessel R/V Altair (see Section 3.4 for further discussion). Low- (low altitude sampling with high vertical resolution) and high- (high altitude sampling with relatively lower vertical resolution) mode wind data were collected and an average consensus was determined over half-hour intervals. However, noting the shallow extent of gulf surges as discussed in Chapter 2, only low-mode data were used.

Figure 14: 915 MHz Doppler clear-air wind profiling radar and Radio Acoustic Sounding System at ISS 4 Los Mochis.

The Research Applications Laboratory (RAP) developed NCAR Improved Moments Algorithm (NIMA hereafter) quality control program was used to correct bad or

questionable profiler data at the ISS sites. Quality control checks for the R/V Altair profiler data were provided by ETL. NIMA makes use of mathematical analyses, image processing techniques, and fuzzy logic in an attempt to imitate human skill in examining profiler spectra (Research Applications Laboratory 2005). Using information from the NIMA program, further quality control was done using the NCAR Winds and Confidence Algorithm (NWCA hereafter). In addition to producing wind speed and direction measurements, this program calculates confidence values that estimate the reliability of the data. Data with a NWCA confidence value of 0.5 or greater are considered dependable (W. Brown 2004, personal communication).

In a separate analysis conducted by the CSU Mesoscale Dynamics Group, it was found that correlations between sounding wind data and cotemporary low-mode profiler wind data with confidence values of 0.5 or greater were 0.85 or higher (P. E. Ciesielski 2005, personal communication). Therefore, assuming the winds measured by the rawinsondes are "upper-air truth," low-mode profiler wind data are highly reliable and used in this study up to approximately 2 km as data coverage above this level with confidence values above 0.5 is low. The relative dryness of the air above 2 km, especially at the northern ISS sites (not shown), may help explain this, since the maximum height to which profilers are able to accurately measure wind speed and direction depends partially on the moisture content of the air (L. Hartten 2005, personal communication).

Unfortunately, quality controlled profiler data could not be obtained for 13 July and 15-16 July at Bahia Kino and 12 July at Los Mochis due to onsite power failures and/or interruptions resulting in the corruption of the raw spectral files (W. Brown 2004, personal communication). However, the original processed data were still available at these times. This information was manually quality controlled through visual checks for temporal and vertical consistency and then merged into the NIMA/NWCA datasets. Other gaps found in the profiler data are relatively short and were due to instrumentation downtime for maintenance and/or data back-up. In addition, one-minute surface winds measured by the ISS enhanced surface observing stations averaged over half-hour intervals were merged with the profiler data to provide better spatial coverage from the first profiler range gate (~120-180 m depending on the site) to the surface (10 m).

In order to describe the spatial and temporal extents of gulf surge wind signatures using this final quality controlled dataset, numerous plots were constructed for each of the ISS sites over the gulf surge time periods up to 2 km. In particular, the evolution of the wind surge was examined given the high temporal resolution of the profiler data. These signatures were then compared to patterns in the surface temperature, moisture, and pressure fields (see Section 3.3.4 for further discussion).

### *3.3.3 Radio Acoustic Sounding System*

The RASS consists of four speakers surrounding the profiler (Fig. 14) that emit a broadband acoustic frequency wave front (Earth Observing Laboratory 2005). The

vertical beam of the profiler tracks changes in the air's index of refraction created by the sound wave. From this tracking and using the relationship between air density and the speed of sound of the wave front, a vertical profile of virtual temperature is obtained.

Due to the proximity of the ISS sites at Puerto Peñasco and Bahia Kino to residential neighborhoods and the unpleasant, high-pitched sound which the RASS emits, site operators were required to shut down the system during nighttime hours from approximately 0400 to 1400 UTC (2200 to 0800 LST). Los Mochis was the only site with 24-hour RASS operations. Unfortunately, gulf surge onset for both GS #1 and GS #2 at Puerto Peñasco and Bahia Kino occurred in the late evening or early morning hours. Thus, the initial surge fronts for the two events examined in this study were not observed by the RASS along the northern gulf. In addition, FOC forecasters noted GS #2 as being restricted to the northern gulf. From this, the only gulf surge initial front that may have been observed by the RASS was at Los Mochis during GS #1. However, it will be shown after careful analysis of the wind profiler data that any gulf surge initial front that may have passed Los Mochis during GS #1 was quite different in structure and intensity from those gulf surge signatures recorded along the northern gulf. This may be due to the fact that the Los Mochis site was several kilometers (~10 km) from the GOC coast and nearby shallow coastal hills may have altered low-level flow from the ocean, whereas the Puerto Peñasco and Bahia Kino sites were much closer (~1-2 km) to the GOC coast. For these reasons, RASS data were not used in this study.

*3.3.4 Enhanced Surface Observing Station*

The ISS enhanced surface observing station consisted of an aneroid barometer, a thermistor (Fig. 15a), a hygristor, an anemometer atop a 10 m tower (Fig. 15b), a series of radiometers (Fig. 15c), and a tipping-bucket rain gauge (Fig. 15d) to respectively measure pressure, temperature, relative humidity, wind speed and direction, radiation, and precipitation at one-minute resolution. However, radiation and precipitation data collected from the ISS sites were not used in this study. The quality of the data collected at the ISS enhanced surface observing stations was excellent, thus requiring no significant quality control effort.

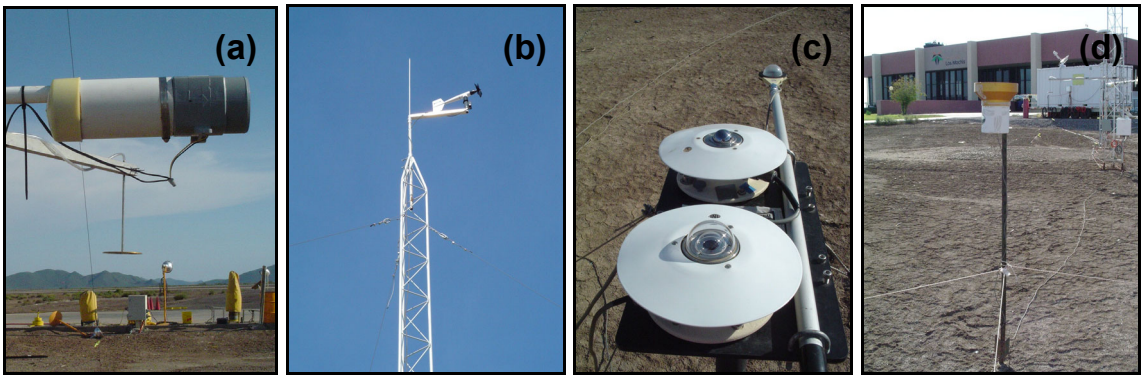


Figure 15: Various ISS surface instruments at Los Mochis; (a) thermistor, (b) 10 m wind tower with anemometer, (c) radiometers, and (d) tipping-bucket rain gauge.

One-minute pressure, temperature, and relative humidity (dewpoint) data averaged over half-hour intervals were plotted and compared against profiler data at the ISS sites to note relationships between gulf surge flow changes aloft and surface patterns. In addition, one-minute surface pressure and temperature observations, and their anomalies from 0000 UTC 7 July – 2359 UTC 14 August means were plotted at the ISS sites to

investigate any high-frequency changes associated with gulf surge onsets in an attempt to identify propagation characteristics and associated dynamical mechanism(s).

Additional high temporal resolution surface observations existed across the southwest United States and Mexico besides those collected at the three ISS sites. Maintained by the NWS in the United States and Servicio Meteorológico Nacional (SMN – Mexican Weather Service) in Mexico, numerous sites reported hourly observations in the standard World Meteorological Organization (WMO hereafter) METAR format. The SMN also maintains a nation-wide network of ten-minute automated surface observing stations. When examining individual time series of surface pressure data at various SMN sites (both WMO and automated), it was discovered that the overall data quality was quite poor and included unrealistic high frequency noise (not shown). Hence, an objective analysis scheme was implemented to remove the most obvious errors. For consistency, however, this scheme was applied to surface pressure data at all sites. Measurements greater than four standard deviations from the site's 0000 UTC 7 July – 0000 UTC 15 August mean were set to missing. Missing data gaps less than or equal to six hours were then linearly interpolated.

To investigate surface pressure patterns associated with gulf surges, hourly station pressure data from the SMN automated sites were reduced to altimeter settings given the station elevation, and were used in conjunction with hourly NWS, SMN, and ISS data to create 25-h running mean surface pressure anomaly maps interpolated onto a regular 1°x1° grid during GS #1. Anomalies from the means were investigated since some sites

reported sea-level pressure while others used altimeter setting. Twenty-five-hour running means were used to smooth the data and remove the diurnal and semidiurnal tidal signals. Unfortunately, large gaps in time (greater than six consecutive hours) existed at many SMN sites during late July, and thus a similar analysis was not plausible for GS #2.

### 3.4 NAME Rawinsondes and Observational Gridded Dataset

In addition to the ISS and GLASS sites, an extensive rawinsonde network (Fig. 12) was deployed during the NAME EOP. In the region from 15°-40°N and 90°-120°W, the NWS supported 23 sites, 10 of which launched four rawinsondes per day during the IOPs, while the SMN supported 13 sites, 5 (2) of which launched six (four) rawinsondes per day during the IOPs. Additional special sites were provided by the Mexican Navy via the vessel R/V Altair at the mouth of the GOC (23.5°N, 108°W), which launched 6 rawinsondes per day during the IOPs over a series of two cruises (7-22 July and 27 July-12 August), and by the Centro de Investigación Científica y de Educatción Superior de Ensenada (CICESE) research vessel R/V Francisco de Ulloa which typically launched 4 rawinsondes per day from 6-16 August throughout the GOC. The U.S. Department of Defense (DOD) provided launch sites at Edwards Air Force Base in California and Yuma. It is important to note that the latter of these sites is actually a composite of rawinsondes launched from four different locations in and near Yuma, each of which had different launch schedules.

The quality controlled data collected from all rawinsonde sites were objectively analyzed using a multiquadric interpolation (Nuss and Titley 1994) onto a 1°x1° grid

over 15°-40°N and 90°-120°W (T2A) two times per day (0000 and 12000 UTC), and over 22°-35°N and 100°-115°W (T1A) four times per day (0000, 0600, 1200, and 1800 UTC) with 25 hPa vertical resolution (surface, 1000 hPa – 50 hPa) (P. E. Ciesielski 2005, personal communication). Due to differing EOP/IOP launch schedules within the T1A, it was helpful in producing the four times per day analysis to create interpolated (linear in time) rawinsonde profiles when actual observational data were not available at the analysis times.

The gridded datasets include information from other instrumentation platforms as well. Profiler data from the three ISS sites were merged into the gridded datasets at those times where rawinsonde winds were unavailable. Given the lack of data over the oceans, NCEP reanalyses data (Kalnay et al. 1996) were used over data-sparse regions of the east Pacific Ocean and Caribbean Sea to assist the analysis. Surface fields were augmented by the NWS and SMN hourly WMO surface observing stations over land and by QuikSCAT surface (10 m) wind data over the oceans. Although not available for this study, subsequent versions of the gridded datasets should include observations collected from the NAME pilot balloon network and NOAA P-3 research aircraft.

Both the T1A and T2A gridded datasets were used extensively to generate various pressure plots and latitudinal cross sections as a means to describe the synoptic and mesoscale environments in which the gulf surges were embedded. These figures also provided valuable insight into the vertical and horizontal extent of the two gulf surge events examined. Topographical elevation data provided by NCAR at 1°x1° resolution

were used in conjunction with gridded height data to determine whether analyses were above or below the surface.

### 3.5 Satellite Data

Geostationary Operational Environmental Satellite (GOES hereafter)-10 data centered about the core monsoon region were obtained from the Cooperative Institute for Research in the Atmosphere (CIRA). Although visible, infrared (IR hereafter), and water vapor imagery were available, only IR data were used in this study. NAM convective features pertaining to gulf surge initiation generally develop along the SMO during the late afternoon and/or early evening and propagate west onto the coastal plain well after sunset. Thus, the usefulness of visible imagery for identifying gulf surges is quite limited. In addition, water vapor imagery was not used since this channel integrates water vapor over a depth of the atmosphere centered about the mid- to upper- troposphere (D. Lindsey, personal communication 2005), whereas gulf surge-related moisture advection is greatest at low-levels. Hence, IR images were examined every 15-30 minutes during both gulf surge periods to determine areas of relative cloudiness and convective activity associated with gulf surge passage. Comparison of these images with the pressure plots generated from the gridded datasets also proved useful in relating convective initiation with pertinent synoptic flow features.

### 3.6 Other NAME Instrumentation Platforms

Several other instrumentation platforms had been deployed during the NAME EOP that will not be specifically used in this study, but may be briefly cited. As already mentioned, the NOAA P-3 research aircraft flew several flights along the GOC during the NAME IOPs, each of which were designed to capture different aspects of the NAM. Also previously mentioned was the deployment of a relatively dense network of pilot balloon sites across the GOC coastal plain and along Baja California to, among other things, better describe the low-level diurnal flow patterns surrounding the GOC.

The NCAR S-band polarimetric (S-POL hereafter) radar was in operation north of Mazatlan near the mouth of the GOC to investigate NAM convection, its diurnal tendencies, and microphysical characteristics. Additional radar data were provided by four SMN C-band radars located nearby. ETL also maintained a site near the S-POL radar which included a vertically pointing S-band profiler, 449 MHz vertical wind profiler, and surface disdrometer. As a means to verify radar estimated rainfall, numerous rain gauges were strategically placed along the GOC coastal plain and SMO foothills. These rain gauges were also deployed to examine rainfall frequency, distribution, and intensity. Smaller instrumentation platforms were also deployed, but are too numerous to mention here. A complete listing of all the data collected during the NAME is available via the 2004 NAME online catalog (http://www.joss.ucar.edu/name /dm/archive/). Though these datasets were not used in this study, all the data collected

from these platforms in addition to those being used for this study will undoubtedly provide further valuable insight into the detailed workings of the NAM.

### 3.7 Anomaly Calculations

Many of the plots described above and analyzed in subsequent chapters involve anomalies. However, anomalies were calculated in one of two ways depending on what was to be investigated. First, as in the case for the half-hour interpolated rawinsonde plots and 25-hour running mean surface pressure plots, the temporal mean was calculated and then subtracted from each individual time. This method emphasized periods when anomalous cooling and moistening relative to the calculated mean accompanied gulf surge passage, as well as anomalous surface pressure increases and/or decreases. Second, as in the case for the one-minute surface pressure and temperature observation plots at the ISS sites, average values were calculated for each minute of the day over a specific period and then subtracted from their corresponding individual time. This method, in essence removed the diurnal cycle from the observations, such that the remaining signal was more representative of effects due to gulf surge passage.

# CHAPTER 4

# SYNOPTIC AND CONVECTIVE ENVIRONMENTS

## 4.1 Mean Upper-Air Atmospheric Fields

In order to properly discuss the two gulf surges identified in Section 3.2, it is important to first understand the mean monsoonal flow and thermodynamic patterns in which these events occurred. Gridded data from the T2A domain were used to calculate average heights, temperatures, mixing ratios, and wind vectors at 0000 (1800 LST) and 1200 UTC (0600 LST) from 1 July – 15 August 2004 in order to identify important diurnal signals. Pressure plots were generated at 950 and 850 hPa (Fig. 16) to best describe low-level features, and at 700 and 200 hPa (Fig. 17) to detail mid- to upper-tropospheric phenomena.

At 950 hPa (Fig. 16), the height fields are relatively weak at both times. However, there is a strong diurnal signal in the wind field over the western Caribbean Sea and areas surrounding the GOC. At 0000 UTC, there is a relatively strong easterly onshore component stretching from the Yucatan Peninsula northward along the Gulf of Mexico coast into Texas. In qualitative agreement with Douglas (1995) (Fig. 3b), there is also strong onshore flow along the entire GOC east coast reflecting the afternoon sea breeze. A similar land/sea interaction along the GOC west coast and Baja California is not

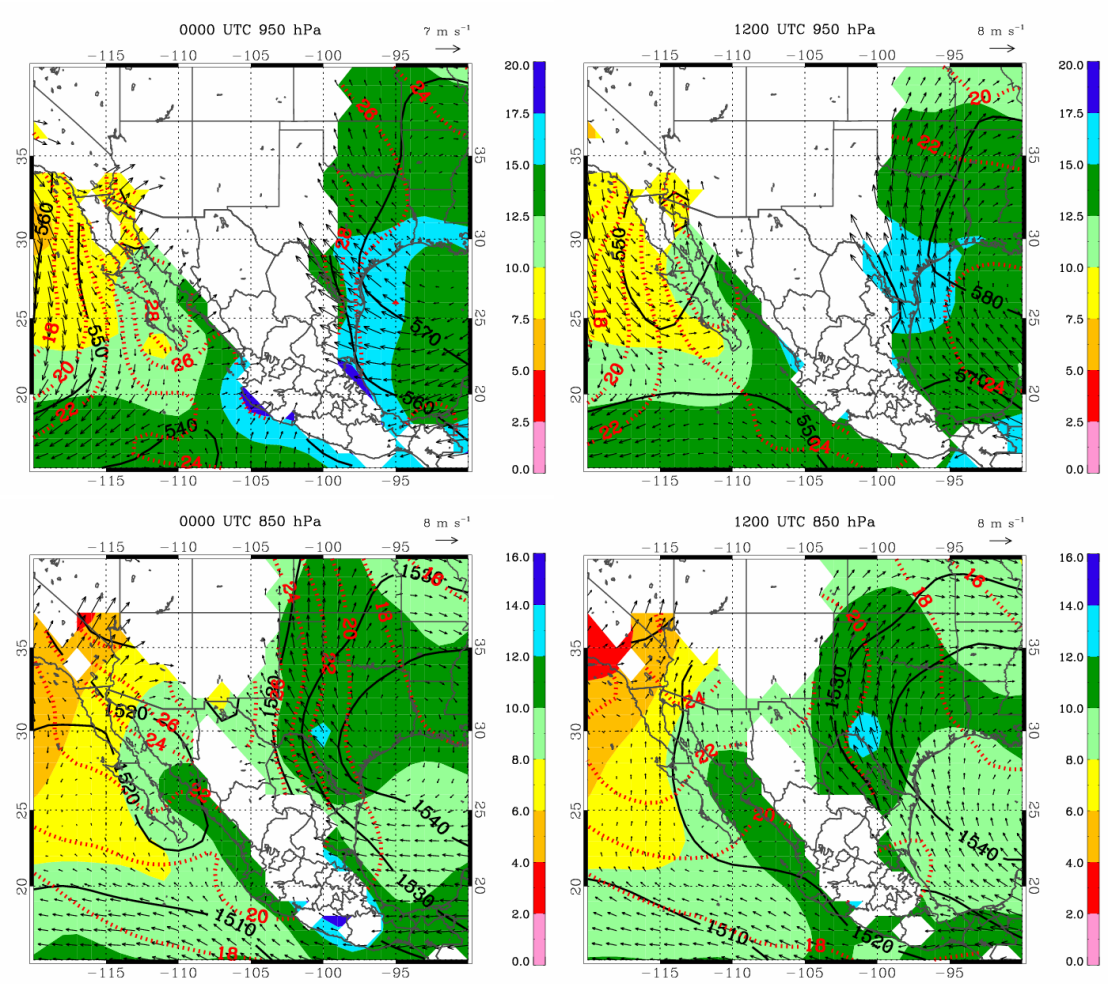


Figure 16: Mean heights (10 m intervals) (black solid), temperatures (2°C intervals) (red dotted), mixing ratios (g $kg^{-1}$) (colored contours), and wind vectors (m $s^{-1}$) at 0000 (left panel) and 1200 UTC (right panel) from 1 July – 15 August 2004 for 950 (top panel) and 850 hPa (bottom panel). White regions represent areas below the surface.

evident most likely due to the lack of rawinsonde observations along the peninsula (Fig. 12) as well as its narrow spatial extent and the relatively course resolution of the gridded dataset. At 1200 UTC, the winds over the Caribbean Sea maintain a more southerly component indicating advection of large quantities of moisture into southern Texas. Further supporting the results of Douglas (1995) (Fig. 3a), there is a distinct turning of the wind from northwesterly west of Baja California to southerly-southeasterly throughout the GOC. The GOC LLJ discussed by Douglas (1995) and later by Douglas

et al. (1998) is also well depicted by strong southeasterly wind vectors at 1200 UTC stretching from near Empalme to Yuma. At both times, winds over the east Pacific Ocean are consistently northwesterly, agreeing with the QuikSCAT results of Bordoni et al. (2004).

Thermodynamically, there is a strong east-west oriented thermal gradient west of Baja California at both times. Associated with daytime heating over the Sonoran Desert, there also exists a strong north-south thermal gradient (~ 8°C) along the GOC stretching from near the gulf's mouth to the southwestern Arizona deserts by 0000 UTC – a result also detailed by Douglas (1995). Low mixing ratios dominate the east Pacific Ocean west of Baja California whereas the greatest moisture resides along the south central coasts of Mexico and the west coast of the Gulf of Mexico at 0000 UTC, and the northeast/ southeast coast of Mexico/Texas at 1200 UTC. Of greater significance to this study, however, is the tongue of moist air along the GOC extending north from the tropical east Pacific Ocean at both times, albeit more prominent at 1200 UTC. The latter feature may be a result of the nocturnal GOC LLJ. This result reaffirms the importance of the GOC/tropical east Pacific Ocean as a prominent NAM low-level moisture source.

The prominent height feature at both times at 850 hPa (Fig. 16) is the westward extension of the southeast United States subtropical high centered about the Texas-Louisiana border. Associated with this phenomenon is a relatively strong anticyclonic turning of the wind. Flow patterns over the GOC and east Pacific Ocean west of Baja California at this level are much weaker than those at 950 hPa, although there still

appears to be a weak LLJ signature over the northern GOC and Sonoran Desert at 1200 UTC. In addition, tropical easterly flow dominates regions south of 20°N, while the relatively strong southwesterly flow over the deserts of Arizona, California, and Nevada at both times may be related to the southwest United States thermal heat low. The prominent thermal gradient west of Baja California noted at 950 hPa is still visible, but much weaker. However, there still exists at both times a north-south thermal gradient of 4°C or more stretching from the deserts of Arizona south to the mouth of the GOC. Regions of maximum moisture content are qualitatively similar to those at 950 hPa, except for being situated slightly farther inland.

At 700 hPa (Fig. 17), a broad region of anticyclonic curvature in the wind field centered along the United States-Mexico border exists as a westward extension of the southeast United States subtropical high. This circulation results in broad southeasterlies across much of Mexico, including regions surrounding the GOC, and southerly flow throughout the deserts of the southwest United States. Not surprisingly, these patterns agree quite well with those documented by Douglas et al. (1993) (Fig. 2b). Although the warmest air is centered about the Four Corners at both times with a thermal ridge extending south along the axis of the SMO, especially at 0000 UTC, thermal gradients at 700 hPa are relatively weak. The strong gradients west of Baja California and along the GOC evident at 950 and 850 hPa are no longer discernable. Interestingly, however, the regions of maximum moisture content at both times are not over the Gulf of Mexico, but centered along the SMO axis and spread longitudinally to the north. Hence, dry air advection accompanies the southeast flow from the Gulf of Mexico into central Mexico.

These observations further emphasize the theories put forth by Douglas et al. (1993) and Stensrud et al. (1995) concerning convection and/or upslope flow over the SMO vertically transporting low-level moisture to the mid-troposphere during the NAM.

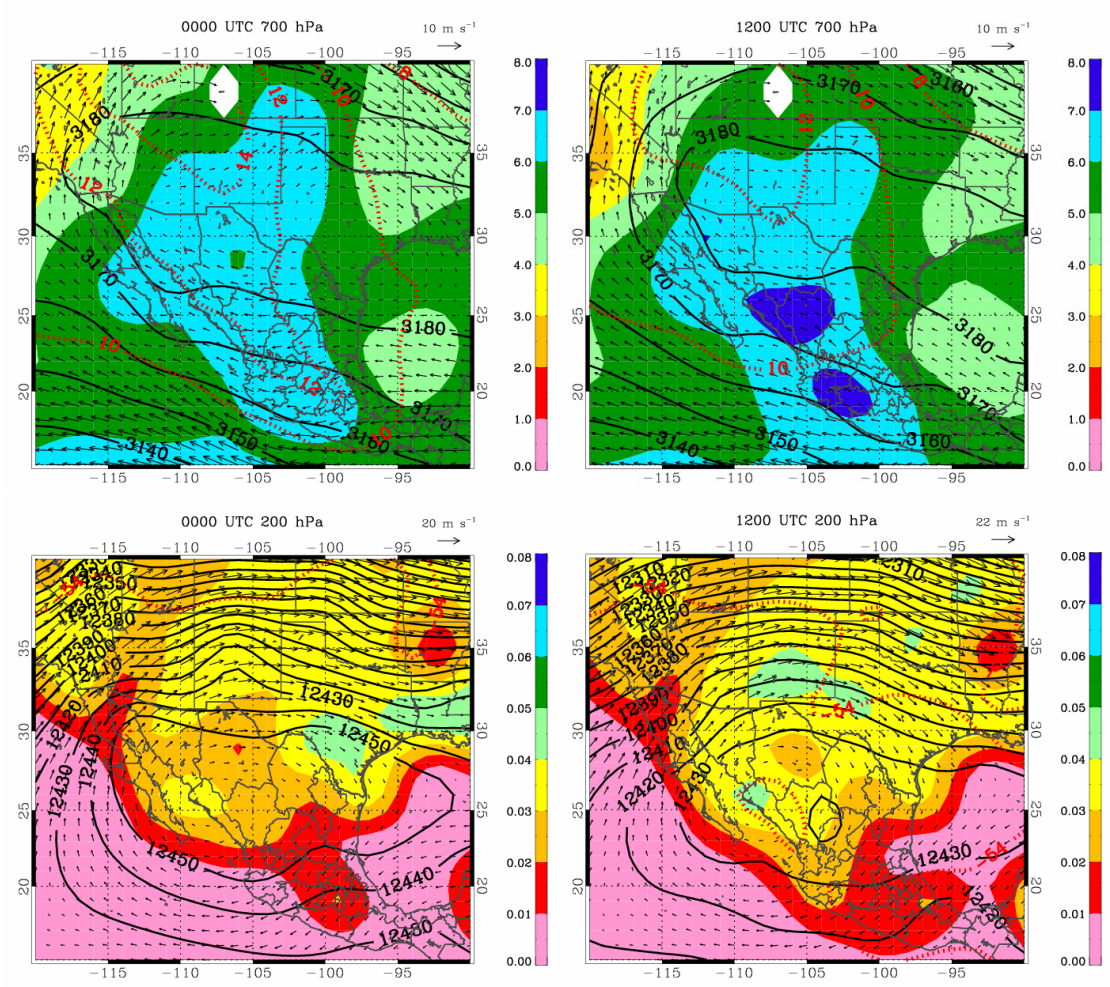


Figure 17: Same as in Fig. 16 except for at 700 (top panel) and 200 hPa (bottom panel).

The dominant height and wind features evident at 200 hPa (Fig. 17) are also qualitatively similar to those at 700 hPa, yet displaced farther south. At both times, the westward extension of the 200 hPa southeast United States subtropical high is centered over north central Mexico, with a relatively tight anticyclonic circulation in the wind field

located over northern Sinaloa – thus deviating from the very broad circulation at 700 hPa. The more southerly position of this upper-tropospheric feature results in predominately westerly flow across northern Mexico and all of the United States, northerly flow along the Gulf of Mexico coast, and easterlies throughout the subtropics, with southwesterly flow along the GOC. In addition, thermal gradients at 200 hPa are practically non-existent, while regions of maximum moisture are confined to areas over land. It is important to note, however, that the reliability of relative humidity data at very low temperatures is poor. Similar plots to those in Figs. 16 and 17 were also constructed at 500 hPa, but are not included here as its dominant features did not greatly differ from those shown at 700 or 200 hPa.

### 4.2 Gulf Surge Synoptic Conditions

Recalling the numerous studies already discussed detailing possible relationships between gulf surge initiation and tropical disturbances or easterly waves (see Section 2.3 for further discussion), it is imperative to investigate the synoptic circulation patterns associated with the two cases presented in this study. Understanding the basic synoptic patterns also provides a background to aid in describing smaller scale (i.e. mesoscale) features. Therefore, pressure maps at 700 and 200 hPa showing heights, temperatures, mixing ratios, and wind vectors were generated from the T2A gridded dataset at 1200 UTC from two days before gulf surge onsets at Puerto Peñasco to two days after. After analyzing plots from numerous levels, these pressures were chosen to best describe dynamical and thermodynamic features in the middle (700 hPa) and upper (200 hPa)

troposphere. 1200 UTC (0600 LST) maps were chosen since both gulf surge events passed Puerto Peñasco in the early morning hours, and the number of days examined (5 days) helps provide detailed information on the time evolution of important features.

### *4.2.1 Gulf Surge #1*

Since gulf surge onset at Puerto Peñasco occurred on 13 July (see Section 3.2) for GS #1, Figs. 18 and 19 detail the prominent synoptic features at 700 and 200 hPa, respectively, from 1200 UTC 11 July (t = -2 d, Day -2) to 1200 UTC 15 July (t = +2 d, Day +2). At 700 hPa (Fig. 18), there are two significant synoptic circulation features – the location and evolution of the westward extension of the southeast United States subtropical high and the northwestward propagation of Tropical Storm Blas. At 200 hPa (Fig. 19), one important feature emerges – the propagation through the subtropical high of a TUTT low as described by Walker and Mock (1982), Whitfield and Lyons (1992), and Pytlak et al. (2005) (see Section 2.3 for further discussion).

The subtropical high's 700 hPa center of circulation on Day -2 is located over eastern Louisiana/western Mississippi and is accompanied by relatively weak, broad anticyclonic flow stretching westward into Arizona and Sonora (Fig. 18). As time progresses, the subtropical high's center weakens and significantly broadens as it builds west and north along the Gulf of Mexico coast and into the southern Great Plains. By Day +2, very broad anticyclonic flow centered near northeast New Mexico dominates the south and southwest United States as well as much of Mexico. Strong cyclonic flow associated

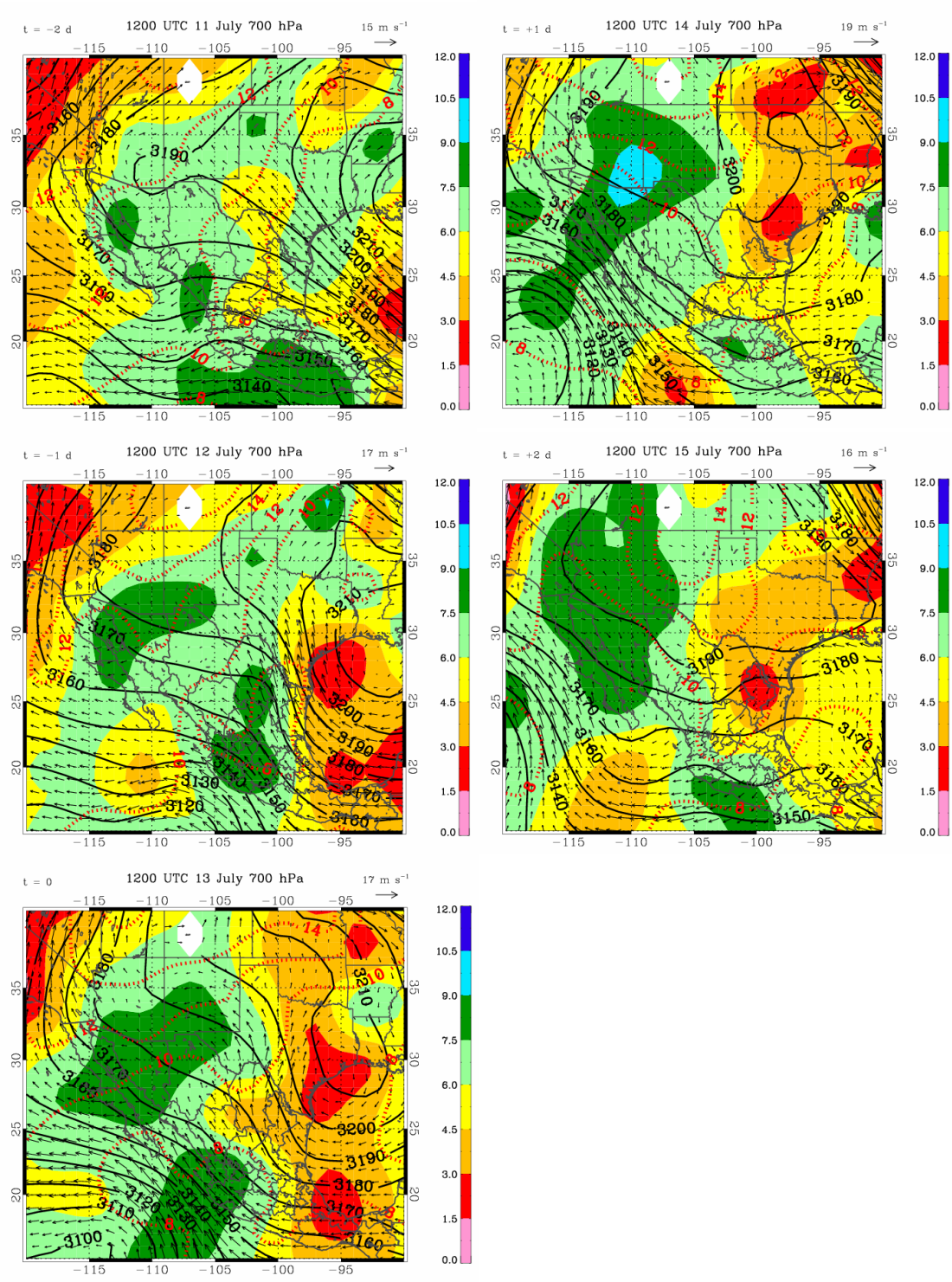


Figure 18: 700 hPa heights (10 m intervals) (black solid), temperatures (2°C intervals) (red dotted), mixing ratios (g $kg^{-1}$) (colored contours), and wind vectors (m $s^{-1}$) at 1200 UTC from t = -2 d (11 July) to t = +2 d (15 July) where t = 0 (13 July) corresponds to day of gulf surge onset at Puerto Peñasco. White regions represent areas below the surface.

with Tropical Storm Blas at 700 hPa is visible south of 20°N and centered near 110°W by Day -1. The consistent northwestward propagation of this system takes its center of circulation south and west of the southern tip of Baja California by Day 0 and out to the open waters of the eastern Pacific Ocean by Day +2. The combined movement of these two important synoptic circulations generate strong height gradients, and thus very strong southeasterly winds, south of the mouth of the GOC by Day 0 and over much of the GOC by Day +1. As a result, significantly cooler and moister air is advected northward into regions surrounding the GOC from the eastern tropical Pacific Ocean. Concurrently, during the time evolution presented in Fig. 18, regions east of the Continental Divide are generally significantly drier than those nearer the GOC, agreeing with the qualitative results of Douglas et al. (1993) (Fig. 2b).

It is interesting to note that the 700 hPa storm track of Tropical Storm Blas agrees relatively well with the movement of cyclonic circulation along the southwest coast of Mexico from the composite anomaly analysis at 925 hPa of Douglas and Leal (2003) (Fig. 6), but is less agreeable with the evolution of the related cyclonic circulation from their 600 hPa composite anomaly analysis (Fig. 7). As per the results of Fuller and Stensrud (2000), the location and movement of this system suggest an important relationship between the tropical disturbance and gulf surge initiation or development. This theory, however, will be discussed further in subsequent sections, as other mechanisms may have also played an important role in gulf surge initiation. Of further interest is the development of an anticyclonic circulation near the mouth of the GOC by Day +2, also evident in the 925 hPa composite anomaly analysis of Douglas and Leal

(2003). Although the relative movement and evolution of the subtropical high do not agree well with the results of Douglas and Leal (2003), the location of Tropical Storm Blas in combination with that of the subtropical high suggest the possibility of a wet surge as defined by Higgins et al. (2004) (Fig. 11a).

At 200 hPa (Fig. 19), a very strong southwest-northeast tilted TUTT low located over central Mexico is embedded within the subtropical high on Day -2, as evident in an enclosed circulation in the wind field. This feature appears to have originated over southeast Texas three days earlier (Pytlak et al. 2005). Also visible at 500 hPa (not shown) albeit much weaker, the low quickly weakens as it propagates northwest along the west coast of Mexico. By Day 0, the TUTT low is no longer identifiable by enclosed height contours, but is still visible as a strong kink in the height field centered near the central GOC stretching south into the Pacific Ocean. The then weakened trough appears to merge with the height feature associated with Tropical Storm Blas by Day +1. As the TUTT low weakened between Days -1 to 0, the subtropical high strengthened over the Four Corners and maintained its dominance throughout the remaining examined period.

A secondary height maximum as a southern extension of this subtropical high over central Mexico on Day 0 soon gave way to another height minimum by Day +2, reminiscent of a propagating TUTT low. This latter feature appears to have originated from a weak cut-off cyclonic circulation over southeast Texas on Day +1. Pytlak et al. (2005), however, suggest that this new TUTT low originated over the western Gulf of Mexico. While 200 hPa thermal gradients in Fig. 19 are extremely weak, it is interesting

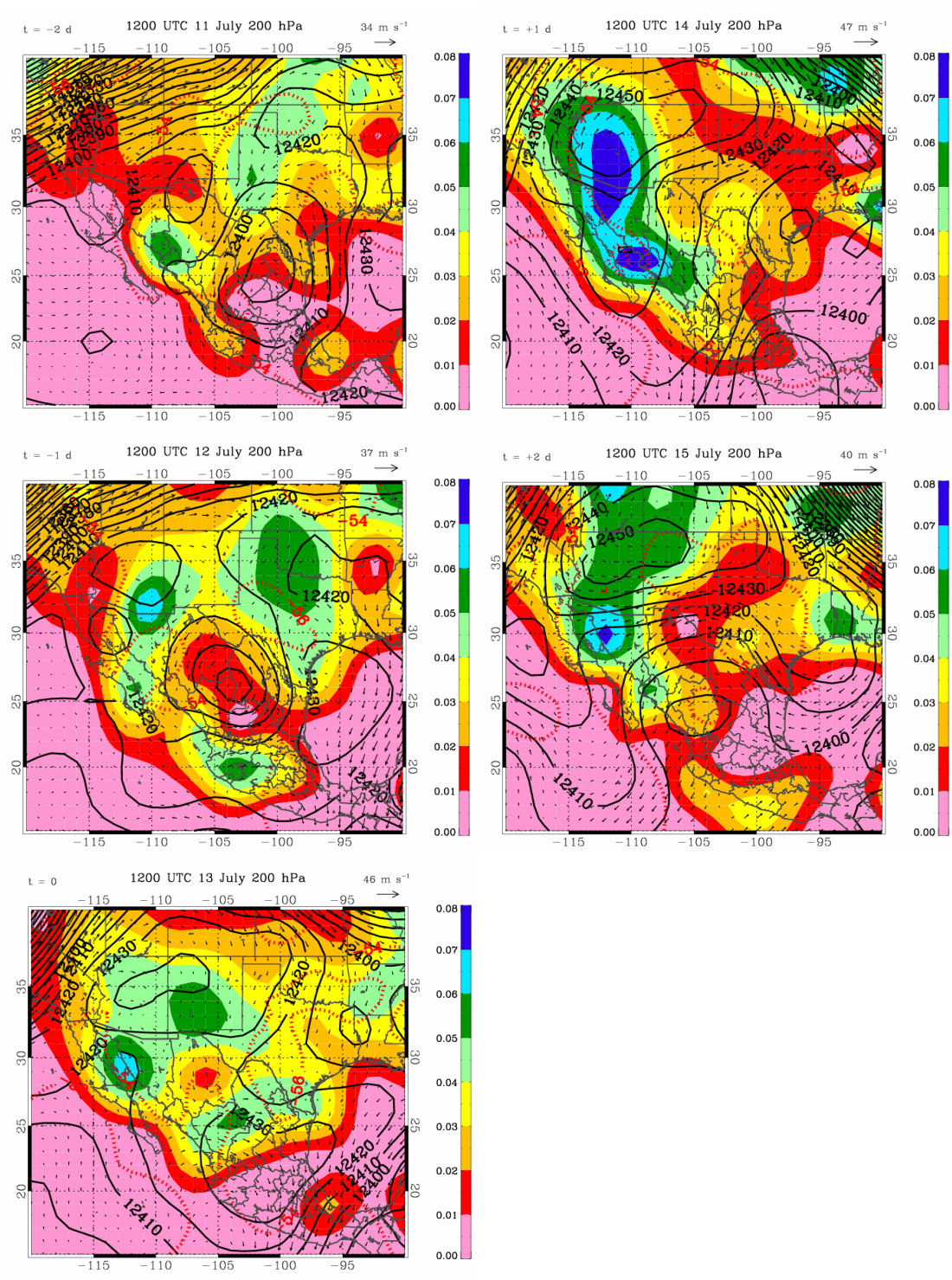


Figure 19: Same as in Fig. 18, except at 200 hPa.

to note that from Day -2 to Day -1 regions of maximum moisture content encircle the inverted trough with local minima at its center.

### *4.2.2 Gulf Surge #2*

Since gulf surge onset at Puerto Peñasco occurred on 21 July for GS #2 (see Section 3.2), Figs. 20 and 21 detail the prominent synoptic features at 700 and 200 hPa, respectively, from 1200 UTC 19 July (t = -2 d, Day -2) to 1200 UTC 23 July (t = +2 d, Day +2). At both levels (Figs. 20 and 21), there are two significant synoptic circulation features – the location and evolution of the subtropical high and an impinging easterly wave (better identified as a TUTT low at 200 hPa). Overall, the synoptic patterns associated with GS #2 are markedly different than those associated with GS #1.

A well-defined subtropical high and associated anticyclonic circulation are well entrenched along the Arizona-Sonora border at 700 hPa from Day -2 to Day 0 (Fig. 20). During this time, the subtropical high remains nearly stationary with little fluctuation. However, on Day 0 a north-south tilted easterly wave is observed over east-central Mexico. It is not until Day +1 when the trough propagates farther west that it interacts with the subtropical high, thus altering its previous position. By Day +2, the easterly wave's axis tilts into a more southwest to northeast orientation and is located near the mouth of the GOC. Concurrently, the subtropical high is no longer visible in the height field, although a very tight anticyclonic circulation in the wind field is noticeable just to the west of northern Baja California.

The combination of these two features on Days 0 to +2 result in strong northeasterly winds between the easterly wave to the south and anticyclonic circulation to the north – a qualitative synoptic pattern reminiscent of that suggested by Higgins et al. (2004) for dry surges (Fig. 11b). Hence, strong warm air and minimal positive moisture advection accompany this 700 hPa flow over the central and southern GOC during Days +1 to +2. This is due to the relatively strong north-south thermal gradient along the GOC and the fact that regions immediately surrounding the GOC are slightly drier than those to the north and east, especially by Day +2. In addition, it is interesting to note that as the easterly wave propagates westward, the subtropical high downstream becomes less well-defined, whereas the westward extension of the southeast United States subtropical high upstream strengthens.

Whereas synoptic signatures associated with Tropical Storm Blas during GS #1 agreed qualitatively well with the composite anomaly analysis at 925 hPa from Douglas and Leal (2003), there was no such system during GS #2. However, certain aspects of the timing and location of the subtropical high relative to the easterly wave during GS #2 somewhat agree with those results at 600 hPa presented in Fig. 7 from Douglas and Leal (2003). These similarities are very general, such that there is a subtropical high centered near the Arizona-Sonora border that is displaced in some way due to a westward propagating cyclonic circulation across central Mexico. Otherwise, there again develops an anticyclonic circulation in the wind field near the mouth of the GOC by Day +2, as was the case with GS #1.

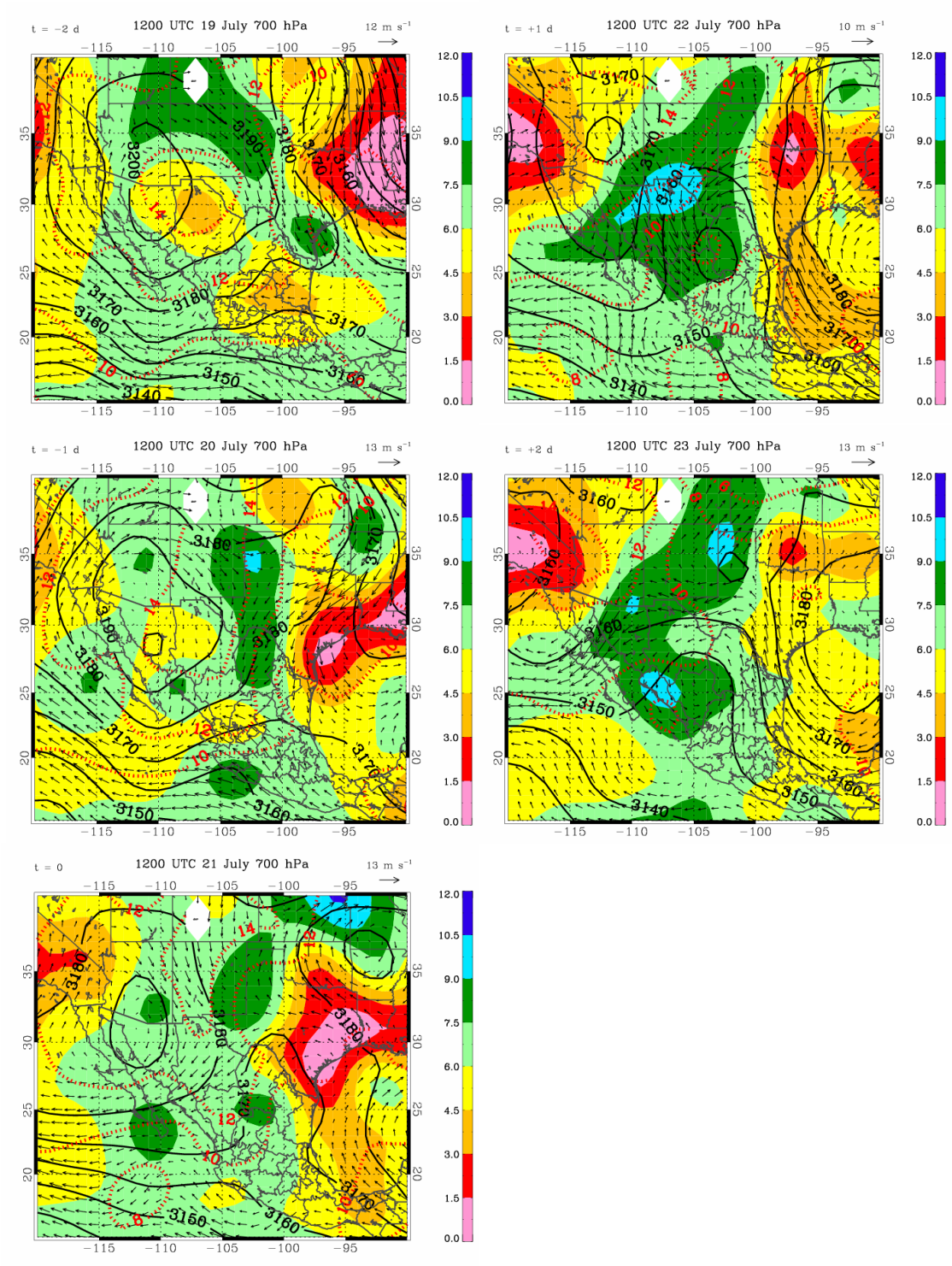


Figure 20: 700 hPa heights (10 m intervals) (black solid), temperatures (2°C intervals) (red dotted), mixing ratios (g $kg^{-1}$) (colored contours), and wind vectors (m $s^{-1}$) at 1200 UTC from t = -2 d (19 July) to t = +2 d (23 July) where t = 0 (21 July) corresponds to day of gulf surge onset at Puerto Peñasco. White regions represent areas below the surface.

At 200 hPa (Fig. 21), the north-south oriented subtropical high is centered over eastern New Mexico with relatively strong northerlies across Texas and southerlies across western Arizona/southeastern California. During the time period examined in Fig. 21, the high's center of anticyclonic circulation progresses clockwise along a comma-shaped track, such that by Day +2, it is located over central Sonora. In addition, the orientation of the high's axis tilts southwest to northeast by Day 0 due to the westward intrusion of the TUTT low along the Gulf of Mexico's western coast. Although proposed by Pytlak et al. (2005) to have originated over the Gulf of Mexico, the southwest-northeast tilted TUTT low seems to be first visible in the height and wind fields on Day -1 over Texas and Louisiana, agreeing relatively well with the general region suggested by Thorncroft et al. (1993) for cut-off lows due to eastward propagating midlatitude thinning troughs.

Whereas the TUTT low at 200 hPa associated with GS #1 decayed substantially over time, the one associated with GS #2 maintains its strength and propagates west to the southwest Texas-Mexico border by Day +2. Noting the location of the easterly wave at 700 hPa on Day +2 (Fig. 20), the easterly wave/TUTT low's vertical axis is aligned southwest to northeast with increasing height, as suggested by the compositing results of Walker and Mock (1982). However, it is uncertain whether the two features are linked or propagate separately, since TUTT lows are much weaker at 700 hPa compared to 200 hPa (Walker and Mock 1982, Whitfield and Lyons 1992), yet easterly waves can be quite strong at 700 hPa (Stensrud et al. 1997). Although 200 hPa thermal gradients are very weak, regions of maximum moisture content seem to propagate around or remain embedded within the subtropical high during the time evolution presented in Fig. 21.

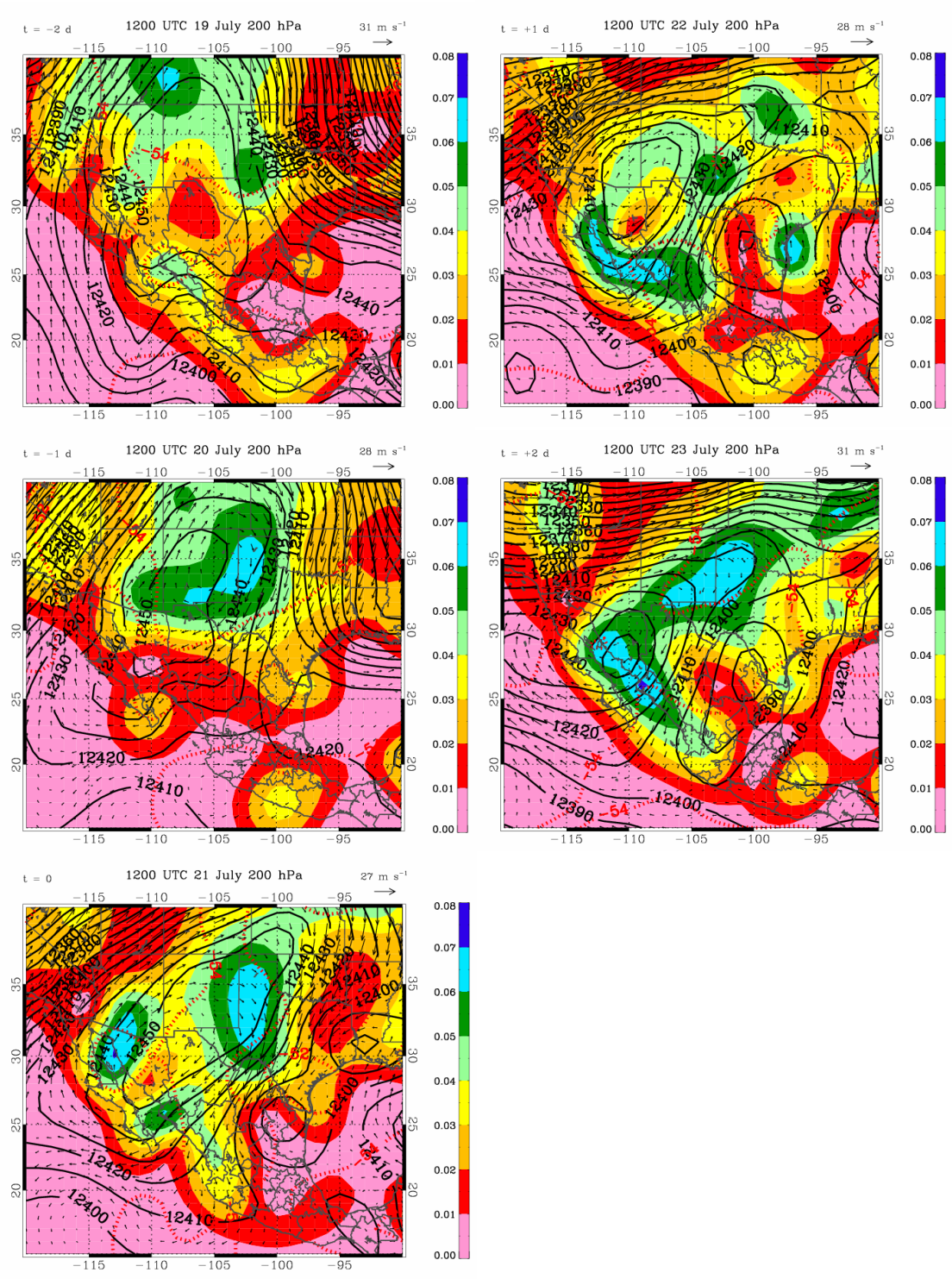


Figure 21: Same as in Fig. 20, except at 200 hPa.

At this point, it is important to mention that neither GS #1 nor GS #2 were preceded by an eastward propagating midlatitude trough, to be soon followed at the same longitudes by a westward propagating cyclonic tropical disturbance south of 20°N across central Mexico, as discussed by Stensrud et al. (1997). Tropical Storm Blas appeared to cross 110°W near 19°N approximately one day prior to gulf surge onset at Puerto Peñasco during GS #1 (Fig. 18), but was not preceded by a midlatitude trough. During GS #2, there again was no midlatitude trough and the cyclonic feature that was observed across central Mexico did not begin to significantly alter the flow near the GOC until Day 0 (Fig. 20).

### 4.3 Gulf Surge Surface Pressure Patterns

As discussed earlier, Hales (1972) and Brenner (1974) noted several common surface characteristics that generally accompany gulf surge passage, including a decrease in temperature, an increase in relative humidity, an increase in sea-level pressure, and a marked wind shift with an increased southerly component (see Section 2.2 for further discussion). From this list, however, the most consistent change to occur between the three ISS sites after examining their surface data during GS #1 was a marked increase in surface pressure (Figs. 25b, 26b, and 27b). Thus, to better understand the spatial and temporal extent of these surface pressure differences as well as their relation to gulf surge passage, the network of surface observation sites maintained by the NWS and SMN were used to describe the 25-h running mean surface pressure anomalies across the core NAM domain from 0000 UTC 13 July to 0000 UTC 15 July every six hours (Fig. 22). Recall,

large surface pressure data gaps accompanied GS #2 at numerous sites (see Section 3.3.4 for further discussion), thus ultimately hindering a similar analysis for the second event.

At 0000 UTC 13 July, the entire region surrounding the GOC is dominated by negative surface pressure anomalies. However, a distinct arc-shape is visible in the -1 hPa isobar and is primarily confined between the coasts of the southern GOC. As time progresses, this arc-shaped feature progresses northwestward along the axis of the GOC, such that by 1800 UTC 13 July, positive surface pressure anomalies have replaced negative values along the majority of the GOC and its coastal plains. This pattern of negative anomalies prior to surge onset replaced by positive anomalies after surge onset agrees qualitatively well with a similar surface pressure analysis conducted by Douglas and Leal (2003) using nine years of NCEP reanalyses data (not shown). It is interesting to note that the northwestward propagation of surface pressure anomalies is primarily confined between the Peninsular Range to the west and SMO to the east. However, it is difficult to tell whether this feature is realistic, or perhaps due to a lack of surface observation sites over the Pacific Ocean and/or SMO, as the results of Douglas and Leal (2003) showed pressure changes extending farther out over the Pacific Ocean.

After 1800 UTC 13 July, pressure changes across the southern GOC are rather uninteresting. However, a large area of positive surface pressure anomalies develops across the Sonoran Desert and into southwestern Arizona and southeastern California. In fact, by 0000 UTC 15 July, these areas maintain surface pressure anomalies of 4 hPa or more above 25-h running mean values. Comparing the surface pressure patterns detailed

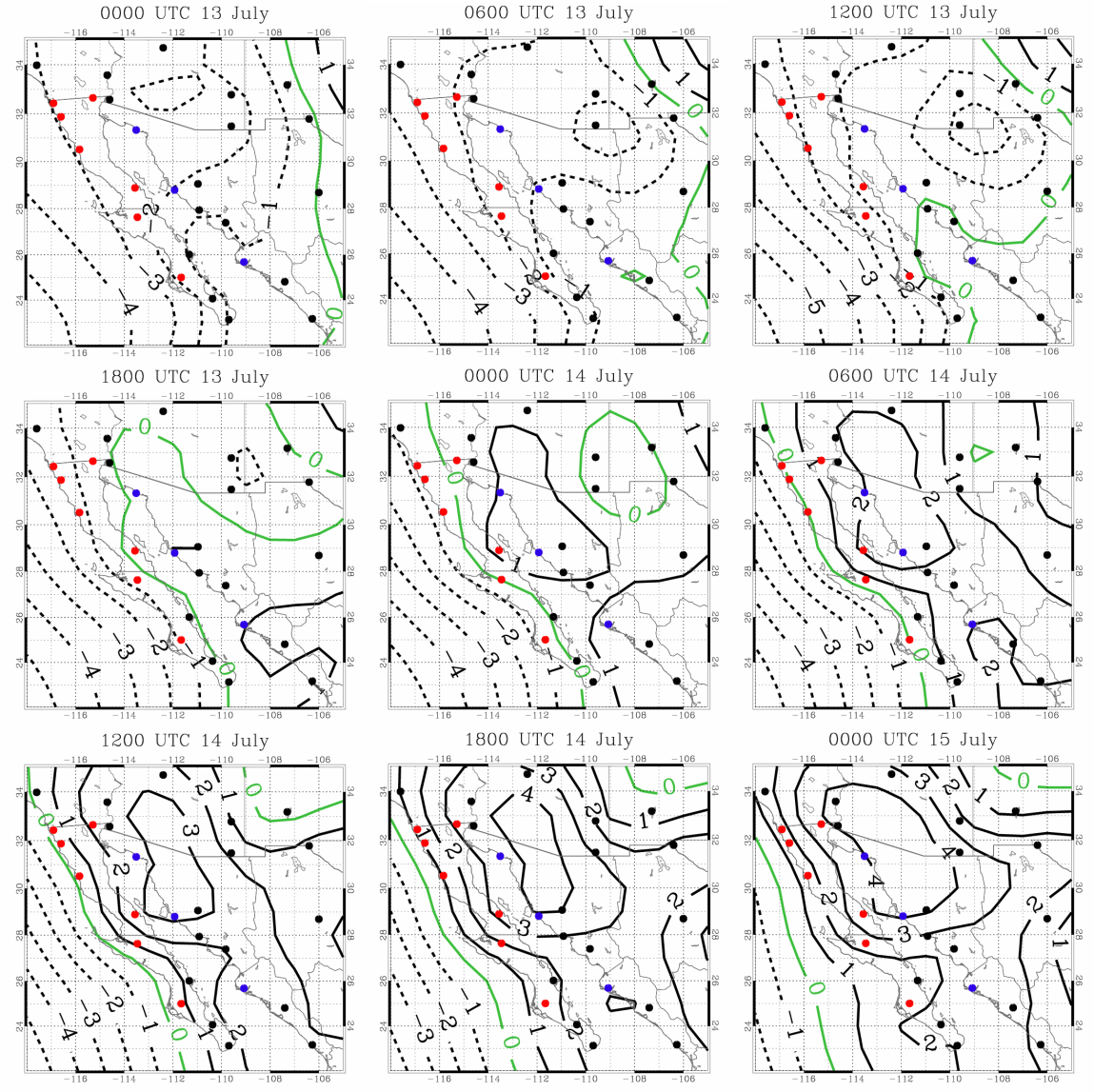


Figure 22: 25-h running mean surface pressure anomaly isobars (hPa) from 0000 UTC 13 July – 0000 UTC 15 July 2004. Anomalies are calculated using 7 July – 15 August means. Dotted contours are negative, green contour equals zero, and solid contours are positive. Black dots represent NWS or SMN WMO sites, red dots represent SMN automated sites, and blue dots represent ISS sites. See Section 3.3.4 for further details.

in Fig. 22 with the timing and propagation of pertinent 700 hPa features from Fig. 18, it is possible that the surface pressure is synoptically driven by Tropical Storm Blas advecting large quantities of cool, moist air northward from the tropical east Pacific Ocean,

especially on 14 July. However, on 13 July, gulf surge passage along the entire length of the GOC may significantly contribute to the pressure anomaly pattern observed.

## 4.4 Gulf Surge Convective Conditions

The relative importance of convective development and propagation across the NAM geographical domain and its relation to gulf surge initiation cannot be ignored. In fact, as mentioned earlier, it was Hales (1972) who first noticed a relationship between convective cloud masses and surges of moisture while studying satellite photographs. More recently, a series of four short studies conducted by Howard and Maddox (1988a,b,c,d) used GOES IR satellite data to detail thunderstorm frequency over Mexico as well as the environmental conditions necessary for the development and evolution of NAM mesoscale convective systems (MCS hereafter). Interestingly, multiple MCSs developed during both gulf surge events and will be suggested to have played a role in surge initiation. After examining hundreds of satellite images, it is important to note that the IR imagery shown below was selected to depict periods when convection appeared to have its greatest extent and/or intensity. These times do not necessarily match with standard synoptic reporting times.

### *4.4.1 Gulf Surge #1*

One day before gulf surge onset (12 July) at Puerto Peñasco, a large MCS develops over the southern GOC coastal plain centered near Los Mochis by 0330 UTC (Fig. 23a).

As time passes, this MCS propagates west-northwest over the GOC and quickly dissipates. Surprisingly, no gulf surge event follows given this large cloud mass near the southern GOC. This MCS most likely developed as a result of various mesoscale processes, such as land/sea interactions, mountain-valley circulations, convective outflows from elevated thunderstorms, and/or convective instability as argued by Howard and Maddox (1988c). In addition, although the MCS developed to the west of the TUTT low's 200 hPa center (Fig. 19), thus seemingly in the region for synoptically forced sinking motion as suggested by Walker and Mock (1982), the 200 hPa low may have still interacted with NAM circulation patterns in such a way as to aid the convective development (Pytlak et al. 2005).

On 13 July, the convective environment becomes increasingly complex with the northwestward propagation of Tropical Storm Blas (Fig. 18). By 0146 UTC 13 July (Fig. 23b), two important convective features emerge. First, a large thunderstorm complex develops over the Sonoran Desert, perhaps as an extension of thunderstorms that first formed over the higher terrain of southeastern Arizona earlier that evening (not shown). Second, a well-defined southeast to northwest oriented line of thunderstorms develops along the SMO axis in Sinaloa. These storms most likely developed as an extension of the intense convection associated with Tropical Storm Blas and/or due to the orographic lift provided by the nearby mountains.

After approximately six hours, the two aforementioned thunderstorm complexes merge together and aid in the development of a significant MCS centered half-way

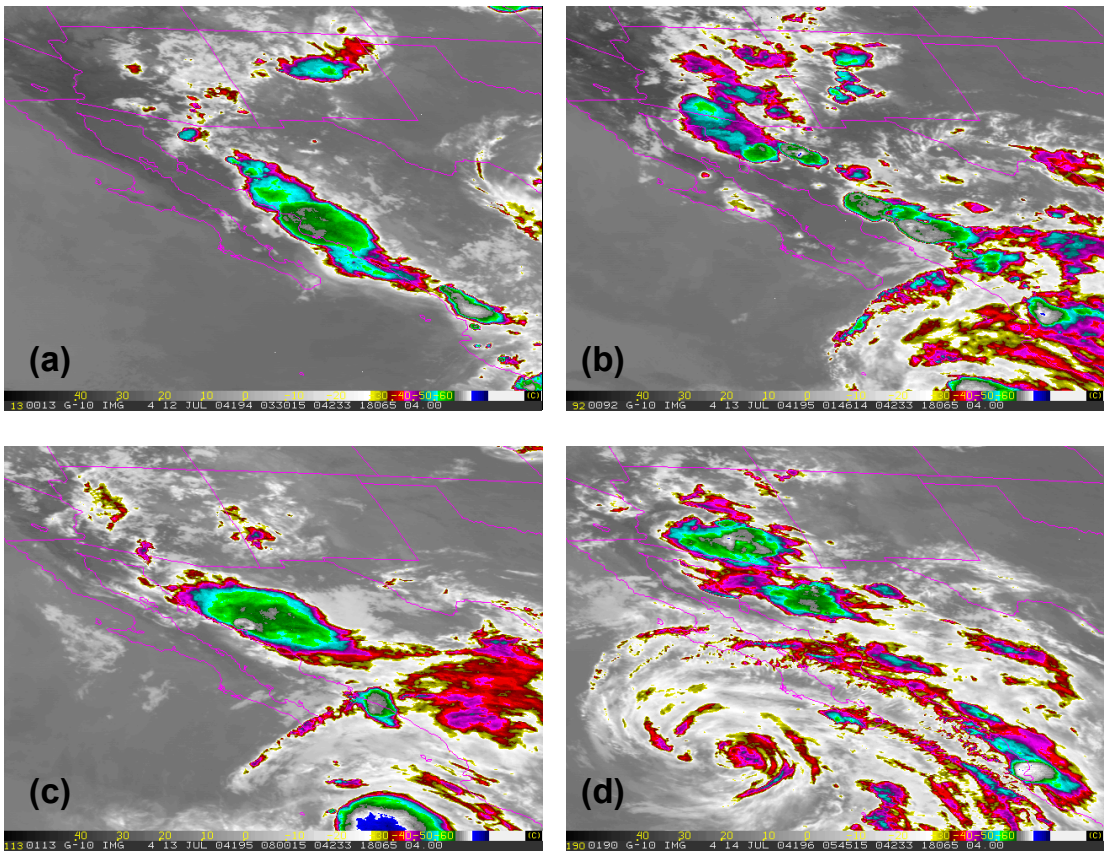


Figure 23: Infrared GOES-10 satellite imagery over the core NAM domain at (a) 0330 UTC 12 July, (b) 0146 UTC 13 July, (c) 0800 UTC 13 July, and (d) 0545 UTC 14 July. Colored contours represent cloud top temperatures (°C).

between Bahia Kino and Los Mochis along the GOC coastal plain by 0800 UTC 13 July (Fig. 23c). A very strong and deep wind surge visible in the profiler data soon follows in the early morning hours at Puerto Peñasco (Fig. 25a), as it had already passed Bahia Kino approximately two hours earlier (Fig. 26a). However, the identification of surge onset at Los Mochis using profiler data proved to be more difficult (Fig. 27a). Hence, GS #1 initiation and propagation is likely tied to the convective development and evolution along the GOC coastal plain throughout the day on 13 July, as well as the propagation of Tropical Storm Blas, even though the tropical system may have only indirectly played a role in initiating convection farther north.

On 14 July, regions immediately surrounding the GOC and eastern tropical Pacific Ocean were dominated by the convective rain bands associated with Tropical Storm Blas, which by 0545 UTC was centered just south and west of the southern tip of Baja California (Fig. 23d). However, of greater interest is the large MCS that developed over the low-deserts of Arizona by this time. As suggested earlier by the synoptic flow patterns at 700 hPa (Fig. 18) and the results of Higgins et al. (2004) as they pertain to defining wet and dry surges, moisture advected by the gulf surge appears to have deeply penetrated the low-deserts of Arizona providing the necessary ingredient for intense convective development and heavy rainfall in this region (McCollum et al. 1995).

*4.4.2 Gulf Surge #2*

One day before gulf surge onset (20 July) at Puerto Peñasco, the convective environment surrounding the GOC is suppressed. However, there is a very large MCS that developed near Guadalajara and propagated west to the eastern tropical Pacific Ocean by 1230 UTC (Fig. 24a). It appears that there was no significant synoptic feature associated with its development (Fig. 19 and 20), but was most likely initiated due to one or more of the mesoscale processes described by Howard and Maddox (1988c). Nonetheless, its relative location to the GOC appears to be too far south to help initiate any kind of gulf surge initiation.

On the following day (21 July, Fig. 24b), the convective environment changes drastically, perhaps due to the westward propagation of the 700 hPa easterly wave across

central Mexico (Fig. 20) combining with various mesoscale processes. Although the position of the 200 hPa TUTT low (Fig. 21) appears too far north and east of the areas of primary convection, it too may have played an important role in initiating the convection. Two MCSs dominate the NAM geographical domain by 0300 UTC. The first, centered over the New Mexico-Texas border, and the second covering much of the GOC coastal plain. While the MCS farther north is quite impressive, it is the MCS across the GOC that is most likely linked to a strong, yet very shallow wind surge again visible in the profiler data at Puerto Peñasco and Bahia Kino soon after (Figs. 28a and 29a). Although these wind signatures could be argued as that only of the GOC LLJ, the qualitative relationship detailed by Hales (1972) and Brenner (1974) between cloud masses across the GOC and subsequent surges of moisture is unmistakable in this case.

The day after gulf surge onset (22 July) at Puerto Peñasco (Fig. 24c), a very similar convective pattern to the day before develops across the core NAM region. By 1045 UTC, a large circular MCS has swept westward over the GOC into a location almost identical to that of the previous day. In viewing successive IR satellite images, it appears that the residual moisture left over from the MCS over the New Mexico-Texas border the previous day helps initiate this new MCS. In addition, the MCS over the GOC helps maintain relatively strong southeasterly flow across the northern GOC via a secondary gulf surge (Figs. 25a and 26a), which appears stronger than that on 21 July. Of further interest, however, is the lack of convective development over the low-deserts of Arizona and New Mexico, differing from GS #1 on the day after gulf surge onset. Given the results of Higgins et al. (2004), this is not surprising, as flow at 700 hPa throughout the

GOC region and southwest United States on 22 July (Fig. 20) had a strong northerly component that appears to have aided in the suppression of convective development despite the influx of low-level gulf surge moisture.

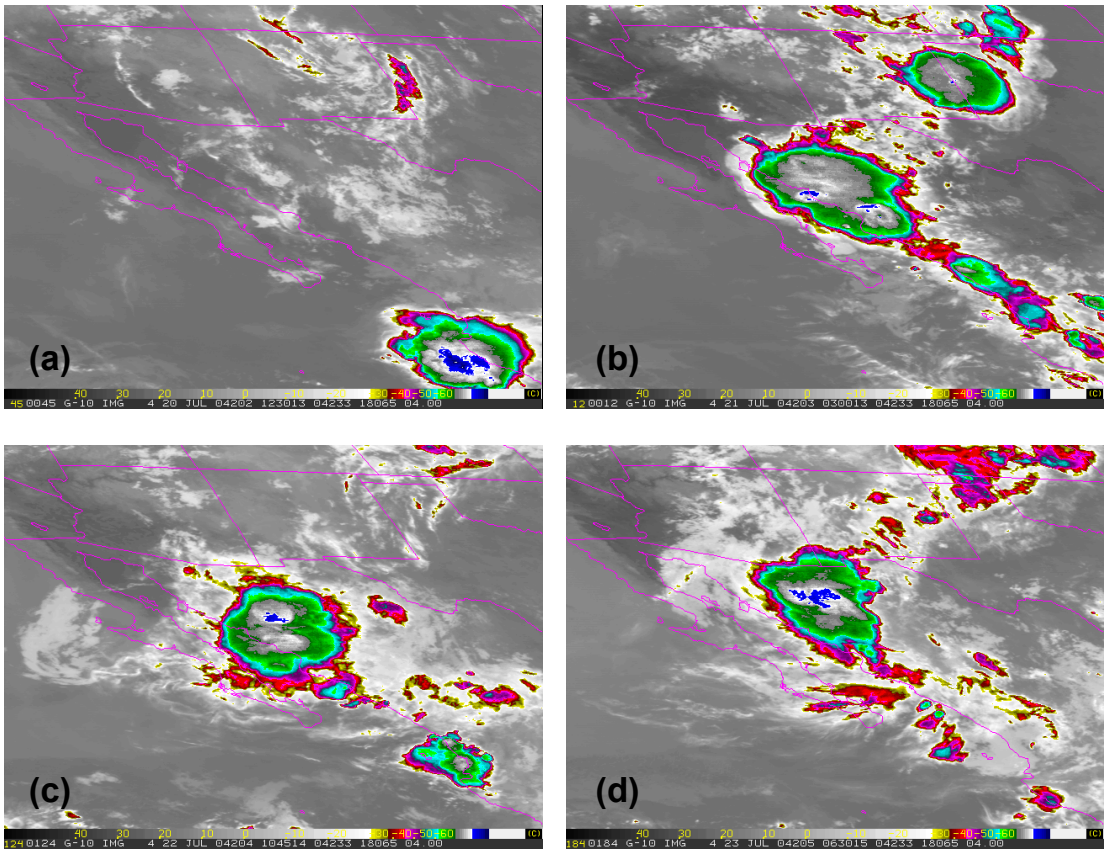


Figure 24: Same as in Fig. 23, except at (a) 1230 UTC 20 July, (b) 0300 UTC 21 July, (c) 1045 UTC 22 July, and (d) 0630 UTC 23 July.

On 23 July (Fig. 24d), yet another MCS develops and is well-entrenched over the Sonoran Desert by 0630 UTC. The northward displacement of this MCS relative to those two days prior may be attributed to the northwest propagation of the 700 hPa easterly wave (Fig. 20). The MCS propagates to the south and slowly dissipates by late-morning as it reaches the GOC. Overall, the convective pattern during GS #2 is very repetitive

and the successive MCSs most likely helped continuously pump low-level moisture northward, such that extremely limited convection finally fired over southeast Arizona by 2000 UTC 23 July (not shown). After viewing successive IR satellite images, the convective development during these several days rotated clockwise around the subtropical high, further aided by the cyclonic circulation provided by the easterly wave to the southeast.

# CHAPTER 5

# GULF SURGE VERTICAL AND HORIZONTAL STRUCTURE

## 5.1 Vertical Structure as Viewed by the ISS Profilers

Prior to the NAME, no wind profilers had ever been placed along the GOC, thus limiting the extent to which gulf surge vertical structure could be understood. Up to this point, Douglas and Leal (2003) have provided the most comprehensive look at gulf surge vertical structure using 12-h rawinsonde data at Empalme over nine years (see Section 2.4 for further discussion). Therefore, the three profiler units positioned at each of the ISS sites and the R/V Altair from 1 July – 15 August 2004 provide a high resolution (i.e. half- hour) first-look at the structure and temporal evolution of the wind signature aloft associated with gulf surge passage. In this section, wind profiler data (including merged surface winds) are presented at the three ISS sites up to 2 km from two days before to two days after day of gulf surge onset at Puerto Peñasco during GS #1 and at only the two northernmost ISS sites during GS #2 for reasons discussed below. In addition, results from the R/V Altair are discussed for GS #1, but not shown since significant features more or less qualitatively agree with those wind signatures depicted at Los Mochis. Half-hour averaged data from the ISS enhanced surface observing stations are also presented to show related changes in surface temperature, dewpoint temperature, and pressure (see Sections 3.3.2 and 3.3.4).

*5.1.1 Gulf Surge #1*

The wind profiler time series in Fig. 25a shows a GOC LLJ wind signature between 1200 and 1800 UTC on 11 July (two days prior to GS #1) up to approximately 0.75 km at Puerto Peñasco. Its structure is similar to that described by Douglas (1995) and Douglas et al. (1998). Following the afternoon sea breeze on 12 July, two convective outflows precede the main gulf surge. The first occurs at approximately 0000 UTC 13 July, as evident in a strong wind shift from southwest to southeast, with maximum wind speeds between 7.5 and 10 m $s^{-1}$ up to 1.0 km. The second occurs at approximately 0400 UTC 13 July, with maximum wind speeds approaching 12.5 m $s^{-1}$ by 0500 UTC up to 0.75 km. Although the second outflow's initial flow direction is from the east, the winds soon turn to the southeast. Both of these outflow boundaries are associated with the thunderstorm complex that developed over the Sonoran Desert depicted in Fig. 23b.

Interestingly, before the local environment can completely recover from these two convective features, the main gulf surge initial front passes Puerto Peñasco at approximately 1000 UTC 13 July from the south-southeast with wind speeds between 10.0 and 12.5 m $s^{-1}$ centered about 0.75 km. Gradual intensification and deepening of this feature occurs, such that by 1400 UTC, maximum wind speeds approach 20 m $s^{-1}$ from the south-southeast near 0.75 km and are close to 10 m $s^{-1}$ from the south just shy of 2.0 km. It is important to note that the strongest winds remain aloft and that the surface signal is not as telling of gulf surge passage even though there is a slight strengthening and turning to the southeast. Overall, the most intense winds do not last long, as the gulf

surge wind signature significantly weakens by 0000 UTC 14 July, perhaps due to strong afternoon vertical mixing within the boundary layer associated with the diurnal signal of the surrounding deserts.

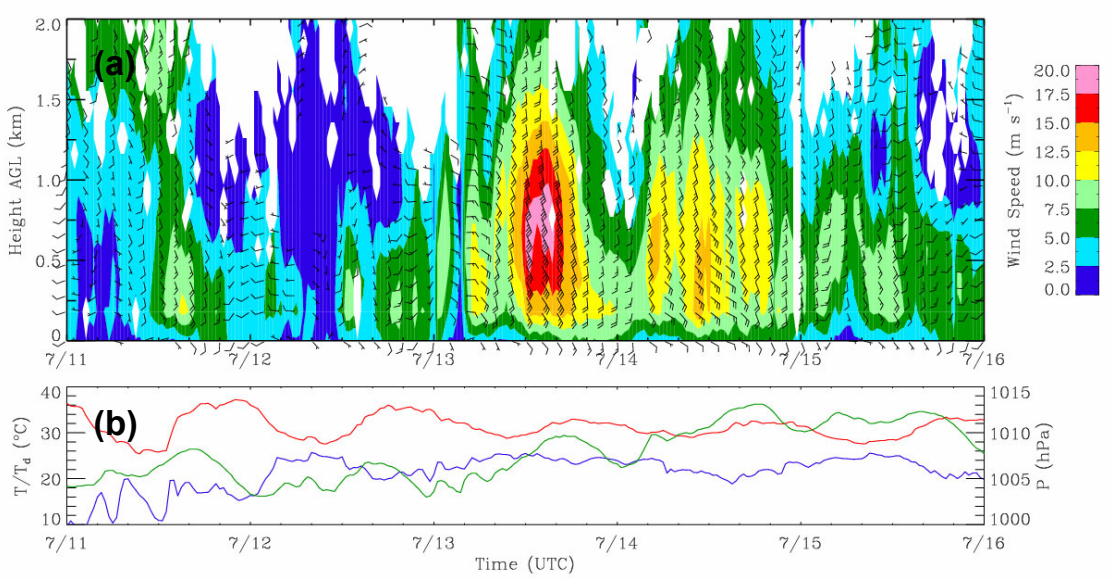


Figure 25: Puerto Peñasco wind profiler data (a) and surface data (b) from 0000 UTC 11 July – 0000 UTC 16 July. In (a), wind speed (colored contours) (m $s^{-1}$) is plotted every half hour and wind barbs every two hours. One full barb equals 5 m $s^{-1}$. Only those times and heights are plotted where NIMA/NWCA confidence values are greater than or equal to 0.5. In (b), surface temperature (red) (°C), dewpoint temperature (blue) (°C), and pressure (green) (hPa) are averaged over and plotted every half hour.

On 14 July, relatively strong flow dominates most of the day up to approximately 1.25 km with maximum speeds from the southeast approaching 15.0 m $s^{-1}$ around 0400 and 1000 UTC. Although this pattern further aids in advecting large quantities of cool moist air northward, it does not appear to be a continuation of the prior day's gulf surge. Rather, this signal is likely due to the northwest propagation of Tropical Storm Blas (Figs. 18 and 23d). By 15 July, the local environment slowly begins to return to its pre-gulf surge condition.

Three important surface features emerge during the time examined in Fig. 25b. First, a strong diurnal thermal signature is visible in the temperature trace during each day. However, this signal is significantly weakened after gulf surge onset as evident in the less extreme daily maximum and minimum temperatures. Interestingly, there also appears to be no significant decrease in the surface temperature concurrent with gulf surge onset, in contrast to the results of Hales (1972) and Brenner (1974). Second, although there is a marked increase in dewpoint temperature early on 12 July for reasons that remain uncertain, there is no dramatic increase associated with gulf surge onset. This has interesting implications for those previous studies that used surface dewpoint temperature data at Yuma to identify gulf surge passages (see Section 2.2 for further discussion). Third, although there are several peaks that make up the pressure curve, there is an overall pattern of pressure increases, especially after gulf surge onset. In fact, there is an approximately 7 hPa increase from prior to surge onset to a maximum value on 14 July.

The overall wind patterns at Bahia Kino on 11-12 July (Fig. 26a) are quite similar to those at Puerto Peñasco. The probable GOC LLJ signature discussed at Puerto Peñasco is stronger and deeper at Bahia Kino, stretching from approximately 1000 to 1400 UTC 11 July, with maximum wind speeds between 10 and 12.5 m $s^{-1}$ from 0.5 to 1.0 km. In addition to the afternoon sea breeze on 12 July, there occurred a relatively strong convective outflow around 0600 UTC with the wind initially from the southeast at approximately 7.5 m $s^{-1}$, strengthening at times to near 12.5 m $s^{-1}$. This outflow was associated with the decaying phase of the MCS that developed near Los Mochis depicted in Fig. 23a.

Whereas gulf surge onset at Puerto Peñasco was preceded by numerous smaller wind maxima likely due to convective features in its vicinity, gulf surge onset at Bahia Kino appears abruptly at 0600 UTC 13 July. Given initial onset from the south-southeast between 5.0 and 7.5 m $s^{-1}$, the gulf surge signature quickly strengthens and deepens, such that at 1000 UTC 13 July, maximum wind speeds are near 20.0 m $s^{-1}$ from the south-southeast at 1.25 km with 10.0 m $s^{-1}$ winds approaching 1.75 km. Again, surface wind patterns are not as suggestive of gulf surge passage given only a slight strengthening and turning to the southeast. The strongest gulf surge-related winds last for approximately six hours, quickly weakening thereafter, again perhaps partly in response to the strong vertical mixing that occurs throughout the boundary layer between 1800 and 0000 UTC.

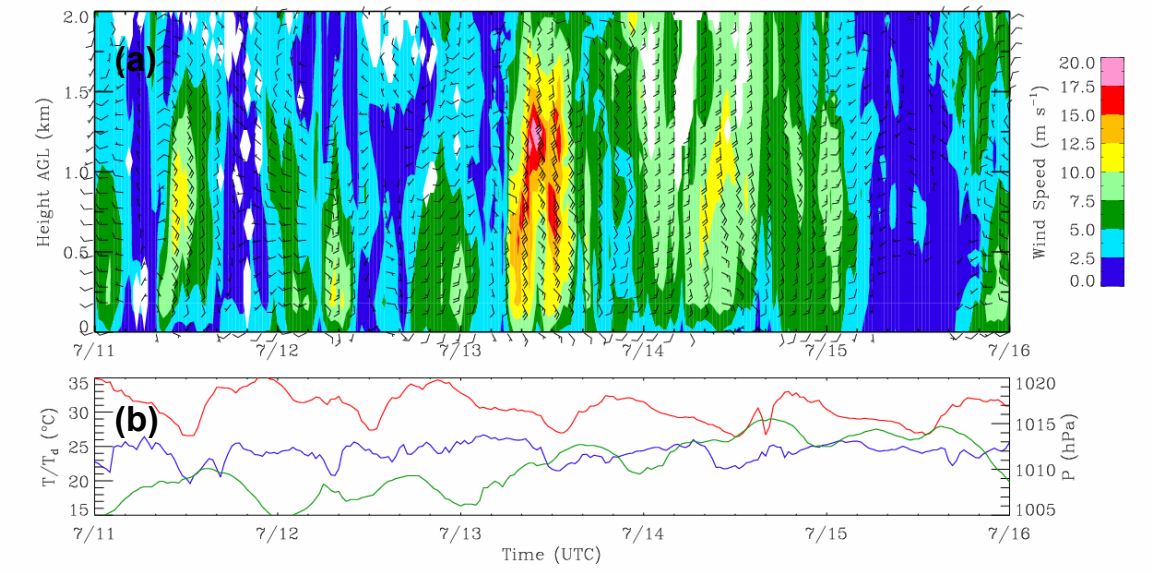


Figure 26: Same as in Fig. 25, except at Bahia Kino.

Relatively strong south-southeasterlies dominate most of the day on 14 July, again likely in response to Tropical Storm Blas. The maximum wind speeds are slightly weaker than those at Puerto Peñasco as well as centered about a higher altitude.

Maximum values between 10.0 and 12.5 m $s^{-1}$ slope upward with time (0.5 to 1.5 km) beginning at 0800 UTC and ending near 1200 UTC. Flow during 15 July is quite weak with no significant features present, except for the low-level afternoon sea breeze centered about 2200 UTC. The same three surface features detailed at Puerto Peñasco also qualitatively hold at Bahia Kino (Fig. 26b), although the weakening of the diurnal thermal signature is not as impressive and the surface pressure increase is approximately 8-9 hPa.

The overall flow patterns throughout the time period examined are very different at Los Mochis (Fig. 27a) compared to those at Puerto Peñasco and Bahia Kino. There is no GOC LLJ signal on 11 July, although a strong sea breeze is evident primarily below 0.5 km centered about 2200 UTC. In addition, two convective outflows pass the site. The first occurs at 1600 UTC 12 July as evident in the strong southeasterly wind stretching up to 1.5 km, albeit stronger near the surface. Also visible at the R/V Altair at 1400 UTC up to 1.0 km with maximum winds near 15.0 m $s^{-1}$ (not shown), this outflow boundary was associated with a few small, yet very intense thunderstorms that developed near Mazatlan shortly after the convection depicted in Fig. 23a. The second occurs at approximately 0400 UTC 13 July as evident in the strong wind shift from southerly to southeasterly with maximum wind speeds near 10.0 m $s^{-1}$. The strong southeast to northwest line of thunderstorms that developed along the SMO in Sinaloa prior to this time were most likely responsible (see Fig. 23b) for this outflow.

The exact structure of the second convective outflow is more difficult to determine since it is embedded within continuous relatively strong (~ 7.5 to 10.0 m $s^{-1}$) south-southeasterly flow up to 2.0 km that begins around 0000 UTC 13 July and continues until 1200 UTC. A similar pattern exists at the R/V Altair from approximately 1600 UTC 12 July to 0400 UTC 13 July, yet is primarily confined to heights above 0.5 km (not shown). Since the overall structures and intensities of these signals are quite different than those gulf surge wind signatures at Bahia Kino and Puerto Peñasco (Figs. 25a and 26a), it is difficult to determine whether or not the southern sites captured the same northward propagating disturbance as depicted at Bahia Kino and Puerto Peñasco.

NOAA WP-3D aircraft measurements during a flight along the GOC as a part of SWAMP-1990 suggest that the height of maximum southerly winds associated with the gulf surge examined increased from north to south (Stensrud et al. 1997). Even though wind speeds are significantly less along the southern gulf compared to the north throughout 13 July, this vertical structure appears to roughly emerge when comparing the heights of the maximum winds between the northern ISS sites (Figs. 25a and 26a) and Los Mochis (Fig. 27a). To account for the vast differences in wind speed, it is quite possible that the gulf surge is significantly enhanced by the GOC LLJ as it propagates north, since as suggested by Douglas (1995), the LLJ may not significantly extend south of the northern GOC. Thus, given the current observations combined with the results of past studies, gulf surge passage along the southern GOC cannot be ruled out for GS #1. However, if the wind signatures at Los Mochis and R/V Altair are that of the gulf surge,

extensive modifications to its overall structure and intensity must have occurred by the time it approached Bahia Kino and Puerto Peñasco.

The strong southeasterly flow primarily above 1.0 km from 2200 UTC 13 July to approximately 1200 UTC 14 July at Los Mochis is undoubtedly due to the passage of Tropical Storm Blas (Fig. 18). It appears that this signal is much weaker below 1.0 km, yet similar patterns associated with Tropical Storm Blas on 14 July at the northern ISS sites maintain some of their more robust features nearer the surface. As discussed above, this may be due to an enhancement of the flow by the GOC LLJ along the northern gulf. Although it is beyond the scope of this study to fully attempt to separate the varying flow effects due to synoptic, GOC LLJ, and gulf surge phenomenon, it is a topic that should be investigated in future work. Otherwise, flow at Los Mochis is weak on 15 July until strong northerlies develop by 1000 UTC from the surface up to 2.0 km.

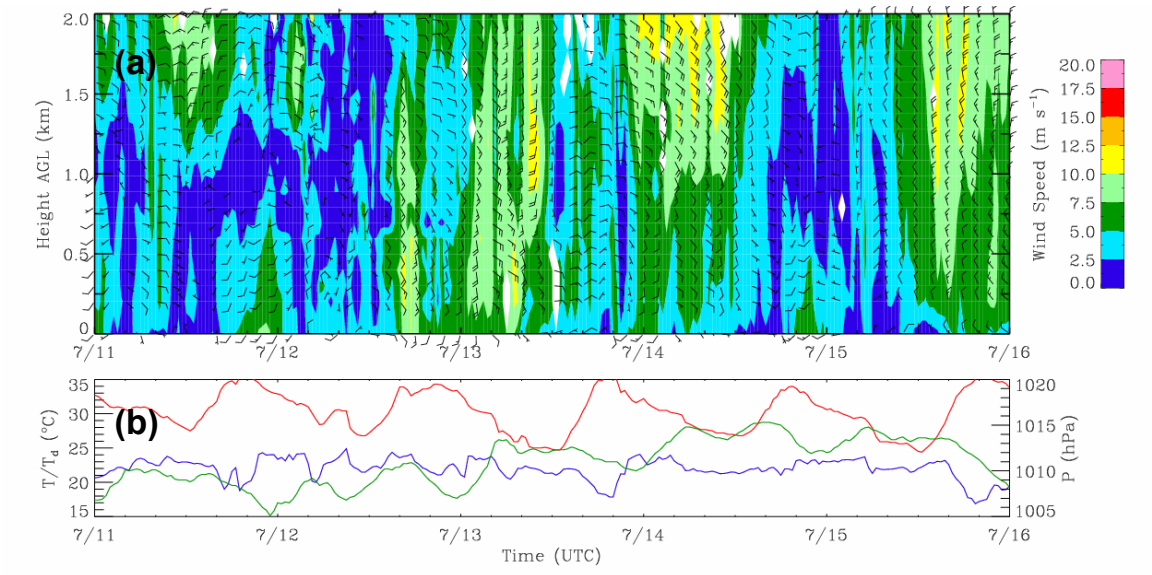


Figure 27: Same as in Figs. 24 and 25, except at Los Mochis.

Of the three surface features observed at Puerto Peñasco and Bahia Kino, only two occur at Los Mochis (Fig. 27b). First, there is little change in the dewpoint temperature. Second, there is a large pressure increase (~ 8.0 hPa) beginning at 0000 UTC 13 July and maxing out by approximately 1600 UTC 14 July. Although the initial substantial pressure increase beginning around 0000 UTC 13 July is most likely associated with the convective outflow that passed the site at 0400 UTC, recall that the northwest propagation of surface pressure anomalies depicted in Fig. 22 may reflect gulf surge passage on 13 July, especially along the southern gulf. Unfortunately, high resolution pressure data was not collected onboard the R/V Altair to allow for detailed comparisons with the other sites. Finally, it is interesting to note that the diurnal thermal signal at Los Mochis does not weaken throughout the examined period. This is perhaps due to the more elevated wind signature or the possibility that the surge's near surface cooling was limited to areas closer to the waters of the GOC, and thus not fully resolved at Los Mochis due to the site's more inland location. At this point, due to the uncertainties surrounding the gulf surge characteristics along the southern GOC, subsequent analyses presented in Chapter 6 for GS #1 will be largely limited to the northern gulf, where there seems to be better continuity of features between Bahia Kino and Puerto Peñasco.

### *5.1.2 Gulf Surge #2*

Given the vast synoptic and convective differences between GS #1 and GS #2, it is not surprising that the gulf surge wind signatures for GS #2 are also markedly different than those associated with GS #1. The pre-gulf surge environment on 19-20 July is very

benign at Puerto Peñasco (Fig. 28a). Besides sea breeze circulations, no flow features of significant interest, including convective outflows transpire. Seemingly abrupt, however, gulf surge onset occurs at approximately 0800 UTC 21 July, as evident in the strong south-southeasterly wind up to 0.75 km. This feature deepens slightly and intensifies, perhaps due to the influence of the GOC LLJ as discussed above for GS #1, such that by 1100 UTC, the strongest winds are located between 0.25 and 0.5 km above ground level and approach 17.5 m $s^{-1}$, while winds between 5.0 and 7.5 m $s^{-1}$ barely extend beyond 1.0 km. As with GS #1, associated surface winds only strengthen slightly and shift to the southeast. By 1800 UTC, significant weakening occurs and the gulf surge signature appears to merge with that of the afternoon sea breeze signal. Any remnants of the gulf surge become completely indiscernible shortly after 0000 UTC 22 July. Although both gulf surges maintain their greatest intensity for approximately eight hours at Puerto Peñasco, GS #2 is significantly shallower than GS #1 – almost by 500 m.

Interestingly, a secondary gulf surge-type wind signature develops on 22 July. This feature is most likely related to the large MCS that developed over the GOC coastal plain depicted in Fig. 24c. Initial onset appears to occur at approximately 0800 UTC, as the winds strengthen slightly and turn to the southeast in the lowest 0.5 km. Steady intensification and deepening occur over the following ten hours, such that by 1800 UTC wind speeds as high as 17.5 m $s^{-1}$ reach 1.25 km and a very confined area centered about 0.75 km nears 17.5 to 20.0 m $s^{-1}$. Areas of greatest intensity weaken quickly afterwards. However, southerly flow of 12.5 m $s^{-1}$ or less remains up to approximately 0.75 km until 0600 UTC 23 July. Although the 22 July wind surge is deeper and stronger than that on

21 July, it is important to emphasize that initial gulf surge onset for GS #2 still occurred on 21 July. Multiple relatively strong south-southeasterly pulses dominate much of the remainder of 23 July up to 1.25 km, most likely associated with the MCS near the Sonoran Desert depicted in Fig. 24d.

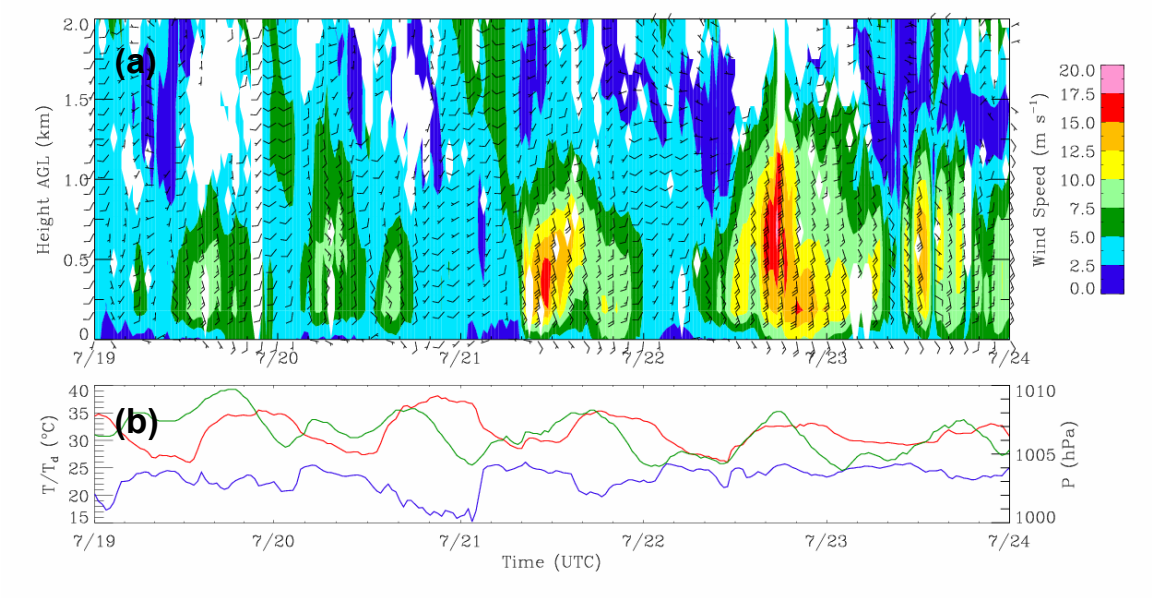


Figure 28: Puerto Peñasco wind profiler data (a) and surface data (b) from 0000 UTC 19 July – 0000 UTC 24 July. In (a), wind speed (colored contours) (m s$^{-1}$) is plotted every half hour and wind barbs every two hours. One full barb equals 5 m s$^{-1}$. Only those times and heights are plotted where NIMA/NWCA confidence values are greater than or equal to 0.5. In (b), surface temperature (red) (°C), dewpoint temperature (blue) (°C), and pressure (green) (hPa) are averaged over and plotted every half hour.

The surface changes associated with gulf surge passage aloft during GS #2 (Fig. 28b) are not as obvious as those during GS #1. First, there is a slight weakening of the thermal diurnal signal after gulf surge passage, similar to that of GS #1. The shallower depth of GS #2 may account for the less dramatic changes. Second, dewpoint temperatures do not change drastically. However, for unknown reasons, there is a marked jump in the surface dewpoint temperature at approximately 0200 UTC 21 July that does not coincide with

gulf surge onset. Third, surface pressures actually decrease slightly during the time period examined, rather than increase as was the case for GS #1.

One of two or perhaps a combination of reasons may account for the very different surface pressure trends between GS #1 and GS #2. First, the depth of cooling associated with GS #2 may not have been extensive enough to significantly alter the surface pressure. Second, northerly flow between the impinging 700 hPa easterly wave to the south and subtropical high to the north (Fig. 20) may have resulted in warm air advection over a significant depth overlying the gulf surge-related cooling. From hypsometric considerations, this deeper warm layer could offset surface pressure increases associated with a shallow cool layer nearer the surface. The latter theory is suggestive of the importance of synoptic circulation patterns, similar to that of Tropical Storm Blas increasing surface pressures during GS #1 on 14 July.

Flow patterns on 19-20 July at Bahia Kino (Fig. 29a) are very similar to those at Puerto Peñasco. No significant features exist except for the well-defined south-southwesterly sea breeze that generally does not extend above 0.5 km and peaks in maximum intensity within a few hours of 0000 UTC each day. However, gulf surge onset interrupts the afternoon sea breeze centered about 0000 UTC 21 July shortly after 0300 UTC 21 July, as evident in the turning of the winds from near westerly to south-southeasterly. Onset is accompanied by wind speeds between 12.5 and 15.0 m $s^{-1}$ from just above the surface up to approximately 1.0 km – slightly deeper than the initial onset at Puerto Peñasco. In addition, whereas the gulf surge signature at Puerto Peñasco

deepens and strengthens with time, the related signature at Bahia Kino only deepens, but maintains its greatest intensity at onset. Due to the relatively early time of surge onset, this pattern may be due to the lack of LLJ enhancement of the surge signature. By 0800 UTC wind speeds approaching 10.0 m $s^{-1}$ extend just above 1.5 km, yet weakening soon follows at all levels, such that the gulf surge signature is no longer visible by 1400 UTC.

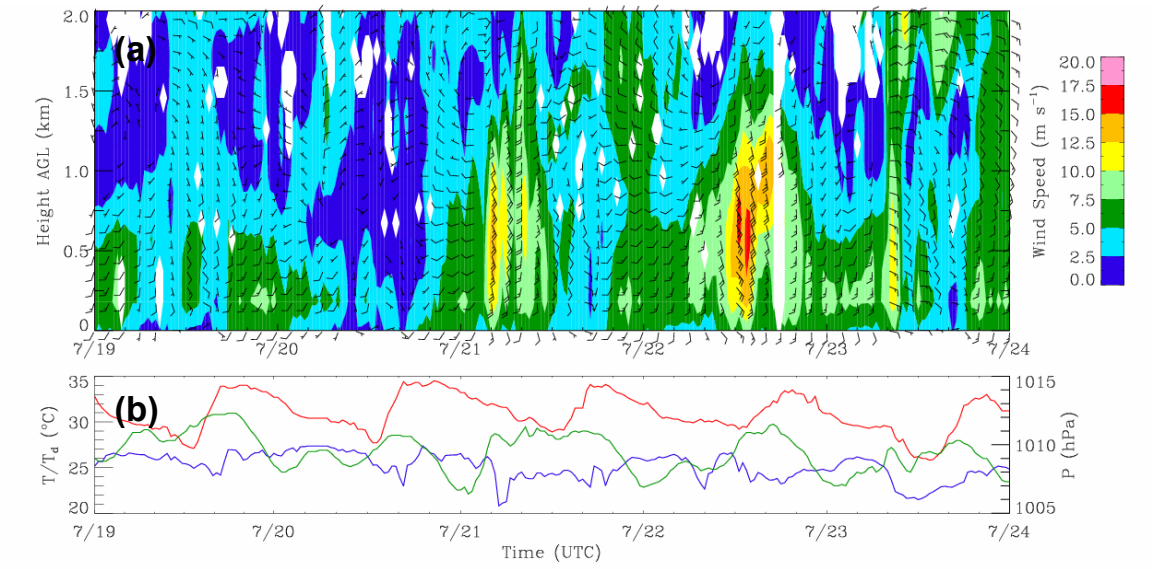


Figure 29: Same as in Fig. 28, except at Bahia Kino.

The secondary gulf surge-type wind signature on 22 July at Puerto Peñasco is also visible at Bahia Kino. Sandwiched between diurnal sea breeze circulations centered about 0000 UTC 22 July and 0200 UTC 23 July, the wind signature's southerly maximum speeds approach 17.5 m $s^{-1}$ by 1200 and 1400 UTC between 0.25 and 0.75 km after initial intensification around 0800 UTC 22 July. Because of the sea-breeze circulations, it is difficult to discern surge onset. Wind speeds from 7.5 to 10.0 m $s^{-1}$ reach almost 1.5 km during the surge's maximum vertical extent and intensity. Gradual weakening occurs after 1400 UTC such that by 0000 UTC 23 July wind speeds no greater

than 10.0 m $s^{-1}$ are observed below 0.5 km. Overall flow patterns on 23 July are not as robust as those at Puerto Peñasco. However, a strong convective outflow associated with the MCS depicted in Fig. 24d passes the site at approximately 0800 UTC, as evident in strong southeasterly winds up to 0.75 km. In addition, Bahia Kino surface patterns match qualitatively well with those described at Puerto Peñasco, except that any weakening of the diurnal thermal signal due to gulf surge passage is extremely weak (Fig. 29b).

Neither the gulf surge wind signature from 21 July nor 22 July is visible in the Los Mochis profiler data (not shown). In fact, the only interesting feature that occurs during the five-day period examined in Figs. 28 and 29 is an afternoon south-southwesterly sea breeze up to 0.5 km, but sometimes extending to 1.0 km. From this, it is evident that GS #2 was limited to the northern GOC. In addition, one significant difference to note between the flow patterns depicted in the above figures for both surges with those of previous studies is that neither GS #1 nor GS #2 were preceded by low-level strong and continuous northerly flow, as shown in the analyses of Douglas and Leal (2003) (Figs. 6 and 8). However, since the results from Douglas and Leal (2003) were composite-based as opposed to examining individual events, it is possible that the two events in this study are atypical in a climatological sense.

### 5.2 Gulf Surge Atmospheric Modifications as Viewed by Rawinsonde Data

In addition to those gulf surge onset surface characteristics described by Hales (1972) and Brenner (1974) (see Section 2.2 for further discussion), the authors noted that gulf

surge-related cooling and moistening is greatest just above the surface and decreases in intensity with height. Douglas and Leal (2003) supported this observation in their compositing analyses using Empalme rawinsonde data (see Section 2.4 for further discussion). Therefore, as a means to investigate the relative gulf surge atmospheric effects (cooling/moistening) and vertical structure in time before and after onsets, half-hour linearly interpolated rawinsonde data (see Section 3.3.1) were examined at six sites along the GOC eastern shore up to 500 hPa from 0000 UTC 10 July to 0000 UTC 17 July for GS #1 (Fig. 30) and from 0000 UTC 18 July to 0000 UTC 25 July for GS #2 (Fig. 31). More specifically, potential temperature and moisture flux (meridional wind component multiplied by mixing ratio) anomalies from 5 July – 16 August means were studied to determine areas of anomalous warming/cooling and northward (positive)/ southward (negative) moisture advection.

*5.2.1 Gulf Surge #1*

Prior to gulf surge onset on 13 July, there appear to be no cohesive moisture flux anomalies propagating between the sites (Fig. 30a-f). However, there is a distinct anomalous warming primarily confined below 600 hPa that dominates most times at each site until gulf surge onset. This warming is especially strong near the surface (+ 4-8°C) in the late afternoons (0000 UTC) due to strong diurnal heating; except for at Los Mochis where it is centered near 800 hPa, and at Mazatlan where it is not nearly as strong. This overall pattern matches qualitatively well with those results put forth by Douglas and

Leal (2003). Their results show anomalous warming of + 2.5°C peaking one day prior to gulf surge onset around 950 hPa at Empalme (Fig. 9).

This overall pattern is abruptly interrupted by GS #1 during the early morning hours on 13 July. Gulf surge onset is easily recognizable by the large maxima of anomalous positive moisture flux and associated cooling from Yuma south to Empalme. These changes are primarily greatest below 800 hPa, in agreement with Douglas and Leal (2003), and last for several hours. However, the greatest anomalous cooling (- 4-8°C) and positive moisture flux (> + 175 m g $s^{-1}$ $kg^{-1}$), which are much stronger than those values provided by Douglas and Leal (2003) (Fig. 9), occur at Puerto Peñasco and Bahia Kino. This is not surprising recalling the gulf surge wind profiler signatures depicted in Figs. 25a and 26a. The less robust signal at Yuma can be related to the fact that Hales (1972) and Brenner (1974) noted that gulf surge intensity weakens as it fans out over the low deserts of Arizona. In addition, relatively strong positive moisture flux anomalies occur at Los Mochis from 1200 UTC 12 July to 1200 UTC 13 July, yet are not accompanied by anomalous cooling until shortly after 0000 UTC 13 July, albeit weak. As with the wind profiler data, it is difficult to discern gulf surge passage along the southern gulf from the thermodynamic anomalies.

Although significant low-level cooling did not occur at Los Mochis or Mazatlan in tandem with gulf surge passage at the northern sites, it is interesting to note the relatively strong cooling (- 2-4°C) that occurs centered about 700 hPa beginning near 0000 UTC 13 July at these sites. Also visible at Empalme around 1200 UTC 13 July, this cooling

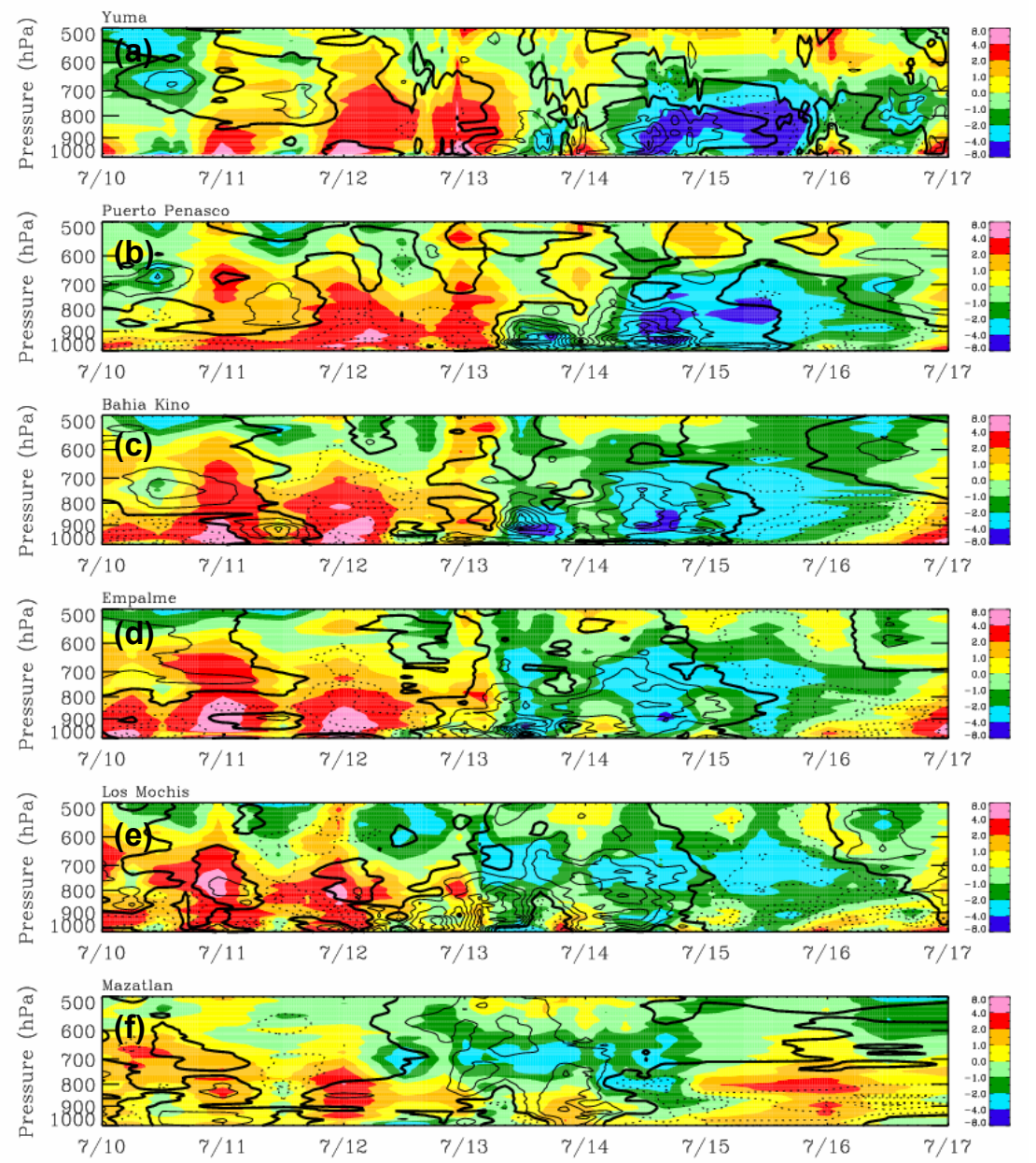


Figure 30: Half-hour interpolated rawinsonde potential temperature and moisture flux anomalies at Yuma (a), Puerto Peñasco (b), Bahia Kino (c), Empalme (d), Los Mochis (e), and Mazatlan (f) from 0000 UTC 10 July to 0000 UTC 17 July. Anomalies are calculated using 5 July – 16 August means. Colored contours represent potential temperature anomalies (K). Solid (dotted) thin black curves represent positive (negative) moisture flux anomalies (m g $s^{-1}$ $kg^{-1}$). Thick solid black curve equals 0 m g $s^{-1}$ $kg^{-1}$, with each successive contour at (±) 25 m g $s^{-1}$ $kg^{-1}$ intervals.

signal is perhaps associated with the northward advection of cool air from the tropical east Pacific Ocean via Tropical Storm Blas. However, mid-tropospheric moistening and evaporational cooling from convection propagating off the SMO may also contribute to this trend. Interestingly, though, the cooling is generally not accompanied by overtly strong concentrated areas of anomalous positive moisture flux, especially at Mazatlan. Nonetheless, the cooling continues for two to three days and deepens to encompass areas nearer the surface by 14 July.

As Tropical Storm Blas propagates northwest, its cooling and moistening effects are seen at Bahia Kino northward by 1200 UTC 14 July as a distinct and separate feature from that of the gulf surge a day prior. Accompanied by relatively strong positive moisture flux anomalies at this time (> + 100 m g $s^{-1}$ $kg^{-1}$), very strong cooling (- 4-8°C) from the surface up to about 800 hPa occurs with - 2-4°C of cooling up to 700 hPa. The positive moisture flux anomalies are associated with the strong south-southeasterly flow throughout the day on 14 July visible in the wind profiler data at the northern ISS sites (Figs. 25a and 26a). Although briefly interrupted around 0000 UTC 15 July due to the diurnal signal, the intense cooling trend related to Tropical Storm Blas continues without significant anomalous positive moisture flux during much of 15 July. Finally, a well-defined anomalous negative moisture flux develops primarily below 700 hPa at most sites by 0000 UTC 16 July.

It is interesting to note that the positive surface pressure anomalies depicted in Fig. 22 over the Sonoran Desert agree extremely well with the timing and strength of maximum

anomalous cooling from Bahia Kino northward in Fig. 30. Additionally, surface pressure rises depicted at the ISS sites (Figs. 25b, 26b, and 27b) correspond qualitatively well to peaks in maximum anomalous cooling in Fig. 30. These results are not surprising since surface pressure quantifies the weight of a column of air above the surface, which is dependent on the column's relative temperature. Thus, cool (warm) air in a layer results in pressure increases (decreases).

*5.2.2 Gulf Surge #2*

Those differences between GS #1 and GS #2 detailed by the synoptic circulation patterns, convective tendencies, and wind profiler data described above are further exemplified when noting areas of anomalous warming/cooling and northward/southward moisture advection. As with GS #1, there appear to be no cohesive moisture flux anomalies propagating between sites prior to gulf surge onset during GS #2 (Fig. 31a-f), although weak disorganized negative anomalies from 18-20 July centered about 800 hPa due appear to dominate Bahia Kino southward. Otherwise, from Empalme north to Puerto Peñasco, extensive anomalous warming occurs to some degree below approximately 600 hPa with the strongest values (+ 2-4°C or greater) centered about 0000 UTC 20 and 21 July extending at least to 800 hPa.

At Yuma, relatively weak anomalous warming above the surface on 18 July extends up to 800 hPa and eventually deepens to 700 hPa by 19 July. Areas nearer the surface from 18-20 July are dominated by the strong thermal diurnal tide with alternating

anomalous warm/cool couplets at 0000 and 1200 UTC respectively. However, on 20 July, anomalous warming does intensify (+ 2-4°C) between 800 and 700 hPa at Yuma. Although pre-gulf surge anomalous warming occurs at Los Mochis and Mazatlan on 18-20 July, it is not as significant as that at the northern sites, especially at lower levels. Maximum anomalous warming at both sites occurs from approximately 0000 UTC 19 July to 0000 UTC 21 July centered about 700 hPa, albeit slightly less robust at Mazatlan.

The overall qualitative pattern of anomalous negative moisture fluxes and warming prior to gulf surge onset is quickly disrupted by the early morning hours on 21 July at Puerto Peñasco and Bahia Kino at low-levels. As was the case with GS #1, this is evident in the maxima of anomalous positive moisture fluxes (> + 125 m g $s^{-1}$ $kg^{-1}$) and relatively strong cooling (- 2-4°C) exclusively below 900 hPa, further emphasizing the much shallower extent of GS #2 as compared to GS #1. The gulf surge signature at Yuma is very weak and appears very similar to the near surface diurnal thermal patterns of previous days. This weakness can most likely be attributed to the loss of gulf surge intensity as it traverses Arizona's low deserts as well as the much shallower extent of the surge. In addition, although seemingly related to the gulf surge signature, the relatively strong low-level cooling at Empalme centered about 1200 UTC 21 July is most likely due to the passage of a strong convective outflow from the east or northeast since the cooling is not accompanied by positive anomalous moisture fluxes. The gulf surge associated cooling and northward moisture advection is short-lived, such that by 0000 UTC 22 July, it is no longer discernable.

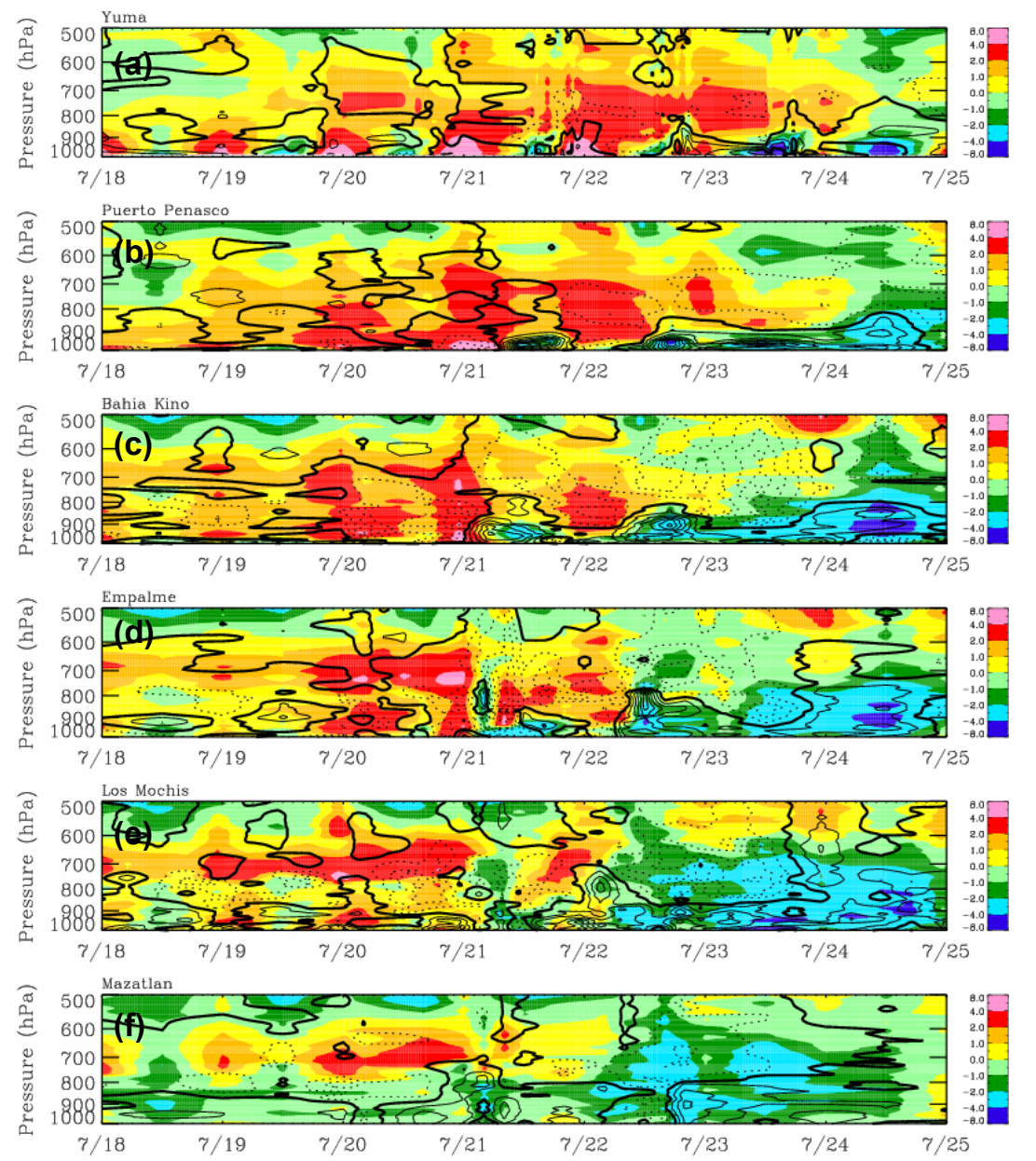


Figure 31: Same as in Fig. 30, except from 0000 UTC 18 July to 0000 UTC 25 July.

After initial gulf surge onset, the secondary gulf surge-type signature on 22 July described in the wind profiler data at Puerto Peñasco and Bahia Kino (Figs. 28a and 29a) is evident as strong anomalous cooling (- 2-4°C or greater) and northward moisture advection (> + 125 m g $s^{-1}$ $kg^{-1}$) from Empalme to Puerto Peñasco up to approximately 800 hPa as it propagates north between 1200 and 1800 UTC. From Bahia Kino to Yuma,

subsequent days are dominated by relatively strong anomalous cooling (- 2-4°C or greater) at low-levels (below 900 hPa on 23 July and up to 800 hPa on 24 July) with occasional bursts of anomalous positive moisture flux (> + 50 m g $s^{-1}$ $kg^{-1}$) generally centered about 1200 UTC. These bursts are most likely associated with the repetitive occurrence of MCSs along the GOC coastal plain as depicted in Fig. 24 during this time as well as the northern GOC LLJ.

Above these features lie a significant depth (100 hPa or greater) of anomalous warming as an extension from pre-gulf surge conditions until approximately 1200 UTC 24 July at Yuma, 0000 UTC 24 July at Puerto Peñasco, and 0000 UTC 23 July at Bahia Kino. It is important to note that it is likely this greater depth of anomalous warming above the shallower anomalous low-level cooling that aided in preventing surface pressures from increasing throughout the gulf surge period examined (Figs. 28b and 29b). In addition, the mid-tropospheric synoptic circulation patterns at the time, which were dominated by relatively strong northerly component flow over much of the GOC between the subtropical high and easterly wave, may have allowed the pre-gulf surge anomalous warming to remain entrenched due to northerly warm air advection, as discussed in Section 5.1.2.

Interestingly, beginning around 0000 UTC 21 July and extending until 1200 UTC 23 July, relatively strong anomalous negative moisture flux (< - 50 m g $s^{-1}$ $kg^{-1}$) dominates levels 800 hPa and above from Los Mochis to Bahia Kino when not interrupted by low-level cool moisture bursts. These vast areas of anomalous negative moisture flux are

most likely associated with the northerly flow downstream from the westerly propagating easterly wave's axis depicted at 700 hPa in Fig. 20. Cohesive thermal anomalies associated with this significant moisture flux anomaly are not necessarily apparent until about 1200 UTC 23 July. At this time, relatively strong anomalous cooling (- 2-4°C) from the surface up to approximately 700 hPa at Los Mochis, 750 hPa at Empalme, and 850 hPa at Bahia Kino emerges. This thermal feature may be due to substantial convective evaporational cooling. Significant anomalous cooling up to about 700 hPa continues until 0000 UTC 25 July with its greatest intensity around 1200 UTC 24 July. This signal is an extension of a seemingly prominent moisture surge that reaches as far north as Yuma, evident in a reversal from negative to positive moisture flux anomalies around 2000 UTC 23 July at Bahia Kino, Empalme, and Los Mochis. Since Mazatlan is south of the easterly wave's center (Fig. 20), it is also important to note that the anomalous cooling (- 2-4°C) centered about 700 hPa during 22-23 July at Mazatlan may be attributed to weak cool air advection from northwesterly flow associated with the low's southwest quadrant.

Although the initial gulf surge onsets for GS #1 and GS #2 maintain some similarities to each other and to the qualitative results of Douglas and Leal (2003), the synoptic, mesoscale, and convective conditions affecting the core NAM region after onsets were vastly different for the two cases examined here. Combining the gulf surge taxonomies of Hales (1972) and Higgins et al. (2004), GS #1 would most likely be considered a strong wet surge, and GS #2 would most likely be considered a weak dry surge. The former strong and wet because of its relatively deep extent across much of the GOC, the

direct or indirect involvement of Tropical Storm Blas, and the convective development over the low-deserts of Arizona the day after surge onset. The latter weak and dry because of its relatively shallow extent, being completely confined to the northern GOC, and the lack of substantial convective development over Arizona/New Mexico in the subsequent days after gulf surge onset.

Of further interest from the information presented above is the fact that the gulf surges examined in this study appear to maintain their greatest intensity for a period less than 12 hours, yet synoptic flow patterns affect their surroundings for periods much longer than 12 hours. Assuming at most a rawinsonde launch schedule at any particular site of twice per day, and noting gulf surge passage times relative to these launches, it is quite possible that rawinsonde data used in previous analyses, especially those of Douglas and Leal (2003), may have been more representative of the synoptic environment rather than the gulf surge environment. Although firm conclusions cannot be made concerning past studies, future research endeavors should more closely consider the time resolution of their data or model runs if gulf surge temporal evolution is to be better understood.

### 5.3 Horizontal Structure as Viewed by the T1A Gridded Dataset

Due to the high vertical and temporal resolution of the wind profiler and rawinsonde data used for this study, it was quite easy to determine in great detail the vertical structure of the two gulf surges examined. However, the horizontal extent of these events is more difficult to resolve due to the somewhat course spatial resolution of the rawinsonde sites,

which formed the basis of the gridded datasets, and the fact that there are no observations located along northern Baja California or over the northern/central GOC waters (Fig. 12). Given this, it is still important to recall the significance and unprecedented nature of the gridded datasets over this region. In order to attempt to define the horizontal extent of GS #1 (GS #2), gridded data from the T1A domain were used to generate 900 hPa (950 hPa) maps showing heights, temperatures, mixing ratios, and wind vectors during the day of initial surge onset at Puerto Peñasco. The levels were chosen noting the approximate pressures from Figs. 30 and 31 in which gulf surge cooling and moistening were the strongest along the northern gulf. Longitude-pressure cross sections showing those parameters detailed in Figs. 30 and 31 are also examined at different latitudes to note relationships with the surrounding terrain features.

### *5.3.1 Gulf Surge #1*

At both 0000 and 0600 UTC, 900 hPa flow throughout the GOC and surrounding areas is light and variable north of Bahia Kino, yet slightly stronger from the south-southeast along the central and southern gulf (Fig. 32). This pattern could reflect the beginnings of the gulf surge as depicted in the Los Mochis profiler data (Fig. 27a). As a result of the relatively weak southerly flow along the northern gulf, the greatest moisture advection at these times is limited to areas surrounding the southern gulf, especially centered about Los Mochis. North-south thermal gradients along the GOC axis are quite large at both times, albeit somewhat stronger at 0000 UTC due to maximum daytime heating over the Arizona deserts. In addition, there are strong east-west thermal gradients

west of Baja California. Slightly cooler air had propagated northward within the GOC by 0600 UTC, as isotherms at 0000 UTC are displaced slightly to the north by 0600 UTC. However, whether this cooling is related to the diurnal cycle or gulf surge-related cooling is uncertain.

Major changes are seen at 1200 UTC, as gulf surge onset has passed both Bahia Kino and Puerto Peñasco by this time. The strongest wind vectors are from the southeast and stretch from Empalme north to Puerto Peñasco. In addition, it appears that the axis of the most intense flow is very near the GOC eastern shores, decaying somewhat over the coastal plains and Baja California. This result could very well be related to the location of the rawinsonde sites during the NAME field campaign and the multiquadric interpolation from these points in the gridded dataset. Complementing this hypothesis, NOAA WP-3D measurements along the northern GOC at approximately 1700 UTC 13 July suggest the greatest gulf surge-related moisture flux (meridional wind component multiplied by specific humidity) is located over the waters of GOC below 900 hPa and not necessarily along the gulf's eastern shores (not shown) (Higgins et al. 2006).

Primarily confined to those areas of strongest southeasterly flow, moisture advection is the most significant from Bahia Kino northward to the low deserts of Arizona and along the GOC eastern shores at 1200 UTC. It is also interesting to note the thermal changes that take place between 0600 and 1200 UTC associated with gulf surge horizontal structure. At 0600 UTC, the 24°C isotherm is located just north of Los Mochis across the GOC. By 1200 UTC, the gulf surge-related cooling displaces this

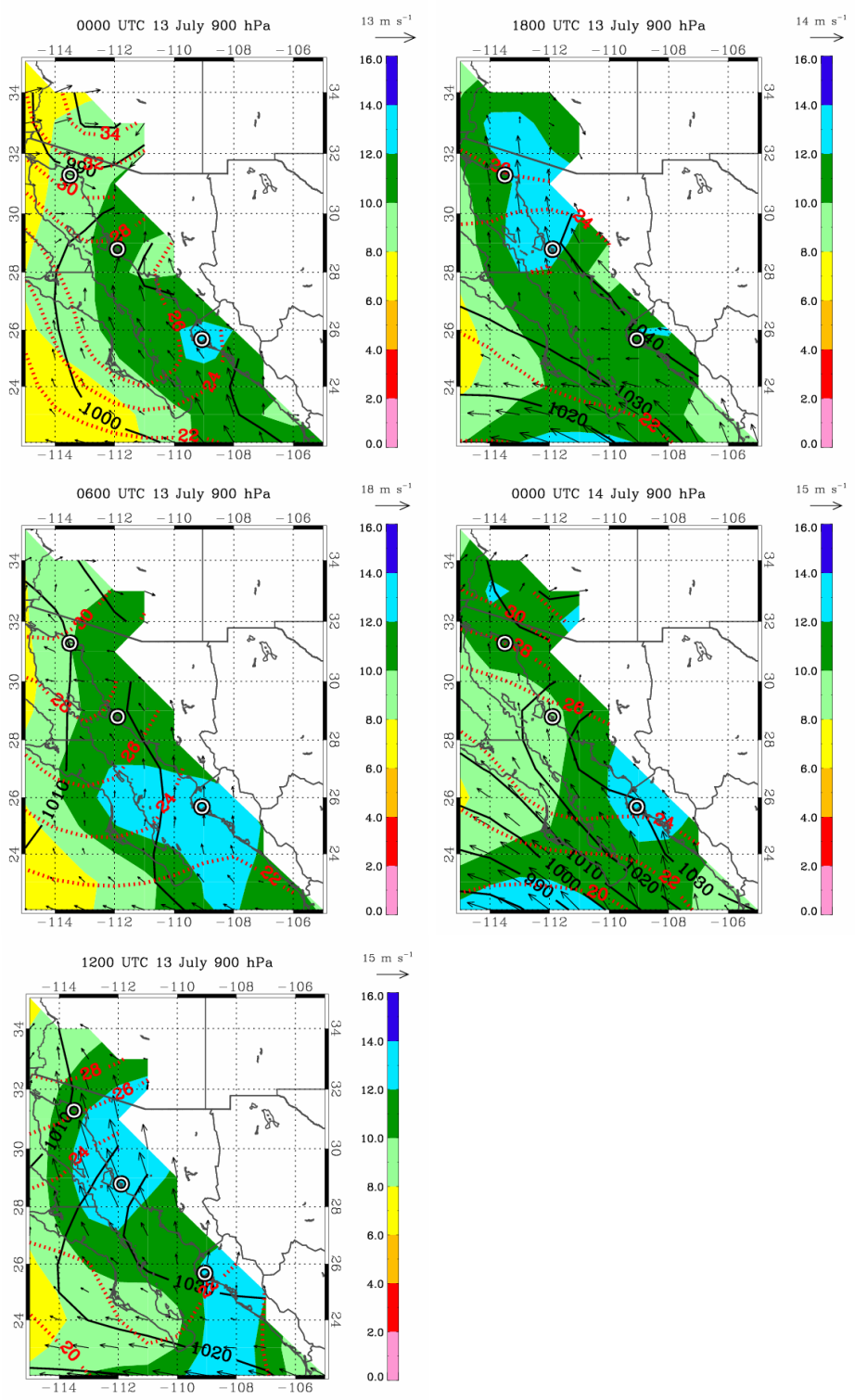


Figure 32: 900 hPa heights (10 m intervals) (black solid), temperatures (2°C intervals) (red dotted), mixing ratios (g $kg^{-1}$) (colored contours), and wind vectors (m $s^{-1}$) from 0000 UTC 13 July to 0000 UTC 14 July. White regions represent areas below the surface. Circles represent the locations of the three ISS sites.

isotherm north of Bahia Kino, resulting in a greater than 4°C cooling at 900 hPa at this site. However, the 22°C isotherm stretching across the mouth of the GOC at 0600 UTC moves very little by 1200 UTC, perhaps suggesting that gulf surge strength at this level and time is not as prominent along the southern gulf.

Although not as strong, the overall gulf surge horizontal structure described at 1200 UTC continues until 1800 UTC. However, the strongest winds from Empalme northward have shifted slightly to a more southerly direction. The most intense moisture advection has shifted slightly farther to the north as well, and the isotherm patterns remain more or less unchanged. The most significant change between these times is the intrusion of Tropical Storm Blas along the mouth of the GOC, as evident in the strong cyclonic flow. In fact, by 0000 UTC 14 July, the tropical disturbance now dominates the flow and moisture advection surrounding the GOC region as the gulf surge signature has since waned toward the north. In addition, thermal patterns at 0000 UTC 14 July seem to be slowly returning to pre-gulf surge conditions.

Examining longitude-pressure cross sections of potential temperature and moisture flux (meridional wind component multiplied by mixing ratio) anomalies from 5 July – 16 August means at 28°N, 30°N, and 32°N latitude up to 500 hPa at 1200 UTC 13 July (Fig. 33a-c) expand upon those results presented above. The gulf surge is evident in the strong positive moisture flux anomalies (at least 100 m g $s^{-1}$ $kg^{-1}$) and relatively strong anomalous cooling (- 2-4°C at 28°N, 30°N and - 0-1°C at 32°N) along the GOC stretching primarily between 110°W to 115°W and generally confined below 800 hPa. It

is also interesting to note that the gulf surge appears not to be connected to any other feature across the longitudinal domain and remains its own entity.

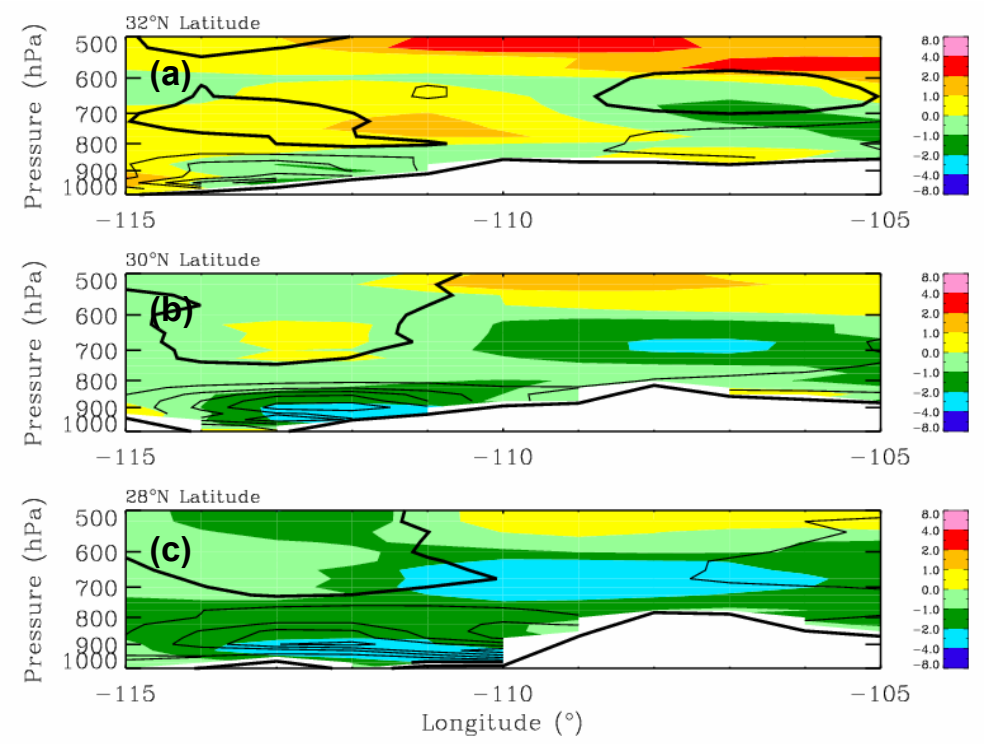


Figure 33: Longitude-pressure cross section of potential temperature and moisture flux anomalies at 32°N (a), 30°N (b), and 28°N (c) latitude at 1200 UTC 13 July. Anomalies are calculated using 5 July – 16 August means. Colored contours represent potential temperature anomalies (K). Solid (dotted) thin black curves represent positive (negative) moisture flux anomalies (m g $s^{-1}$ $kg^{-1}$). Thick solid black curve equals 0 m g $s^{-1}$ $kg^{-1}$, with each successive contour at (±) 25 m g $s^{-1}$ $kg^{-1}$ intervals. White regions represent areas below the surface.

In the vertical, the gulf surge does not extend above the local terrain maximum along the SMO. Horizontally, the surge is strongest along the eastern shores of the GOC at 30°N, as discussed above. Additionally, at 32°N, the surge is not strongest over the Colorado River Valley (114°W-115°W) as suggested by Hales (1972) and Brenner (1974), but rather just to the east of this area. When this structure is compared with the

contradicting aircraft results from Higgins et al. (2006), it appears most likely to be associated with the course spatial resolution of the rawinsonde data, which serves as the basis for the gridded datasets. At 28°N, it appears that the gulf surge is strongest over a broader area stretching from the GOC coastal plain to the eastern slopes of the Baja California Peninsular Range.

*5.3.2 Gulf Surge #2*

At 0000 UTC 21 July (Fig. 34), the overall 950 hPa flow and thermodynamic patterns match qualitatively well with those of the 0000 UTC mean state at 950 hPa (Fig. 16). Northwesterly flow dominates regions west of Baja California with a strong turning of the winds to south-southeasterly across the southern GOC. In addition, relatively strong onshore flow along the GOC coastal plain is visible throughout the central and northern gulf as a result of the strong sea breeze. Strong north-south and east-west thermal gradients exist along the GOC and west of Baja California respectively. Maximum moisture resides along the southern GOC, especially centered about Los Mochis.

GS #2 first emerges at 0600 UTC as relatively strong southeast winds centered and confined about Bahia Kino advect significant moisture northward. Light mesoscale offshore flow seems to dominate the GOC coasts south of this point with light and variable winds elsewhere. Thermal patterns change little from 0000 UTC and a more pronounced tongue of moisture (> 12.0 g $kg^{-1}$) exists along most of the eastern GOC. The gulf surge is fully developed by 1200 UTC, as strong southeast winds stretch from

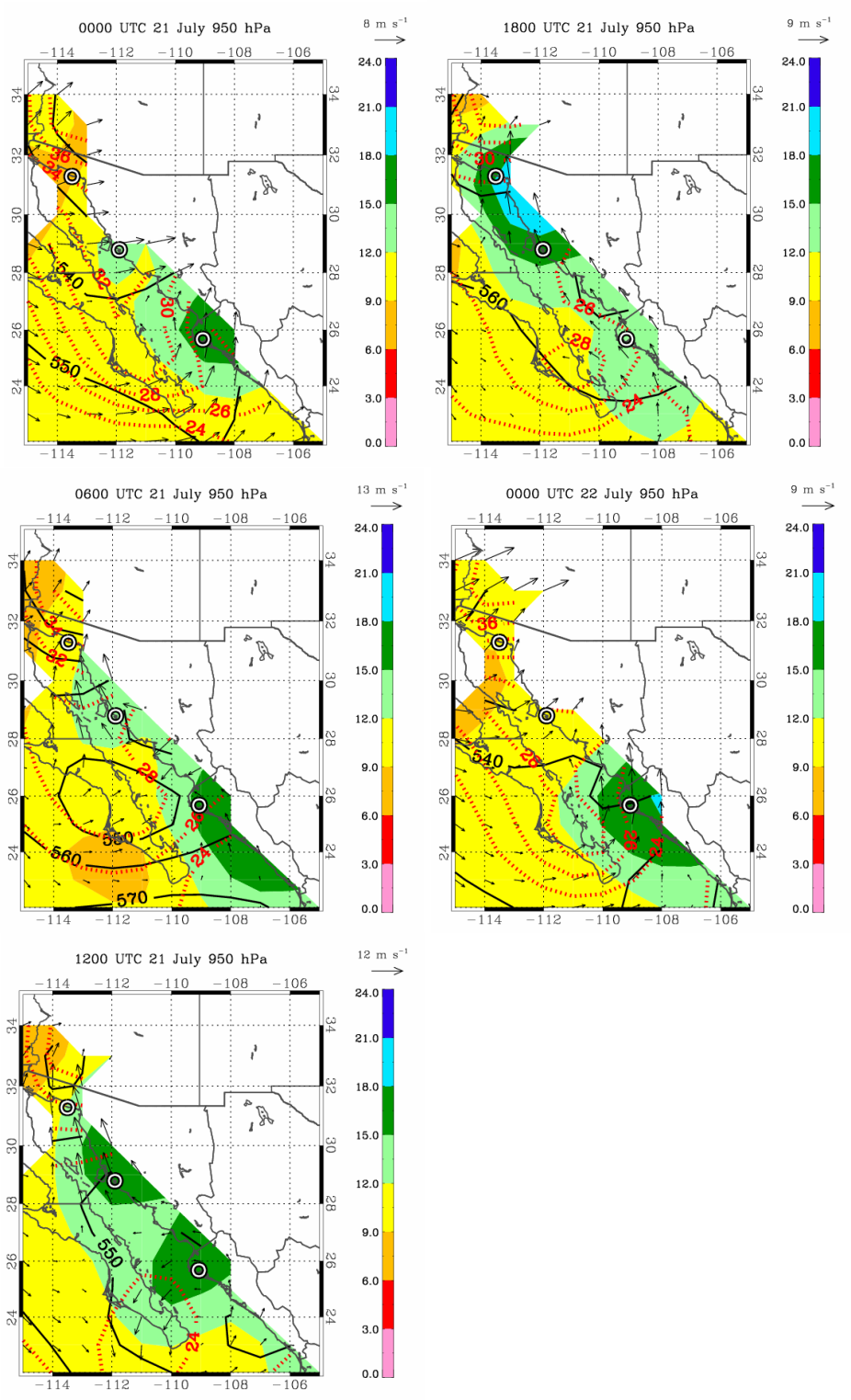


Figure 34: Same as in Fig. 32 except at 950 hPa and from 0000 UTC 21 July to 0000 UTC 22 July.

Bahia Kino northward to the low-deserts of Arizona. In addition, the axis of strongest winds seems to follow the GOC east coastline, as was the case for GS #1. Wind intensity decays significantly with distance away from this axis.

Although significant moisture advection occurs at 1200 UTC north of Bahia Kino during GS #2, it is not nearly as impressive in horizontal extent as that which accompanied GS #1. However, similar thermal changes to those observed during GS #1 occur between 0600 and 1200 UTC. At 0600 UTC, the 26°C isotherm lies across the GOC south of Los Mochis. By 1200 UTC, this contour is displaced just north of Bahia Kino due to gulf surge passage, resulting in a cooling of approximately 4°C at this site. Conversely, very similar temperatures remain stationary over the southern GOC between 0600 and 1200 UTC, further suggesting the horizontal extent of GS #2 was limited to the northern GOC.

The gulf surge remains intact at 1800 UTC, albeit slightly weaker with maximum winds still stretching from Bahia Kino to southern Arizona. At this time, gulf surge winds have turned more southerly, especially from Puerto Peñasco into Arizona, and remain most intense along the GOC coastal plain. Although thermal patterns seem to be returning to their pre-gulf surge conditions, northward moisture advection is significantly stronger than at 1200 UTC north of Puerto Peñasco. The short-lived surge is no longer discernable by 0000 UTC 22 July, and the overall flow and thermodynamic patterns surrounding the GOC at this time match remarkably well with those only 24 hours earlier (0000 UTC 21 July).

As with GS #1, longitude-pressure cross sections at 28°N, 30°N, and 32°N latitude up to 500 hPa at 1200 UTC 21 July (Fig. 35a-c) are examined to further understand the horizontal structure of GS #2. The gulf surge is evident in maxima of positive moisture flux anomalies (at least 50 m g $s^{-1}$ $kg^{-1}$) and anomalous cooling (- 2-4°C at 28°N and - 1-2°C at 30°N) along the GOC stretching primarily between 110°W to 115°W and confined below 900 hPa. However, it is extremely difficult to distinguish a definite gulf surge-type signature at 32°N, most likely due to the overall shallowness of the surge and its inability to deeply penetrate the low deserts of Arizona.

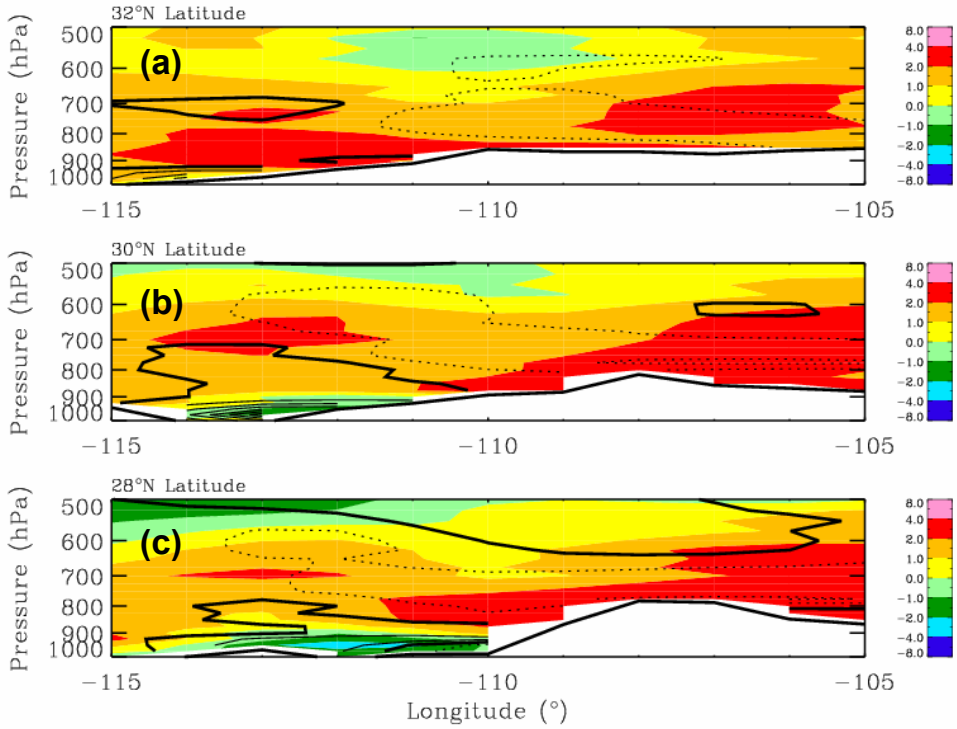


Figure 35: Same as in Fig. 33, except for 1200 UTC 21 July.

Nonetheless, the horizontal patterns depicted at 28°N and 30°N match qualitatively well with those described for GS #1, but again appear slightly askew compared with the

aircraft results of Higgins et al. (2006). The gulf surge-related cooling and moistening spread farther longitudinally at 28°N than at 30°N, where surge effects are primarily limited to the GOC and its coastal plain. Recalling that the overall intensity of GS #1 exceeded that of GS #2 as measured by maximum wind speeds in the profiler data, gulf surge strength may be linked, among many other things, to its vertical, but not horizontal structure. Comparing the two events examined here shows significant vertical structural differences, yet very similar horizontal patterns. Needless to say, high resolution mesoscale model runs need to be conducted to verify these structures and possible relationships to gulf surge strength.

# CHAPTER 6

# PROPAGATION CHARACTERISTICS AND DYNAMICAL MECHANISM

## 6.1 Gulf Surge Propagation Speeds

Upon examining minute-resolution surface data from the ISS enhanced surface observing stations; it was found that gulf surge onsets were accompanied by distinct surface patterns on time scales less than one hour. Using surface data from Bahia Kino and Puerto Peñasco, these signals can be tracked and used to calculate gulf surge propagation speed between the sites– a parameter useful for helping determine dynamical mechanisms. To this end, one-minute surface pressure and temperature anomaly plots (see Section 3.3.4) are presented at Bahia Kino and Puerto Peñasco during the day of surge onset (13 July for GS #1 and 21 July for GS #2). Recall from Section 3.7 that the diurnal cycle has been removed from the anomalies presented here so that true meteorological signals remain.

### *6.1.1 Gulf Surge #1*

Three distinct pressure features appear at Puerto Peñasco (Fig. 36a) prior to gulf surge onset (Fig. 36d). Strong anomalous pressure rises of approximately 2 and 1 hPa begin at

0000 and 0330 UTC respectively. Associated with these signals, the temperature anomaly dips nearly 2°C at 0045 UTC and 1°C at 0445 UTC. These patterns suggest the passage of a convective outflow, or gravity current. Not surprisingly, such convective signatures are evident in the wind profiler data (Fig. 25a) and coincide with the patterns discussed here. A third anomalous pressure rise of approximately 1 hPa begins at 0730 UTC. However, there is no distinct thermal trend to accompany this signal. Although the exact reason for this anomalous pressure rise is uncertain, it may be a result of a mesoscale convective feature between 0.75 and 1.25 km, as evident in a turning of the wind from easterly to more southeasterly in the wind profiler data (Fig. 25a).

In Section 5.1.1, it was noted that the initial front of GS #1 passed Puerto Peñasco at approximately 1000 UTC 13 July (Fig. 25a). Coincidentally, a nearly 0.75 hPa anomalous pressure rise occurs over a one hour period beginning at 1000 UTC, leveling off slightly, and then additionally increasing slightly more than 0.5 hPa in the following hour (Fig. 36d). Therefore, an approximately 1.25 hPa pressure rise accompanies the two hours immediately after gulf surge onset. Interestingly, during this time there are anomalous thermal increases of approximately 0.6 and 0.7°C that match relatively well in time with the two pressure pulses. After 1200 UTC, the anomalous pressure curve continues to gradually rise and increases approximately 1 hPa more by 0000 UTC 14 July, perhaps due to the relatively strong low-level southerly flow throughout the period in combination with the GOC LLJ (Fig. 36a). Concurrently, the anomalous thermal curve reaches a maximum around 1300 UTC and decreases substantially throughout the remainder of the day by about 5.0°C. From this, it is interesting to note that the

anomalous thermal curve does not decrease immediately after surge onset, yet steadily increases for another three hours. This may be the result of gulf surge-related cooling not affecting the surface until sometime later when the anomalous thermal curve decreases.

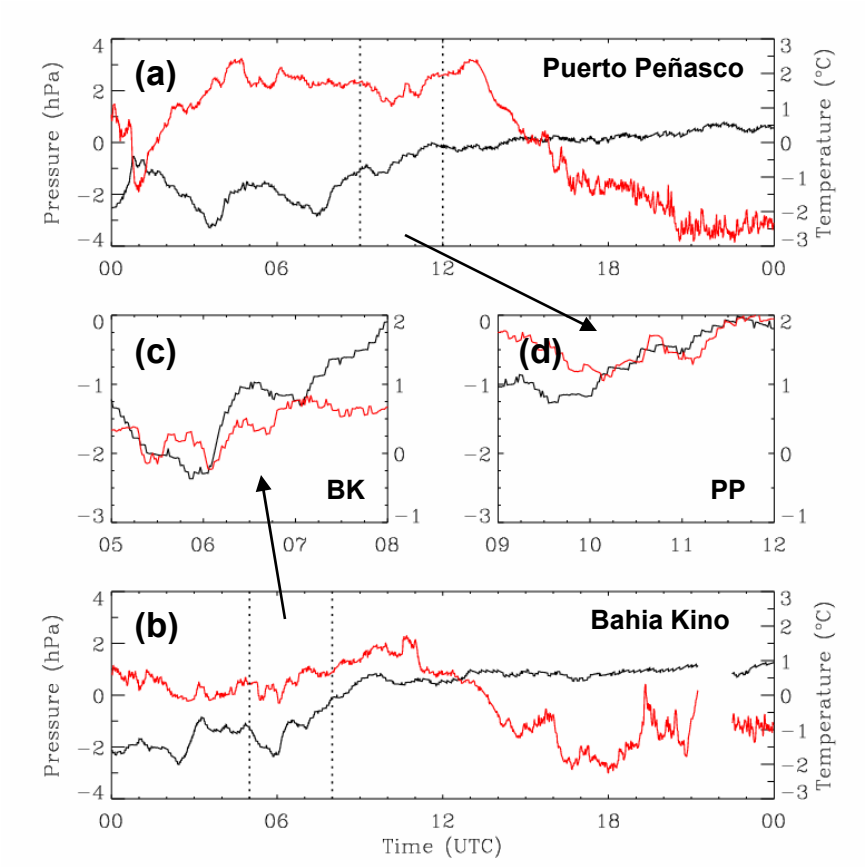


Figure 36: Minute surface pressure (black) (hPa) and temperature (red) (°C) anomalies at Puerto Peñasco (a) and Bahia Kino (b) for 13 July. Anomalies are calculated using 0000 UTC 7 July – 2359 UTC 14 August means. Panels (c) and (d) are three hour subsets as noted by the dotted vertical curves in panels (a) and (b) surrounding the time of gulf surge onset at Bahia Kino and Puerto Peñasco, respectively.

At Bahia Kino, only one distinct pressure feature appears (Fig. 36b) prior to gulf surge onset (Fig. 36c). Beginning around 0230 UTC, the pressure anomaly curve increases slightly more than 1.0 hPa, followed by an approximate 0.4°C decrease in the temperature anomaly shortly after 0300 UTC. Although this surface signal is not related

to a significant flow feature in the wind profiler data (Fig. 26a), its similarities to the patterns prior to surge onset described at Puerto Peñasco suggest a convective outflow. It is possible that the half-hour resolution of the profiler data was not high enough to capture this particular feature.

Initial gulf surge onset passed Bahia Kino around 0600 UTC 13 July as shown in the profiler wind data (Fig. 26a). As was also the case at Puerto Peñasco, a distinct double-pulsed structure in the pressure and temperature anomaly curves occurs during the two hours following initial gulf surge onset (Fig. 36c). Beginning near 0600 UTC, the pressure anomaly increases approximately 1.25 hPa within the hour, slightly decreasing thereafter, only to increase an additional 1.0 hPa from the maximum reached during the first pulse. In total, the pressure anomaly increased approximately 2.25 hPa – stronger than that at Puerto Peñasco, suggesting a slight weakening of the surge as it propagated north. This pressure increase was also accompanied by anomalous temperature increases – the first approximately 0.75°C and the second slightly more than 0.5°C. These thermal pulses agree qualitatively well in time with those of the pressure curve. In addition, the pressure anomaly pattern matches very closely to that at Puerto Peñasco after 1200 UTC, although it only increases an additional 0.5 hPa (Fig. 36b). However, the thermal curve continues to increase until approximately 1030 UTC, then decreases sharply, such that by 1800 UTC, almost 4.0°C of anomalous cooling have occurred.

Assuming that the pressure and temperature signals discussed above at the two northern ISS sites are a result of the same northward propagating disturbance along the

GOC, the gulf surge's propagation speed can be calculated. Four hours separated the gulf surge surface signals between the two sites, and from Section 5.1.1, surge onset appears to have been from the south-southeast. For the purposes of this calculation, it is assumed the direction of initial onset is 160°. Presuming the gulf surge's initial wave front is perpendicular to this direction, 295.3 km separate Bahia Kino and Puerto Peñasco along this path, resulting in a propagation speed of 20.5 m $s^{-1}$. However, it is possible that the wind profiler did not capture the exact timing of gulf surge onset and thus the most accurate direction of propagation. Therefore, Table 2 lists propagation speeds assuming varying initial wind directions from south (180°) to southeast (130°) every 10° as a means to better understand the uncertainty associated with this calculation. For clarification purposes, the distance traversed is determined by the latitudes of the two sites and assumes that the wave front is perpendicular to the initial direction of propagation. In addition, the elapsed time for each calculation is four hours.

Table 2: GS #1 initial direction and corresponding distance traversed needed to calculate propagation speed assuming four hours of elapsed time between Bahia Kino and Puerto Peñasco. Yellow highlights suggest most probable propagation speed based on wind profiler information.

| INITIAL DIRECTION | DISTANCE TRAVERSED | PROPAGATION SPEED |
|---|---|---|
| 180° | 277.5 km | 19.3 m $s^{-1}$ |
| 170° | 281.8 km | 19.6 m $s^{-1}$ |
| 160° | 295.3 km | 20.5 m $s^{-1}$ |
| 150° | 320.4 km | 22.3 m $s^{-1}$ |
| 140° | 362.3 km | 25.2 m $s^{-1}$ |
| 130° | 431.7 km | 30.0 m $s^{-1}$ |

*6.1.2 Gulf Surge #2*

The overall pressure and temperature anomaly patterns on 21 July (Fig. 37) are more complex than those on 13 July (Fig. 36). However, similar signals to those during GS #1 accompany initial surge onset. Prior to gulf surge passage at Puerto Peñasco (Fig. 37a), the most prominent surface feature is an anomalous pressure increase of slightly more than 0.5 hPa that begins just before 0600 UTC. Not related to any blatantly obvious thermal pattern, reasons for this pressure signal remain uncertain.

According to the analyses presented in Section 5.1.2, initial onset at Puerto Peñasco for GS #2 occurred around 0800 UTC 21 July (Fig. 28a), which agrees well with the timing of the surge-related anomalous surface pressure and temperature increases depicted in Fig. 37d. Within 30 minutes of 0800 UTC, the pressure anomaly increases approximately 1.1 hPa, more or less oscillating near this new level until 1000 UTC. In addition, the temperature anomaly increases nearly 2.75°C during the same two hour period. After 1000 UTC, the surface pressure trace continues its oscillatory behavior about its new post-surge level until about 1300 UTC, where it then begins to significantly decrease to pre-surge levels by 1600 UTC (Fig. 37a). This distinctly different pressure pattern that emerges only a few hours after surge onset during GS #2 as compared to that during GS #1 may be attributed to the weaker nature of the second surge. Temperature anomalies after 1000 UTC and throughout the remainder of the day slowly decrease such that by 0000 UTC 22 July, 4.0°C of anomalous cooling have occurred, similar to the thermal pattern associated with GS #1 at Puerto Peñasco.

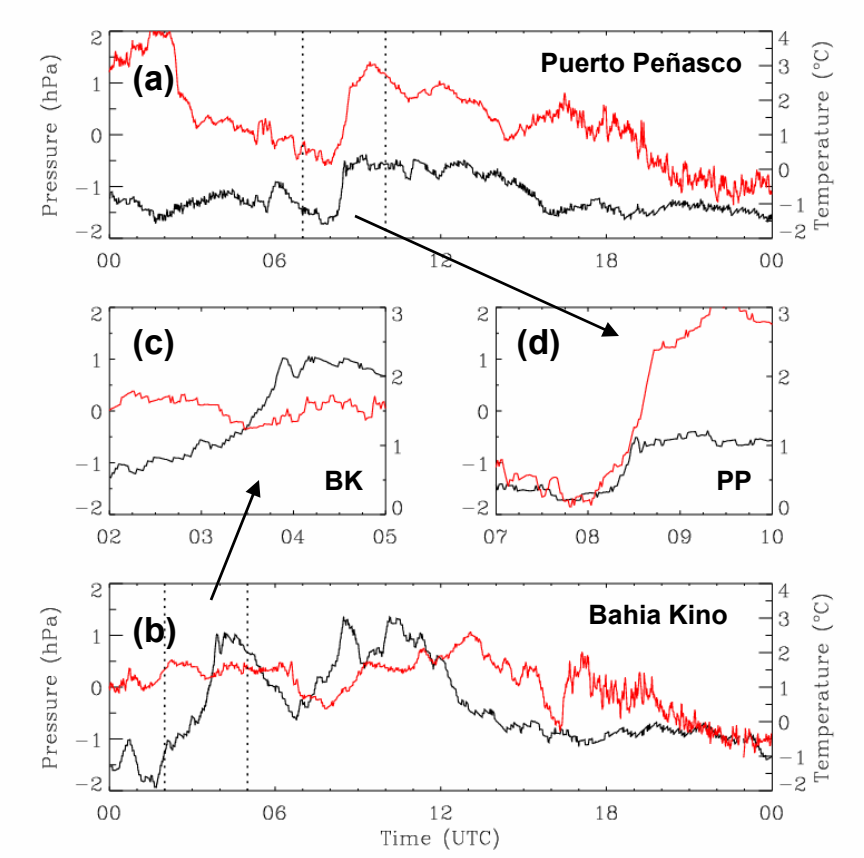


Figure 37: Same as in Fig. 36, except for 21 July.

Prior to gulf surge onset at Bahia Kino, there is very little of significant interest (Fig. 37b). Initial surge onset occurs shortly after 0300 UTC 21 July according to the wind profiler data (Fig. 29a), agreeing qualitatively well with the surface pressure and temperature anomaly results (Fig. 37c). Beginning at 0330 UTC, a strong anomalous pressure increase of approximately 1.5 hPa occurs within 30 minutes, remaining thereafter near the post-surge level until about 0500 UTC (Fig. 37c). Since the initial anomalous pressure rise at Puerto Peñasco is slightly less than that at Bahia Kino, it is again suggested that the surge slightly weakened as it propagated north. In addition, given the same hour and a half time frame between surge onset and 0500 UTC, the temperature anomaly oscillates numerous times, yet increases by about 0.5°C overall.

Reasons for the significant pressure and temperature anomaly decreases shortly after 0500 and 0630 UTC (Fig. 37b) respectively are uncertain, even after examining the wind profiler data in great detail. These signals rebound back to or above gulf surge-related levels by 0830 and 0900 UTC. Soon after 1000 UTC, the pressure anomaly significantly decreases, similar in fashion to that at Puerto Peñasco after 1300 UTC, such that pre-surge levels are regained by 1600 UTC. In addition, after its unexplained decrease near 0630 UTC, the temperature anomaly slowly increases until 1300 UTC, after which it gradually decreases through the remainder of the day, excepting the significant feature centered about 1600 UTC – also similar in fashion to the pattern at Puerto Peñasco.

Noting the initial gulf surge onset times from above, the propagation speed of the surge can be calculated using an identical method as that done for GS #1. Four and one-half hours separated the gulf surge-related surface signals between Bahia Kino and Puerto Peñasco, and onset appears to have been from the south-southeast in line with the discussion in Section 5.1.2. For the purposes of this calculation, it is assumed the direction of initial onset is 150°. As with GS #1, assuming the gulf surge's initial wave front is perpendicular to this direction, 320.4 km separate Bahia Kino and Puerto Peñasco along this path, resulting in a propagation speed of 19.8 m $s^{-1}$. Table 3 details the same information as presented in Table 2, except an elapsed time of four and one-half hours, instead of four is used to calculate the propagation speeds.

Similar plots to those depicted in Figs. 36 and 37 were also generated for 22 July at the two sites in an attempt to describe the propagation speed of the strong gulf surge that

followed GS #2 (not shown). Unfortunately, continuity between surface patterns and wind signals aloft (Figs. 28a-29a) at the time of surge onset were difficult to discern. However, from the wind profiler data it seems that approximately four to five hours elapsed between the most intense wind signatures noted at Bahia Kino and Puerto Peñasco on 22 July. Since the initial front most likely came from the south-southeast, similar propagation speeds to those in Tables 2 and 3 would result.

Table 3: Same as in Table 2, except for GS #2 and assuming an elapsed time of 4.5 hours.

| INITIAL DIRECTION | DISTANCE TRAVERSED | PROPAGATION SPEED |
|---|---|---|
| 180° | 277.5 km | 17.1 m $s^{-1}$ |
| 170° | 281.8 km | 17.4 m $s^{-1}$ |
| 160° | 295.3 km | 18.2 m $s^{-1}$ |
| 150° | 320.4 km | 19.8 m $s^{-1}$ |
| 140° | 362.3 km | 22.4 m $s^{-1}$ |
| 130° | 431.7 km | 26.6 m $s^{-1}$ |

With initial gulf surge fronts from the south to southeast presented in Tables 2 and 3, propagation speeds for GS #1 range from 19.3 to 30.0 m $s^{-1}$, and from 17.1 to 26.6 m $s^{-1}$ for GS #2. Thus, it is very clear that the calculated propagation speed is highly dependent upon the direction of the flow perpendicular to the surge's initial front. Uncertainties can be large if this direction is unknown or grossly estimated. However, since the surge is likely channeled along the GOC, it is unlikely that the estimated direction is off by more than approximately 10°. Since the gulf surge signatures depicted in Figs. 25a-26a and 28a-29a exhibit their most robust features above the surface, it is unclear whether the surface wind can be trusted as the most accurate measurement of the

surge's initial front. Ideally, higher time resolution data from the wind profilers would prove most useful in better resolving such issues. Although propagation speeds calculated here agree with the range of speeds calculated by Stensrud et al. (1997) (10-23 m $s^{-1}$), they are faster than that calculated by Hales (1972) (~ 15.4 m $s^{-1}$), as discussed in Section 2.2.

### 6.2 Boundary Layer Evolution

Although the half-hour interpolated rawinsonde plots depicted in Figs. 30 and 31 were useful in determining the amount and extent of gulf surge-related anomalous moistening and cooling, they provided little information regarding the boundary layer's evolution due to gulf surge passage. To this end, 0000, 0600, 1200, and 1800 UTC rawinsonde temperature, dewpoint temperature, and wind data at Puerto Peñasco are plotted from 12-14 July for GS #1 and from 20-22 July for GS #2 up to 800 hPa. Identical plots were generated for Bahia Kino, but are not included here since similar qualitative features associated with gulf surge passage occur at both sites. However, it is important to note that these features are more pronounced and easier to distinguish at Puerto Peñasco, especially for GS #2. Besides the fact that significant features at Bahia Kino are at slightly lower pressures, the most significant difference between the two sites is that the Bahia Kino thermodynamic profiles are slightly cooler and moister than those at Puerto Peñasco.

*6.2.1 Gulf Surge #1*

On 12 July, boundary layer winds are primarily light and variable at each sounding time (Fig. 38). A strong thermal inversion exists at 0600 UTC between 990 and 975 hPa, and at 1200 UTC from the surface up to 995 hPa. These inversions, especially the one at 1200 UTC, are most likely linked to nighttime radiative cooling over the Sonoran Desert, which results in the development of a low-level stable layer decoupled from the drier, warmer air aloft. On the other hand, the profiles at 0000 and 1800 UTC appear to be well-mixed over a significant depth due to daytime heating and sufficient vertical mixing of boundary layer air.

Significant changes occur, however, on 13 July due to gulf surge passage. Most notably, a strong, yet shallow thermal inversion develops by 0000 UTC confined between 985 and 980 hPa. As the evening progresses, this inversion layer deepens (1000-985 hPa) and extends to very near the surface at 0600 UTC. Thermal conditions both above and below the inversions at 0000 and 0600 UTC remain close to neutral, or well-mixed, and relatively dry. In addition, wind profiles shift dramatically from west-southwesterly at 0000 UTC to east-southeasterly at 0600 UTC, perhaps in association with the convective outflows discussed above. Gulf surge onset occurs at 1000 UTC and thus the 1200 UTC sounding reflects the boundary layer changes associated with surge passage.

Three important features from the 1200 UTC 13 July profiles deserve attention. First, the base of the thermal inversion at 0600 UTC is vertically displaced approximately 45

hPa at 1200 UTC (from 1000 to 955 hPa ~ 450 m). Assuming the height of the low-level thermal inversion at 1200 UTC 12 July is representative of normal conditions at this time at Puerto Peñasco, the upward shift of the low-level inversion between 0600 and 1200 UTC 13 July is most likely due to gulf surge passage. Second, in comparing the 1200 UTC thermodynamic profiles on 12 and 13 July, significant cooling (~ 8°C at 980 hPa)

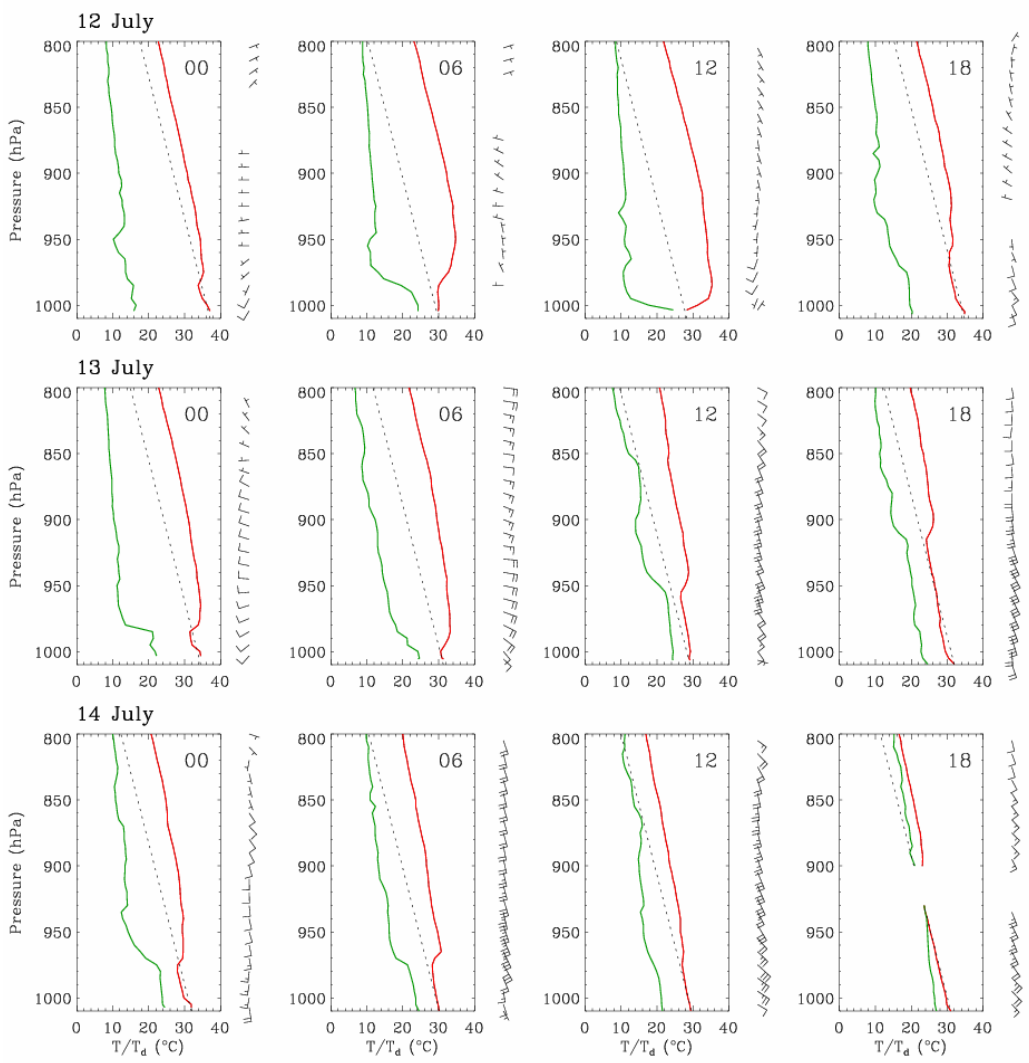


Figure 38: Puerto Peñasco rawinsonde temperature (red) (°C), dewpoint temperature (green) (°C), and wind (1 full barb = 5 m s$^{-1}$) profiles at 0000, 0600, 1200, and 1800 UTC from 12-14 July. Black dotted curve represents reference dry adiabat. Profile gaps are bad or questionable data as determined by the quality control procedure (Section 3.3.1).

and moistening (dewpoint increases by ~ 14°C at 980 hPa) occur both above and below the thermal inversion, consistent with the results depicted in Fig. 30 at Puerto Peñasco. Third, strong gulf surge winds at 1200 UTC are from the south-southeast throughout the column, with the greatest speeds of 15.0 to 17.5 m $s^{-1}$ located within the thermal inversion layer (960-940 hPa). It is again interesting to note, as done in Section 5.1.1, that the near surface winds are not as indicative of gulf surge passage as those aloft.

At 1800 UTC 13 July, gulf surge signatures are still visible. The 1200 UTC thermal inversion is vertically displaced even farther by approximately 40 hPa. However, the extent to which this additional uplift is due to gulf surge passage is unclear since vertical mixing due to the diurnal cycle becomes increasingly strong during daylight hours. Otherwise, the gulf surge-related cooling and moistening continue, as areas below the thermal inversion are well-mixed and contain the strongest wind speeds up to 15.0 m $s^{-1}$. Although the post-surge environment on 14 July remains relatively cool and moist compared to those thermodynamic profiles on 12 July, there appear to be no distinct features that evolve on that day at Puerto Peñasco, as was evident with the increasing thermal inversion heights on 13 July. Winds on 14 July remain strong throughout the boundary layer from the south-southeast, especially at 0600 and 1200 UTC with maximum speeds between 15.0 and 17.5 m $s^{-1}$. However, as discussed above in several sections, this flow pattern is likely due to Tropical Storm Blas and not the gulf surge.

*6.2.2 Gulf Surge #2*

Although the overall boundary layer evolutions on the days before and after day of surge onset are quite different during GS #2 as compared to GS #1, similar characteristics to those discussed above occur related to gulf surge passage. On 20 July, a low-level thermal inversion is present between 990 and 980 hPa at 0000 UTC (Fig. 39). Interestingly, this inversion is also present at 0600 and 1200 UTC at nearly the same pressure levels, albeit slightly weaker than at 0000 UTC. Above these inversions, the thermodynamic structure of the boundary layer is close to neutral and relatively dry. In addition, the 1800 UTC sounding is very similar to the 1800 UTC 12 July sounding depicted in Fig. 38. Winds throughout the day are primarily light and range in direction from the southwest to southeast.

Despite varying wind patterns, the thermodynamic structures of the 1800 UTC 20 July and 0000 UTC 21 July soundings are qualitatively similar. However, a strong thermal inversion appears between 1000 and 990 hPa at 0600 UTC 21 July most likely in response to nighttime radiative cooling as suggested above. Near neutral conditions remain above this inversion. In addition, the overall wind pattern below 900 hPa shown at 0000 UTC changes little by 0600 UTC. Above this level, a greater westerly component emerges at 0600 UTC. Subsequently, significant changes appear by 1200 UTC as initial gulf surge onset occurs at 0800 UTC at Puerto Peñasco.

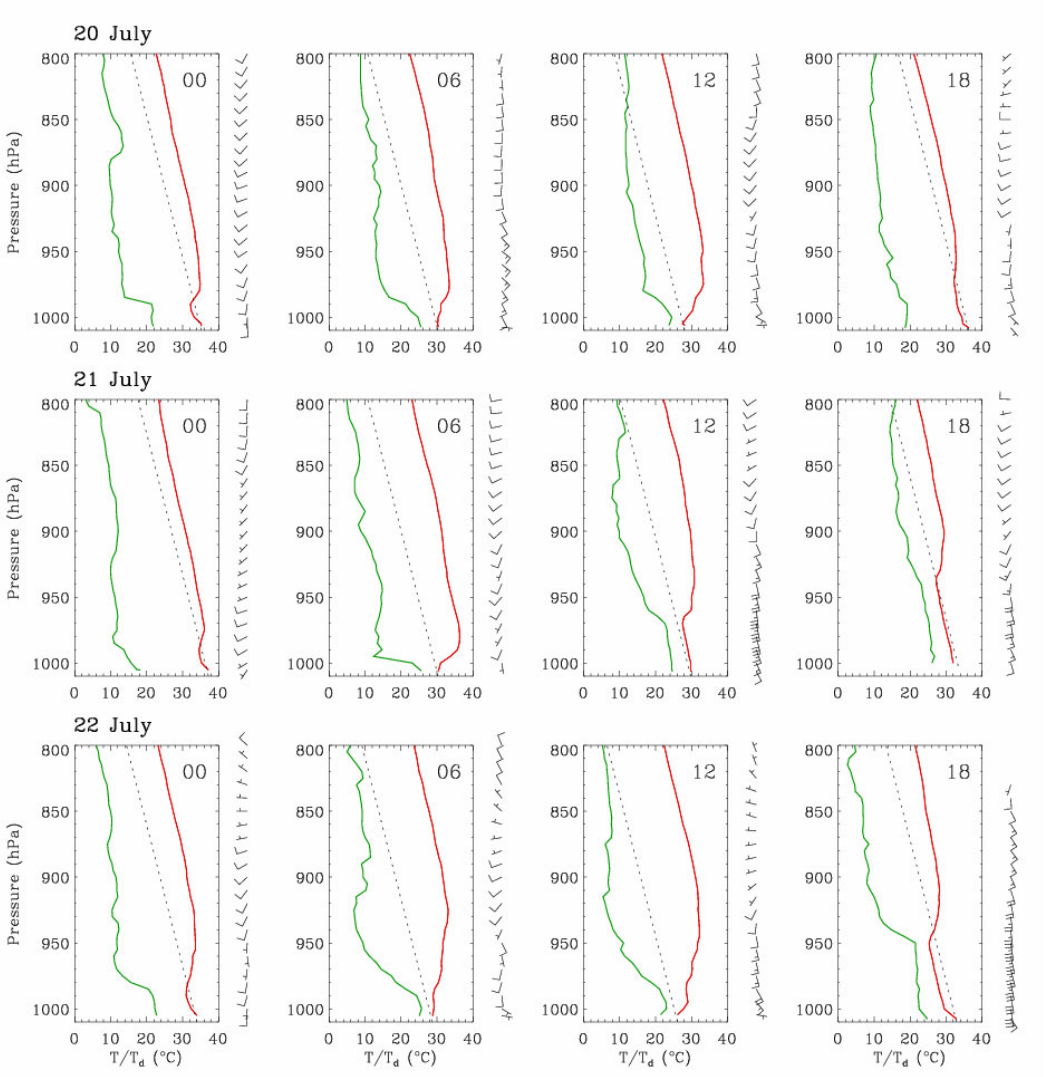


Figure 39: Same as in Fig. 38, except from 20-22 July.

As was the case with GS #1, there are three important features to note from the 1200 UTC 21 July sounding. First, the base of the low-level inversion at 0600 UTC lifts approximately 30 hPa (~ 300 m) to 970 hPa at 1200 UTC. The local environment below the inversion is very well-mixed. This displacement can most likely be attributed to gulf surge passage since the base of the thermal inversion 24 hours earlier is near 1000 hPa – the same as that at 0600 UTC 21 July. Thus, GS #2 did not lift the well-mixed boundary layer nearly as much as GS #1. Second, significant cooling (~ 5°C at 980 hPa) and

moistening (dewpoint increases by ~ 8°C at 980 hPa) occur when compared to the 1200 UTC 20 July sounding, although it is most prominent below 950 hPa. Third, relatively strong gulf surge-related southerly winds extend up to 920 hPa with maximum speeds from 15.0 to 17.5 m $s^{-1}$ between 980 and 960 hPa – very near the thermal inversion. These results are consistent with the analyses presented in previous chapters, which showed that GS #2 was shallower than GS #1.

At 1800 UTC 21 July, the gulf surge-related wind signature is much weaker than at 1200 UTC. However, the base of the thermal inversion at 1200 UTC is raised an additional 35 hPa to 935 hPa – a nearly identical displacement to that between 1200 and 1800 UTC 13 July for GS #1. Again, it is possible that much of this lift is due to strong diurnal afternoon heating. Of greater interest, though, is the significant moistening above the thermal inversion that occurs between 1200 and 1800 UTC, whereas the thermal curve remains mostly unchanged. Finally, whereas the 14 July sounding profiles (Fig. 38) reflect the passage of Tropical Storm Blas, the 22 July sounding profiles show evidence of the stronger secondary gulf surge passage as depicted in Fig. 28a. More specifically, between 1200 and 1800 UTC, the low-level inversion height dramatically increases, substantial cooling and moistening occur below 950 hPa, and strong south-southeasterly winds extend to near 900 hPa.

### 6.3 Proposed Gulf Surge Dynamical Mechanism

Up to this point, Zehnder (2004) has provided the most comprehensive analyses of probable gulf surge dynamical mechanisms using dynamical arguments and modeling experiments (see Section 2.6 for further discussion). Primarily due to a lack of high resolution spatial and temporal observational data over the NAM region, similar studies using only observations have been non-existent. To the knowledge of this author, the data collected during the 2004 NAME allows for the first-ever attempt to describe the dynamics necessary to initiate and maintain a northward propagating gulf surge along the GOC. Zehnder (2004) proposed four possible dynamical mechanisms - gravity currents, ageostrophic isallobaric flow, Rossby edge waves, and barrier Kelvin waves. Only linear theory was considered for such disturbances. Three possibilities remained after having dismissed ageostrophic isallobaric flow due to very slow propagation speeds. Therefore, in this section, the validity of the other three mechanisms will be tested against the observational results discussed throughout this study.

First, consider gravity currents, or convective outflows. This mechanism can be dismissed after considering two important characteristics of gravity currents. Gravity current onset is accompanied concurrently by a significant decrease in surface temperature (Simpson 1997, Ralph et al. 2000), and the dense fluid associated with gravity currents must propagate at least as fast as the leading initial front (Ralph et al. 2000). However, gulf surge onset for both GS #1 and GS #2 at Puerto Peñasco and Bahia Kino were accompanied by anomalous surface temperature warming as depicted in Figs.

36 and 37. In addition, agreeing qualitatively with the modeling results of Stensrud et al. (1997), the wind speeds depicted by the profiler data in Figs. 25a-26a and 28a-29a are much slower immediately after gulf surge onset (~ 5.0-12.5 m $s^{-1}$) than the calculated propagation speeds from Section 6.1 in Tables 2 and 3 (~ 20.0 m $s^{-1}$). This suggests any impending dense fluid would lag behind the current's initial front. Both observational results contradict fundamental gravity current behavior, thus negating gravity currents as a viable gulf surge dynamical mechanism for the two events studied here.

Second, consider Rossby edge waves and barrier Kelvin waves. To distinguish these two mechanisms, Zehnder (2004) noted that isentropes follow the curvature of the earth's surface and are tightly packed near the summits of coastal mountain ranges for Rossby edge waves, and intersect the surface for barrier Kelvin waves. Examining longitude-pressure cross sections from the T1A gridded dataset at several latitudes along the GOC prior to and during gulf surge passages (not shown), revealed isentropic surfaces that intersect the western slope of the SMO and slant downward to the west. This pattern was most prevalent at latitudes primarily between Los Mochis and Bahia Kino, but also as far south as Mazatlan at times. On the other hand, distinct isentropic patterns along the Peninsular Range were not obvious. Although Zehnder (2004) suggested Rossby edge waves as a more probable gulf surge mechanism compared to barrier Kelvin waves, these observational results favor the latter mechanism. This may be due to the fact that Zehnder (2004) did not include nonlinear processes within the study's model simulations, thus limiting the extent to which large changes in gradients can be accurately resolved.

Interestingly, however, the observed gulf surge propagation speeds calculated in Section 6.1 (~ 20 m $s^{-1}$) are too fast to suggest pure linear Kelvin wave theory (~ 10 m $s^{-1}$ or less). Propagation speeds of approximately 20 m $s^{-1}$ seem to fall more in line with nonlinear wave phenomena, such as atmospheric or internal bores (bores hereafter), which have been observationally found to propagate at speeds greater than 15.0 m $s^{-1}$ across portions of Oklahoma (Haase and Smith 1984 and Fulton et al. 1990) and the Mid-Atlantic States (Koch et al. 1991). Propagation speeds of bores over northern Australia, also famously referred to as morning glories, are generally less – typically on the order of 10.0 m $s^{-1}$ (Noonan and Smith 1986).

Bores are shallow-water phenomena that can be responsible for horizontal mass transport and resemble a hydraulic jump, in which fluid depth significantly increases after passage (Simpson 1997). Bores are typically generated when dense gravity current outflows from thunderstorms impinge on less dense low-level stable layers and their associated thermal inversions. These inversions tend to be induced by nighttime radiative cooling and the thermodynamic state of the local environment above them is normally close to neutral (Menhofer et al. 1997, Skamarock et al. 1999). Depending on the depth of the gravity current compared to that of the low-level stable layer, partial or complete blocking causes the less dense layer to lift, which then generally propagates out ahead of the gravity current atop the thermal inversion as a series of undulations, or waves (Simpson 1997). This initiation process was beautifully captured and discussed in much greater detail by two separate observational studies – Fulton et al. (1990) and Koch et al. (1991). Bores can also develop due to colliding gravity currents (Simpson 1997) or sea

breezes, as has been shown to be the initiating mechanism for bores over Cape York Peninsula in northeast Australia (Clarke et al. 1981 and Noonan and Smith 1986).

Noting these characteristics, bore onset is generally accompanied by distinct surface features including a marked increase in pressure due to increased fluid depth, an increase in temperature due to vertical mixing of warmer air from above the thermal inversion to the surface, and a distinct wind shift in the direction of propagation (Simpson 1997). After passage, the surface pressure generally remains at its newly elevated level for at least several hours and the bore's undulations most often are visibly identified by a series of roll clouds (Clarke et al. 1981).

Many of the bore-like features discussed here are also evident within the observations presented above for both surge events. The thermodynamic environment prior to surge passage consists of a low-level thermal inversion (Figs. 38 and 39), most likely due to nighttime radiative cooling, although in some instances may be enhanced by subsidence to the lee of the SMO. Areas above the inversions are close to neutral. Extensive areas of convection develop along the GOC coastal plain prior to surge passage, undoubtedly providing the gravity currents necessary to trigger bore initiation (Figs. 23 and 24). There is a distinct increase in the depth of the well-mixed boundary layer from before to after surge passage (Figs. 38 and 39). At the surface, surge onset is accompanied by marked increases in both the anomalous pressure and temperature profiles (Figs. 36 and 37). In addition, the pressure anomaly remains essentially elevated for at least several hours following surge passage, especially during GS #1. Finally, observed gulf surge

propagation speeds match quite well with observed bore speeds from other studies (Tables 2 and 3).

Given these similarities, however, one very important set of results do not appear to fit the model of a bore-like disturbance – the gulf surge wind signatures evident in the profiler data (Figs. 25a-26a and 28a-29a). Using a Multiple Antenna Profiler Radar (MAPR hereafter) during the 2002 International $H_2O$ Project (IHOP) in Kansas and Oklahoma, Brown et al. (2003) observed a bore-like event on 4 June. The MAPR uses a spaced antenna technique, allowing it to make measurements every 1-5 minutes, which is much finer temporal resolution than available from the wind profilers at the ISS sites (30 minutes) during the NAME. The MAPR reflectivity (a), vertical velocity (b), and five-minute consensus winds (c) from this event are shown in Fig. 40. From this figure, there are three distinct pulses associated with the bore-like feature visible in the reflectivity profile (Fig. 40a). The pulses last at least 20 minutes and are respectively centered about 0650, 0720, and 0810 UTC. Also accompanied by rising/sinking motion couplets (Fig. 40b), each pulse maintains maximum wind speeds from the south-southwest no greater than 30.0 m $s^{-1}$ primarily below 1.0 km (Fig. 40c). However, the depths of maximum winds appear to undulate in phase with those pulses evident in the reflectivity and vertical velocity profiles.

Noting the coarser temporal resolution of the profiler data depicted in this study, it is possible that similar bore-like features to those in Fig. 40c passed the ISS sites during gulf surge onset, but could not be resolved. However, although Fig. 40 depicts only one

case, the gulf surge-related wind signatures shown in Chapter 5 for both events appear dissimilar to features presented in Brown et al. (2003). ISS gulf surge wind signatures for both events generally maintained their most robust features for several hours with no obvious undulating patterns present, despite GS #1 being accompanied by two anomalous surface pressure/thermal pulses within two hours after onset (Fig. 36c and d). Therefore, although it seems as if the correct environment necessary for bore-like development exists prior to gulf surge passage, as well as bore-like features emerging in tandem with

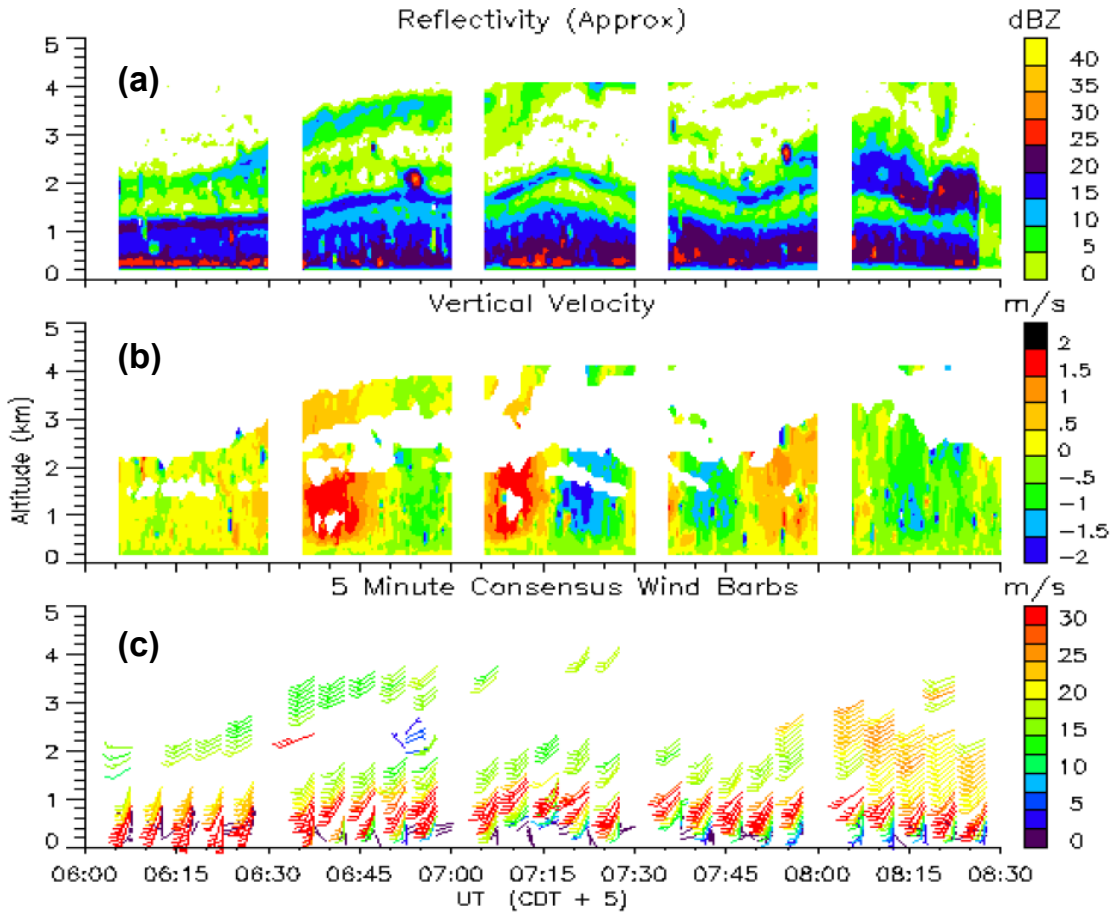


Figure 40: Reflectivity (dBZ) (a), vertical velocity (m $s^{-1}$) (b), and five-minute consensus wind barbs (m $s^{-1}$) (c) of a bore-like event on 4 June 2002 during IHOP. From Brown et al. (2003) Fig. 1.

gulf surge onset at the surface and within the boundary layer, it appears from the profiler data that the two gulf surge events examined here cannot fully be described as undulating bores. However, since it is also possible for a bore to propagate as a single disturbance, similar to that of a solitary wave (Simpson 1997), the validity of this possibility must be examined and discussed.

Recalling that the isentropic analyses discussed above suggested a linear Kelvin wave-like disturbance along the central and/or southern GOC, and gulf surge initial onset is consistent with bore-like features across the northern GOC, there appears to be a hybrid of dynamical mechanisms occurring during gulf surge initiation and propagation. Interestingly, in studying coastally trapped disturbances (CTD hereafter) along the California coast using a 3D non-hydrostatic model, Skamarock et al. (1999) noted that initial development of the CTD is due to a deepening of the cool marine layer along the coast via onshore synoptic flow (Fig. 41). From the shallow water *u*-component momentum equation (Equation 1) (Kundu and Cohen 2002), the first term on the left-hand-side is set to zero assuming no cross barrier flow (i.e. $u = 0$) given a north-south coastline. Since $\partial h / \partial x$ is positive where $h$ is the marine layer depth, the meridional component, $v$, in Equation 2 must be positive. Therefore, southerly flow, as denoted by the *'X'* in Fig. 41 develops along the barrier in response to this deepening marine layer, and a linear Kelvin wave-like CTD is able to propagate north as a smooth waveform (Skamarock et al. 1999). The CTD also decays exponentially away to the west from the north-south barrier.

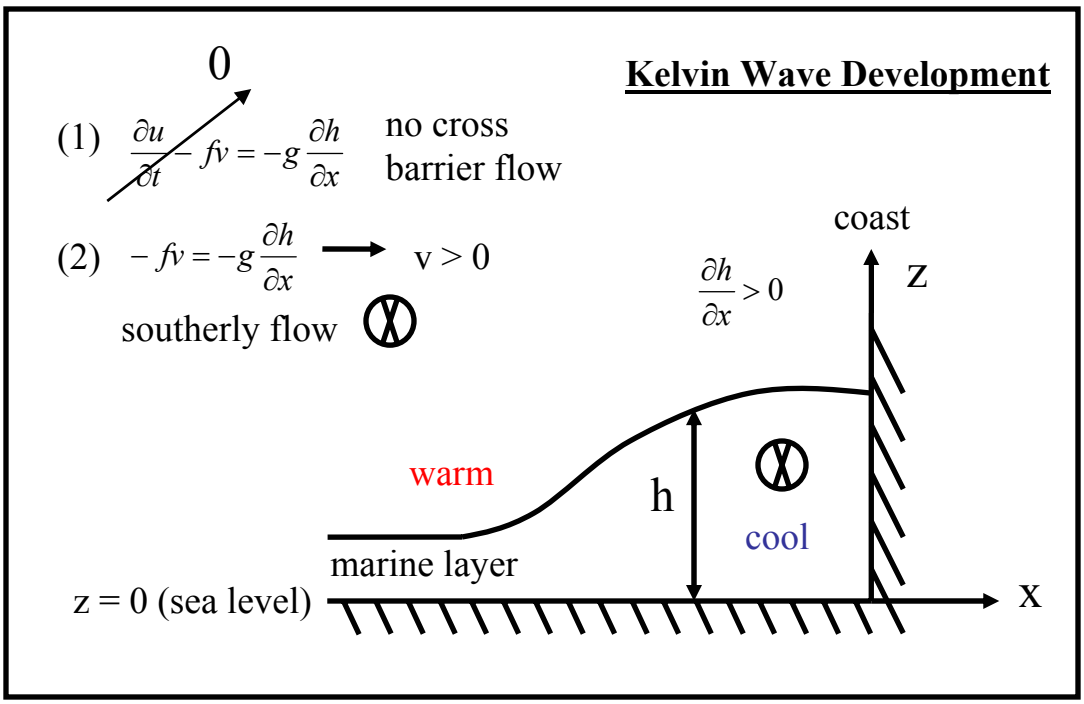


Figure 41: Conceptual schematic of Kelvin wave development along a north-south coastal barrier. Adapted from Kundu and Cohen (2002) and Reason and Steyn (1992).

Skamarock et al. (1999) also notes that the CTD can quickly steepen along its leading edge due to the development of nonlinearities, thus increasing its propagation speed (Ralph et al. 2000). These nonlinearities are related to the much greater height of the CTD compared to that of the marine layer in those areas to which it is propagating. In addition, as the leading edge of the CTD continues to steepen, it is possible that it develops bore or gravity current-like characteristics unless the associated nonlinearities are balanced by dispersive effects (Reason and Steyn 1992). In the latter instance, if a balance is achieved, nonlinear semi-geostrophic theory dictates a special solitary wave solution for the CTD.

Therefore, applying the observations and discussion presented above to gulf surges, the following conceptual model is presented as a means to suggest a probable gulf surge dynamical mechanism for the two events examined in this study. Figures 41 and 42 provide conceptual schematic diagrams to help illustrate the most important points. If Tropical Storm Blas played a more direct role in gulf surge initiation during GS #1, the patterns depicted in Fig. 42 should be located farther south.

- Aided by various mesoscale processes (Howard and Maddox 1988c) as well as synoptic forcing such as Tropical Strom Blas during GS #1 (Figs. 18-21), NAM convection begins to develop along the SMO axis during the afternoon and propagates west to the SMO foothills and GOC coastal plain by the late evening and early morning (Figs. 23 and 24).
- Significant evaporational cooling due to heavy convective rainfall over the SMO foothills and GOC coastal plain help develop a surface mesohigh (Fig. 42a).
- Aided by Coriolis deflection and the developing surface anticyclonic circulation (Fig. 42a), cool air is piled up against the SMO along the mesohigh's northern extent, in a similar fashion to the marine layer depth increasing along the California coast due to synoptic onshore flow (Fig. 41). This process results in isentropes that intersect the surface and slope upward with distance towards the mountains, as discussed above.
- Southerly flow develops along the SMO in response to this "cool-air damming" (Fig. 41) and a barrier induced disturbance similar to a linear Kelvin wave begins

to propagate north as a gulf surge (Fig. 42a). In addition, horizontal transport of cool moist air from the central or southern GOC regions accompanies this flow.

- As the gulf surge propagates north away from the now decaying convection and weakened mesohigh (Fig. 42b), it encounters areas where a low-level nighttime stable layer is present with near neutral conditions aloft (Figs. 38 and 39). Therefore, nonlinearities increase along the leading edge of the disturbance due to the much greater depth of the surge compared to that of the low-level stable layer.
- As a result, the gulf surge's initial front quickly steepens (Fig. 42b) and acquires bore-like characteristics, as evident in the increased depth of the well-mixed boundary layer after surge passage (Figs. 38 and 39), the surface anomaly characteristics associated with surge onset (Figs. 36 and 37), and the observed propagation speeds (Tables 2 and 3).
- The now nonlinear system propagates at a much faster speed and its timing of passage along the northern gulf coincides more or less with that of GOC LLJ (Fig. 42b). Therefore, it is quite plausible that the gulf surge wind signatures merge with that of the LLJ, except at Bahia Kino during GS #2 where the timing of the two features does not appear to agree as well (Figs. 25a-26a and 28a-29a).
- Upon exiting the immediate GOC region and into the low deserts of the southwest United States, the gulf surge horizontally expands and significantly weakens, as previously discussed by Hales (1972) and Brenner (1974).
- Depending on the synoptic flow patterns at the time (Figs. 18-21) (Higgins et al. 2004) and the depth and strength of the moisture transport, significant convective

development may occur over Arizona/New Mexico in the hours following surge passage (Figs. 23 and 24).

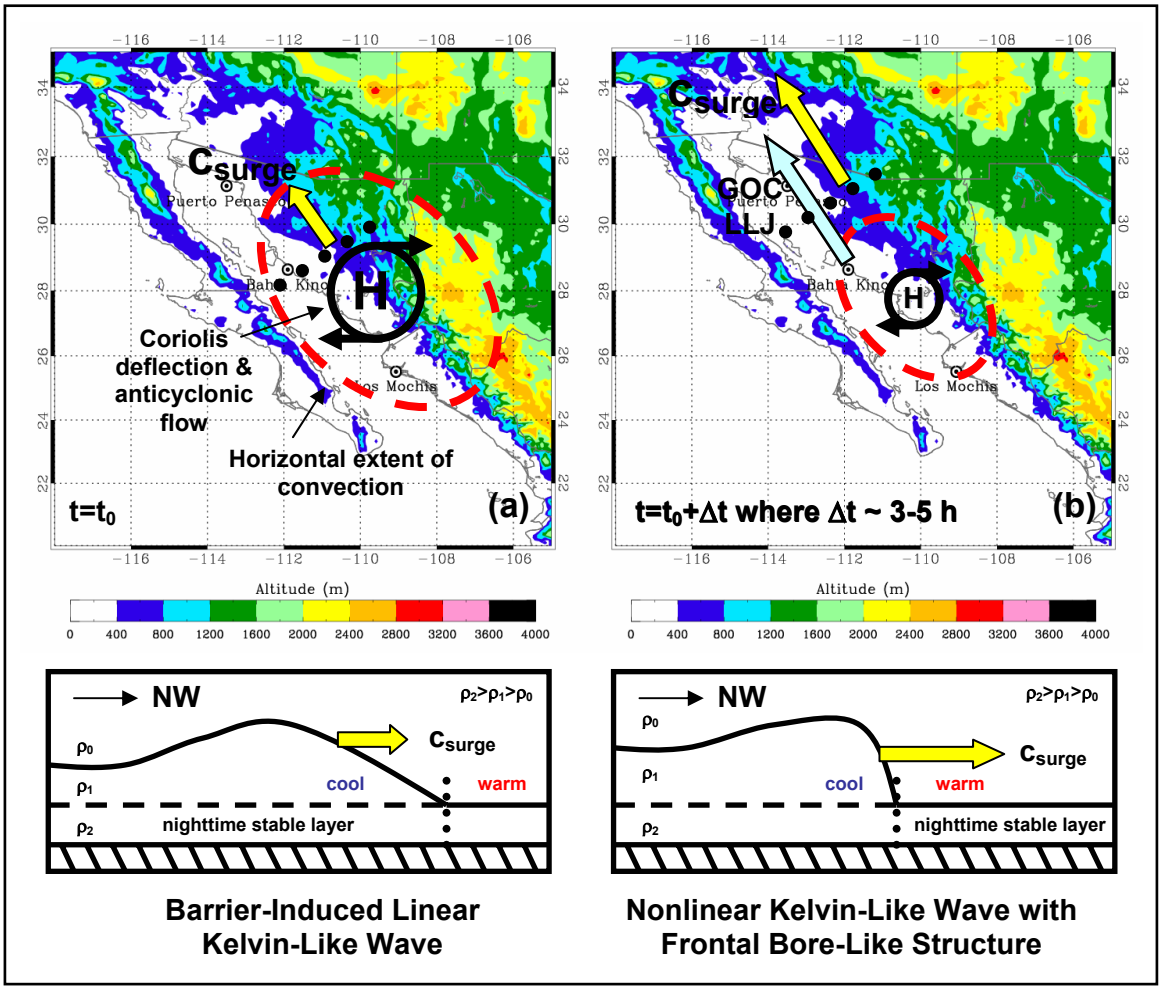


Figure 42: Conceptual schematic detailing the evolution of proposed gulf surge dynamical mechanism at times $t_0$ (a) and $t_0+\Delta t$ (b). Top panels depict approximate extent of monsoon convection (red dashed), associated surface mesohigh (H) with anticyclonic circulation, and gulf surge onset (black dotted). The yellow arrows ahead of gulf surge onset represent propagation speeds and the light blue arrow in (b) represents the GOC LLJ. Colored contours represent altitude above sea level (m). Bottom panels depict gulf surge horizontal structure (~ hundreds of km) where $\rho_2>\rho_1>\rho_0$. The dotted lines and propagation vectors correspond to those in the top panels.

The above conceptual model is oversimplified and undoubtedly does not explain all the details of the observations. However, the idea of a barrier induced linear Kelvin wave-like disturbance that quickly steepens along its leading edge due to evolving nonlinearities, such that bore-like characteristics accompany gulf surge onset seems to agree qualitatively well with the gross characteristics presented from the data above. It is important to note that since the SMO slopes away from the GOC coast from south to north and the fact that gulf surge strength appears to be strongest over the ocean waters (Hales 1972, Brenner 1974, Higgins et al. 2006), this model cannot be used to sufficiently describe the horizontal structure of the surge events examined here as they relate to the complex terrain surrounding the GOC. Unfortunately, observations presented in this study did not allow for detailed analyses over areas of the ocean, Peninsular Range, or SMO foothills. Thus, it is unknown how these geographical features may have influenced gulf surge strength, structure, and propagation. However, future analyses using pilot balloon, aircraft, or precipitation data collected during the NAME field campaign may help resolve some of these issues.

In addition, this model only applies to the two gulf surge events examined in this study. It is uncertain whether the results presented here can be applied in part or in whole to other gulf surge events. Given the enormous topographical complexity of the GOC region combined with the varying effects of synoptic, mesoscale, and convective features surrounding gulf surge events, it is suggested that high-resolution mesoscale model runs be conducted to verify the gulf surge observations presented here and to determine whether or not the proposed dynamical mechanism is plausible for describing gulf surges.

# CHAPTER 7

# SUMMARY AND CONCLUSIONS

## 7.1 Summary

Gulf surges are complex atmospheric phenomena, yet extremely important to the North American Monsoon (NAM) as they relate to northward horizontal transport of cool, moisture-laden air to the low deserts of the southwest United States and northwest Mexico. It is this moisture that can be responsible for explosive convective development over the NAM region. The spatial and temporal resolutions of the 2004 North American Monsoon Experiment (NAME) observational networks are unprecedented and have afforded detailed analyses of the NAM heretofore not possible. Case studies of two gulf surge events were presented in which several aspects of their behavior were investigated.

Gulf surge #1 (GS #1, on 13 July) was relatively strong and deep (~ 800 hPa), resulting in the development of a large mesoscale convective system (MCS) over southern Arizona on 14 July. The surge most likely traversed the entire length of the Gulf of California (GOC). However, its basic structure appears to have changed drastically as it propagated north, evident in the ISS wind profiles. Extensive convection along the Sierra Madre Occidental (SMO) and GOC coastal plain developed after 0000 UTC 13 July apparently in response to various mesoscale processes, Tropical Storm Blas,

and a 200 hPa inverted trough, or tropical upper tropospheric trough (TUTT). This convective activity most likely played an important role in gulf surge initiation. Surge passage was observed along the northern GOC as a strong increase in south-southeasterly flow (up to 20.0 m $s^{-1}$ around 0.75 km at Puerto Peñasco and 1.25 km at Bahia Kino), anomalous cooling (- 4-8°C), and anomalous positive moisture flux (> + 175 m g $s^{-1}$ $kg^{-1}$). Overall, surface signals related to surge passage were relatively weak compared to those 1-2 km above the surface, with the exception of substantial increases in surface pressure and a distinct weakening of the diurnal thermal pattern.

Initial surge onset along the northern gulf for GS #1 occurred within one hour, as evident in strong anomalous surface pressure (> 0.75 hPa) and temperature (> 0.5°C) increases coincident with increased south-southeasterly flow from the profiler winds. Pressure increases were most likely associated with the increased depth of the well-mixed boundary layer, whereas thermal increases appeared to be related to the vertical mixing of warmer air from above the nighttime inversion to the surface. Assuming a direction of initial propagation from 160°, similar surface signals were traced between Bahia Kino and Puerto Peñasco, resulting in a surge propagation speed of 20.5 m $s^{-1}$.

Gulf surge #2 (GS #2, on 21 July) was weaker and shallower (~ 900 hPa) than GS #1. Little to no convective development over Arizona/New Mexico occurred the following day due to surge passage. Whereas GS #1 traversed the entire length of the GOC, GS #2 was primarily confined along the northern GOC. An impressive MCS developed over the SMO by 0000 UTC 21 July, perhaps in response to mesoscale processes and the 700 hPa

easterly wave. This system quickly propagated west to the GOC coastal plain between Bahia Kino and Los Mochis, therefore most likely playing an integral role in surge initiation.

Similar characteristics to those during GS #1 were observed during GS #2. Anomalous cooling (- 2-4°C) and positive moisture fluxes (> + 125 m g $s^{-1}$ $kg^{-1}$) were generally weaker and associated surface signals were more difficult to discern. In fact, surface pressures slightly decreased several hours after surge onset. It appears that this can be related to the weakness of the surge combined with the synoptic flow patterns at the time. Initial gulf surge onset for GS #2 was also accompanied by similar surface characteristics (> 1.0 hPa pressure increase and > 0.5°C temperature increase) to those described for GS #1. However, these changes occurred over one-half hour. Assuming an initial direction of propagation from 150°, these surface signals were also tracked, resulting in a surge propagation speed of 19.8 m $s^{-1}$ between Bahia Kino and Puerto Peñasco.

The horizontal extent of both gulf surges was difficult to accurately discern due to the relatively course spatial resolution of the observations that served as the basis for the gridded datasets. Noting the extremely complex topography of the GOC region, the extent to which gulf surge strength and structure is influenced by the Peninsular Range, GOC, SMO and its foothills is not well understood. Nevertheless, from the observations presented in this report, it was still possible and reasonable to propose a dynamical

mechanism that could perhaps partially explain the northward propagation of the two gulf surge events examined here.

The analyses suggest a hybrid of mechanisms. Strong evaporational cooling associated with convective rainfall over the SMO foothills and GOC coastal plain can aid in the development of a surface mesohigh (Fig. 42). The anticyclonic flow around this system, in combination with Coriolis deflection, piles cooler air along the north-south barrier of the SMO, thus inducing south-southeasterly flow and a linear Kelvin wave-like disturbance that propagates north. As the surge moves north, it can encounter an environment conducive to the development of nonlinearities along its leading edge. These nonlinearities are evident in the surface and boundary layer observations as characteristics similar to those of atmospheric bores or solitary waves. Nonlinear Kelvin wave-like disturbances with bore-like features along their leading edges may not entirely account for what is actually occurring, but provides a basis to build from in future research endeavors.

**7.2 Conclusions**

Although the two events examined in this report are most likely not representative of all gulf surges, the results presented throughout Chapters 4-6 provide insight towards better understanding the vertical/horizontal structures and dynamical mechanisms of such phenomena. Several important conclusions can be deduced from this work. While some reinforce ideas presented in Chapter 2, others question previous studies. Conclusions

from both categories are listed below, although new findings presented here can most likely be attributed to the high temporal and spatial resolutions of the observations collected during the 2004 NAME field campaign.

- In addition to mesoscale processes, synoptic circulation patterns including those of subtropical ridges, tropical cyclones, mid-tropospheric easterly waves, and inverted troughs, or TUTTs can potentially enhance the development of NAM-related convection, which is apparently closely tied to gulf surge initiation.
- Preceded by strong anomalous warming, gulf surge-related cooling, moistening, and increased south-southeasterly flow are greatest from immediately above the surface up to approximately 800 hPa.
- Initial atmospheric modifications related to gulf surge passage are generally observed over 12 hours or less. Further significant cooling and/or moistening may occur afterwards, but seem to be related to other features not directly linked to surge passage, including various synoptic circulations and/or convective activity.
- Surge onset occurs abruptly in the early morning hours and is difficult to discern using only surface data, especially along the southern GOC. Onset is accompanied by increases in surface pressure and temperature, but seemingly little change in the surface dewpoint temperature. Surface cooling does not occur until several hours after initial surge onset. Surface winds are also not nearly as suggestive of surge passage; however they do appear to strengthen slightly and shift to the south-southeast.

- As gulf surges propagate from the southern to northern GOC, their vertical structure seems to significantly change, perhaps due to the influence of the northern GOC LLJ, although the method and extent to which this may occur is very uncertain.
- Gulf surge strength is perhaps related to its vertical structure and the surrounding synoptic, mesoscale, and convective environments.
- Gulf surge horizontal structure is still not well understood due to the lack of observations along Baja California, the GOC, and SMO foothills. Future analysis of aircraft, pilot balloon, and precipitation data may help resolve this issue.
- Propagation speeds along the northern GOC are approximately 20.0 m $s^{-1}$ for the two cases studied.
- The observations suggest a nonlinear Kelvin wave-like disturbance with atmospheric bore or solitary wave-like characteristics along its leading edge as the dynamical mechanism responsible for gulf surge northward propagation.
- High temporal and spatial resolution mesoscale model runs must be conducted to verify the observations and proposed dynamical mechanism.

The results presented in this report reveal the complexity of gulf surges and the environments in which they propagate. Since several questions still remain, however, future work should focus on further integrating other observational platforms from the 2004 NAME field campaign (i.e. aircraft, pibal, radar, precipitation) into the gridded datasets as a means to more accurately compare against model simulations. Only then may a more complete picture emerge concerning gulf surge behavior.

## REFERENCES


Adams, D. K., and A. C. Comrie, 1997: The North American Monsoon. *Bull. Amer. Meteor. Soc.,* **78,** 2197-2213.

Anderson, B. T., J. O. Roads, and S. Chen, 2000b: Large-scale forcing of summertime monsoon surges over the Gulf of California and the southwestern United States, *J. Geophys. Res.,* **105,** 24455-24467.

Anderson, B. T., J. O. Roads, S. Chen, and H. H. Juang, 2000a: Regional simulation of the low-level monsoon winds over the Gulf of California and southwestern United States, *J. Geophys. Res.,* **105,** 17955-17969.

Badan-Dangon, A., C. E. Dorman, M. A. Merrifield, and C. D. Winant, 1991: The lower atmosphere over the Gulf of California, *J. Geophys. Res.,* **96,** 16877-16896.

Bordoni, S., P. E. Ciesielski, R. H. Johnson, B. D. McNoldy, and B. Stevens, 2004: The low-level circulation of the North American Monsoon as revealed by QuikSCAT, *Geophys. Res. Lett.,* **31,** 1-4.

Brenner, I. S., 1974: A surge of maritime tropical air – Gulf of California to the southwestern United States, *Mon. Wea. Rev.,* **102,** 375-389.

Brown, W. O. J., J. O. Pinto, T. Yu, D. B. Parsons, and T. Weckwerth, 2003: NCAR integrated sounding system observations at IHOP. Preprints, *12th Symposium on Meteorological Observations and Instrumentation, 83rd Annual Amer. Meteor. Soc. Meeting,* Long Beach, CA, Amer. Meteor. Soc., CD-ROM, 10.4.

Bryson, R. A., and W. P. Lowry, 1955: Synoptic climatology of the Arizona summer precipitation singularity. *Bull. Amer. Meteor. Soc.,* **36,** 329-339.

Carleton, A. M., 1986: Synoptic-dynamic character of 'bursts' and 'breaks' in the south-west U.S. summer precipitation singularity, *J. Climatol.,* **6,** 605-623.

Clarke, R. H., R. K. Smith, and D. G. Reid, 1981: The morning glory of the Gulf of Carpentaria: An atmospheric undular bore, *Mon. Wea. Rev.,* **109,** 1726-1750.

Douglas, M. W., 1995: The summertime low-level jet over the Gulf of California, *Mon. Wea. Rev.,* **123,** 2334-2347.

_____, and S. Li, 1996: Diurnal variation of the lower-tropospheric flow over the Arizona low desert from SWAMP-1993 observations, *Mon. Wea. Rev.,* **124,** 1211-1224.

_____, and J. C. Leal, 2003: Summertime surges over the Gulf of California: Aspects of their climatology, mean structure, and evolution from radiosonde, NCEP reanalysis, and rainfall data, *Wea. Forecasting,* **18,** 55-74.

_____, R. A. Maddox, K. Howard, and S. Reyes, 1993: The Mexican monsoon. *J. Climate,* **6,** 1665-1677.

_____, A. Valdez-Mananilla, and R G. Cueto, 1998: Diurnal variation and horizontal extent of the low-level jet over the northern Gulf of California, *Mon. Wea. Rev.,* **126,** 2017-2025.

Dunn, L. B., and J. D. Horel, 1994a: Prediction of central Arizona convection. Part I: evaluation of the NGM and Eta model precipitation forecasts, *Wea. Forecasting,* **9,** 495-507.

_____, and _____, 1994b: Prediction of central Arizona convection. Part II: further examination of the Eta model forecasts, *Wea. Forecasting,* **9,** 508-521.

Fuller, R. D., and D. J. Stensrud, 2000: The relationship between tropical easterly waves and surges over the Gulf of California during the North American Monsoon, *Mon. Wea. Rev.,* **128,** 2983-2989.

Earth Observing Laboratory, cited 2005: Integrated Sounding System (ISS). [Available online at http://www.atd.ucar.edu/rtf/facilities/iss/]

Fulton, R., D. S. Zrnić, and R. J. Doviak, 1990: Initiation of a solitary wave family in the demise of a nocturnal thunderstorm density current, *J. Atmos. Sci.,* **47,** 319-337.

Glickman, T. S., M. Frey, R. G. Hendl, and R. T. Podsiadlo, 2000: *Glossary of Meteorology.* 2d ed. American Meteorological Society, 855 pp.

Gochis, D. J., A. Jimenez, C. J. Watts, J. Garatuza-Payan, and W. J. Shuttleworth, 2004: Analysis of 2002 and 2003 warm-season precipitation from the North American Monsoon Experiment Event Rain Gauge Network, *Mon. Wea. Rev.,* **132,** 2938-2953.

Hales, J. E. Jr., 1972: Surges of maritime tropical air northward over the Gulf of California, *Mon. Wea. Rev.,* **100,** 298-306.

_____, 1974: Southwestern United States summer monsoon source – Gulf of Mexico or Pacific Ocean?, *J. Appl. Meteor.,* **13,** 331-342.

Haase, S. P., and R. K. Smith, 1984: Morning glory wave clouds in Oklahoma: A case study, *Mon. Wea. Rev.,* **112,** 2078-2089.

Higgins, R. W., Y. Yao, and X. L. Wang, 1997: Influence of the North American monsoon system on the U. S. summer precipitation regime, *J. Climate,* **10,** 2600-2622.

_____, W. Shi, and C. Hain, 2004: Relationships between Gulf of California moisture surges and precipitation in the southwestern United States, *J. Climate,* **17,** 2983-2997.

_____, and Coauthors, 2006: The North American Monsoon Experiment (NAME) 2004 field campaign and modeling strategy, *Bull. Amer. Meteor. Soc.,* in press.

Holton, J. R., 1992: *An Introduction to Dynamic Meteorlogy.* 3d ed. Academic Press, 511 pp.

Howard, K. W., and R. A. Maddox, 1988a: A satellite-based climatology of warm season thunderstorms over Mexico. Preprints, *III InterAmerican and Mexican Congress of Meteorology,* Mexico City, Mexico, 414-418.

_____, and _____, 1988b: Mexican mesoscale convective systems - a satellite perspective. Preprints, *III InterAmerican and Mexican Congress of Meteorology,* Mexico City, Mexico, 404-408.

_____, and _____, 1988c: Mexican mesoscale convective systems - large-scale environmental conditions. Preprints, *III InterAmerican and Mexican Congress of Meteorology,* Mexico City, Mexico, 395-399.

_____, and _____, 1988d: Mexican mesoscale convective systems - two case examples. Preprints, *III InterAmerican and Mexican Congress of Meteorology,* Mexico City, Mexico, 89-93.

Jurwitz, L. R., 1953: Arizona's two-season rainfall pattern, *Weatherwise,* **6,** 96-99.

Joint Office for Science Support, cited 2005: NAME Field Catalog. [Available online at http://www. joss.ucar.edu/cgi-bin/catalog/name/report/index]

Kelley Jr., W. E., and D. R. Mock, 1982: A diagnostic study of upper tropospheric cold lows over the western north Pacific, *Mon. Wea. Rev.,* **110,** 471-480.

Koch, S. E., P. B. Dorian, R. Ferrare, S. H. Melfi, W. C. Skillman, and D. Whiteman, 1991: Structure of an internal bore and dissipating gravity current as revealed by raman lidar, *Mon. Wea. Rev.,* **119,** 857-887.

Kundu, P. K., and I. M. Cohen, 2002: *Fluid Mechanics.* 2d ed. Academic Press, 730 pp.

McCollum, D. M., R. A. Maddox, and K. W. Howard, 1995: Case study of severe mesoscale convective system in central Arizona, *Wea. Forecasting,* **10,** 643-665.

Menhofer, A., R. K. Smith, M. J. Reeder, and D. R. Christie, 1997: "Morning-Glory" disturbances and the environment in which they propagate, *J. Atmos. Sci.,* **54,** 1712-1725.

NAME Science Working Group, cited 2005: NAME Science and Implementation Plan. [Available online at http://www.cpc.ncep.noaa.gov/products/precip/monsoon/NAME.html]

Noonan, J. A., and R. K. Smith, 1986: Sea-breeze circulations over Cape York Peninsula and the generation of Gulf of Carpentaria cloud line disturbances, *J. Atmos. Sci.,* **43,** 1679-1693.

Nuss, W.A., D. W. Titley, 1994: Use of multiquadric interpolation for meteorological objective analysis, *Mon. Wea. Rev.,* **122,** 1611–1631.

Pytlak, E., M. Goering, and A. Bennett, 2005: Upper tropospheric troughs and their interaction with the North American Monsoon. Preprints, *19th Conf. on Hydrology, 85th Annual Amer. Meteor. Soc. Meeting,* San Diego, CA, Amer. Meteor. Soc., CD-ROM, JP2.3.

Ralph, F. M., L. Armi, J. M. Bane, C. Dorman, W. D. Neff, P. J. Neiman, W. Nuss, and P. O. G. Persson, 1998: Observations and analysis of the 10-11 June 1994 coastally trapped disturbance, *Mon. Wea. Rev.,* **126,** 2435-2465.

_____, P. J. Neiman, P. O. G. Persson, J. M. Bane, M. L. Cancillo, J. M. Wilczak, and W. Nuss, 2000: Kelvin waves and internal bores in the marine boundary layer inversion and the relationship to coastally trapped wind reversals, *Mon. Wea. Rev.,* **128,** 283-300.

Rasmusson, E. M., 1967: Atmospheric water vapor transport and the water balance of North America, *Mon. Wea. Rev.,* **95,** 403-426.

Reason, C. J. C., and D. G. Steyn, 1992: The dynamics of coastally trapped mesoscale ridges in the lower atmosphere, *J. Atmos. Sci.,* **49,** 1677-1692.

Reitan, C. H., 1957: The role of precipitable water vapor in Arizona's summer rains. Tech. Rep. on the Meteorology and Climatology of Arid Regions 2, 21 pp.

Research Applications Laboratory, cited 2005: Wind Profiler Quality Control Algorithms and Software. [Available online at http://www.rap.ucar.edu/technology/profiler/]

Rowson, D. R., and S. J. Collucci, 1992: Synoptic climatology of thermal low-pressure systems over south-western North America, *Int. J. Climatol.,* **12,** 529-545.

Sellers, W. D, and R. H. Hill, 1974: *Arizona Climate 1931-1972,* 2d ed. The University of Arizona Press, 616 pp.

Schmitz, J. T., and S. L. Mullen, 1996: Water vapor transport associated with the summertime North American Monsoon as depicted by ECMWF analyses, *J. Climate,* **9,** 1621-1634.

Simpson, J. E., 1997: *Gravity Currents in the Environment and the Laboratory.* 2d ed. Cambridge University Press, 244 pp.

Skamarock, W. C., R. Rotunno, and J. B. Klemp, 1999: Models of coastally trapped disturbances, *J. Atmos. Sci.,* **56,** 3349-3365.

Stensrud, D. J., R. L. Gall, S. L. Mullen, and K. W. Howard, 1995: Model climatology of the Mexican monsoon, *J. Climate,* **8,** 1775-1794.

_____, _____, and M. K. Nordquist, 1997: Surges over the Gulf of California during the Mexican monsoon, *Mon. Wea. Rev.,* **125,** 417-437.

Tang, M., and E. R. Reiter, 1984: Plateau monsoons of the Northern Hemisphere: a comparison between North America and Tibet, *Mon. Wea. Rev.,* **112,** 617-637.

Thorncroft, C. D., B. J. Hoskins, and M. E. McIntyre, 1993: Two paradigms of baroclinic-wave life-cycle behaviour, *Quart. J. Roy. Meteor. Soc.,* **119,** 17-55.

U.S. Census Bureau, cited 2005: American FactFinder Data Sets with Thematic Maps. [Available online at http://factfinder.census.gov/servlet/TMSelectedDatasetPageServlet?_lang=en]

Whitfield, M. B., and S. W. Lyons, 1992: An upper-tropospheric low over Texas during summer, *Wea. Forecasting,* **7,** 89-106.

Zehnder, J. A., 2004: Dynamic mechanisms of the gulf surge, *J. Geophys. Res.,* **109,** 1-14.

## APPENDIX

## LIST OF COMMONLY USED ACRONYMS

| | |
|---|---|
| ATD | Atmospheric Technology Division |
| ASPEN | Atmospheric Sounding Processing Environment |
| CSU | Colorado State University |
| CTD | Coastally Trapped Disturbance |
| ECMWF | European Centre for Medium-Range Weather Forecasts |
| EOP | Extended Observing Period |
| ETL | Environmental Technology Laboratory |
| FOC | Forecast Operations Center |
| GLASS | GPS Loran Atmospheric Sounding System |
| GOC | Gulf of California |
| GOES | Geostationary Operational Environmental Satellite |
| GPS | Global Positioning System |
| GS | Gulf Surge |
| GTS | Global Telecommunications System |
| IOP | Intensive Observing Period |
| IR | Infrared |
| ISS | Integrated Sounding System |
| LLJ | Low-Level Jet |

| | |
|---|---|
| MAPR | Multiple Antenna Profiler Radar |
| MCS | Mesoscale Convective System |
| NAM | North American Monsoon |
| NAME | North American Monsoon Experiment |
| NCAR | National Center for Atmospheric Research |
| NCEP | National Centers for Environmental Prediction |
| NERN | NAME Event Rain Gauge Network |
| NIMA | NCAR Improved Moments Algorithm |
| NOAA | National Oceanic and Atmospheric Administration |
| NWCA | NCAR Winds and Confidence Algorithm |
| NWS | National Weather Service |
| PSU | Pennsylvania State University |
| RAP | Research Applications Laboratory |
| RASS | Radio Acoustic Sounding System |
| SMN | Servicio Meteorológico Nacional (Mexican Weather Service) |
| SMO | Sierra Madre Occidental |
| S-POL | S-band Polarimetric |
| SWAMP | Southwest Area Monsoon Project |
| T1A | Tier 1 Array |
| T2A | Tier 2 Array |
| TUTT | Tropical Upper-Tropospheric Trough |
| WMO | World Meteorological Organization |